NASA/TM–2017-219022

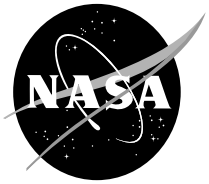

Mathematical Modeling of Electrodynamics Near the Surface of Earth and Planetary Water Worlds

Robert H. Tyler

September 2017

NASA STI Program ... in Profile

Since its founding, NASA has been dedicated to the advancement of aeronautics and space science. The NASA scientific and technical information (STI) program plays a key part in helping NASA maintain this important role.

The NASA STI program operates under the auspices of the Agency Chief Information Officer. It collects, organizes, provides for archiving, and disseminates NASA's STI. The NASA STI program provides access to the NTRS Registered and its public interface, the NASA Technical Reports Server, thus providing one of the largest collections of aeronautical and space science STI in the world. Results are published in both non-NASA channels and by NASA in the NASA STI Report Series, which includes the following report types:

TECHNICAL PUBLICATION. Reports of completed research or a major significant phase of research that present the results of NASA Programs and include extensive data or theoretical analysis. Includes compilations of significant scientific and technical data and information deemed to be of continuing reference value. NASA counter-part of peer-reviewed formal professional papers but has less stringent limitations on manuscript length and extent of graphic presentations.

TECHNICAL MEMORANDUM. Scientific and technical findings that are preliminary or of specialized interest, e.g., quick release reports, working papers, and bibliographies that contain minimal annotation. Does not contain extensive analysis.

CONTRACTOR REPORT. Scientific and technical findings by NASA-sponsored contractors and grantees.

CONFERENCE PUBLICATION. Collected papers from scientific and technical conferences, symposia, seminars, or other meetings sponsored or co-sponsored by NASA.

SPECIAL PUBLICATION. Scientific, technical, or historical information from NASA programs, projects, and missions, often concerned with subjects having substantial public interest.

TECHNICAL TRANSLATION. English-language translations of foreign scientific and technical material pertinent to NASA's mission.

Specialized services also include organizing and publishing research results, distributing specialized research announcements and feeds, providing information desk and personal search support, and enabling data exchange services.

For more information about the NASA STI program, see the following:

- Access the NASA STI program home page at http://www.sti.nasa.gov
- E-mail your question to help@sti.nasa.gov
- Phone the NASA STI Information Desk at (757) 864-9658

Write to:

NASA STI Information Desk

Mail Stop 148

NASA Langley Research Center

Hampton, VA 23681-2199

NASA/TM–2017-219022

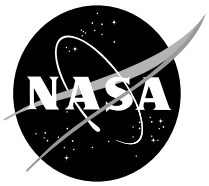

Mathematical Modeling of Electrodynamics Near the Surface of Earth and Planetary Water Worlds

Robert H. Tyler
University of Maryland, College Park, MD

National Aeronautics and
Space Administration

Goddard Space Flight Center
Greenbelt, MD 20771

September 2017

Level of Review: This material has been technically reviewed by technical management.

Mathematical modeling of electrodynamics near the surface of Earth and planetary water worlds

Robert H. Tyler

Abstract An interesting feature of planetary bodies with hydrospheres is the presence of an electrically conducting shell near the global surface. This conducting shell may typically lie between relatively insulating rock, ice, or atmosphere, creating a strong constraint on the flow of large-scale electric currents. All or parts of the shell may be in fluid motion relative to main components of the rotating planetary magnetic field (as well as the magnetic fields due to external bodies), creating motionally-induced electric currents that would not otherwise be present. As such, one may expect distinguishing features in the types of electrodynamic processes that occur, as well as an opportunity for imposing specialized mathematical methods that efficiently address this class of application. The purpose of this paper is to present and discuss such specialized methods. Specifically, thin-shell approximations for both the electrodynamics and fluid dynamics are combined to derive simplified mathematical formulations describing the behavior of these electric currents as well as their associated electric and magnetic fields. These simplified formulae allow analytical solutions featuring distinct aspects of the thin-shell electrodynamics in idealized cases. A highly efficient numerical method is also presented that is useful for calculations under inhomogeneous parameter distributions. Finally, the advantages as well as limitations in using this mathematical approach are evaluated. This evaluation is presented primarily for the generic case of bodies with water worlds or other thin spherical conducting shells. More specific discussion is given for the case of Earth, but also Europa and other satellites with suspected oceans.

Department of Astronomy, University of Maryland at College Park
and NASA Goddard Space Flight Center
Geodesy and Geophysics Laboratory, Code 61A, Greenbelt, MD 20771
Email: robert.h.tyler@nasa.gov; Tel: 301-614-6472

Contents

1 Introduction

1.1 Scope and goals

This paper treats the mathematical modeling of electrodynamics near the surface of planetary bodies with electrically conducting fluid shells that may be in relative motion. Fundamentally, this involves the calculation of the behavior of electric charge and electric currents as they interact with material media and momentum. This interaction is mediated through the electric and magnetic fields and so governing equations often involve these as variables. Attention is restricted to applications where the traditional approximations in magnetohydrodynamics apply. This essentially focuses on macro-scale phenomena involving the dynamics of the media where conduction electric currents dominate over other types of electric current (e.g. displacement, advection). In the application to Earth, the conduction electric currents involved then reside predominantly in the oceans, secondarily in the conducting solid Earth, and only negligibly in the relatively insulating lower atmosphere or even the conducting upper atmosphere where a tensor conductivity implicitly represents electric current types beyond simple conduction. While the example of Earth is heavily relied upon for the purposes of discussion, this study is aimed at describing a methodology applicable to a generic class of planetary bodies having a global or large-scale conducting shell near the surface. Expected extraterrestrial applications primarily comprise water worlds on icy satellites in the Solar System and conjectured exoplanets with oceans.

While the well-studied equations of magnetohydrodynamics form a complete set of governing equations for all intended applications, they are more complicated than what is needed here. In these equations, the equations describing the dynamics of mass and momentum of material media, and the equations describing the electrodynamics of charge and electric current are coupled. As a result, both sets of equations must be solved simultaneously. Such is the case in the highly conducting Earth's core, or in rarified plasmas because in these cases either the higher prominence of electric currents or the lower prominence of material momentum allow a near equipartition in the energy densities carried in the electrodynamic and material momentum components. Such is not the case near the surface of the Earth. The material dynamics (e.g. ocean flow) are controlled primarily by energy inputs not directly related to the internal electrodynamics, and because of the relatively low electrical conductivity of the media very little of this energy is transferred to the electromagnetic fields. External energy fluxes into the electrodynamic components are also small compared to the mechanical and thermodynamic energy fluxes arriving from the atmosphere and gravitational forcing, and so it is the situation that the electrodynamic component of the magnetohydrodynamic system near the surface of the Earth has very little energy and therefore can contribute little to changing the dynamical behavior of the bulk material. One may describe this then as a restricted magnetohydrodynamic system where the "coupling" is only in one direction—transfer of kinetic energy can appreciably drive electric currents but the electromagnetic Lorentz forces on the material flow are insignificant (at least on time scales less than about 1000 years, and with geomagnetic field amplitudes closely similar to the present (Tyler, 2006)). Similarly, the Ohmic heat generated by electric currents can usually be considered to be unimportant in the thermodynamic balance. This greatly simplifies calculations because the equations for the electrodynamics can usually take the mechanical and thermodynamic variables as prescribed (ocean flow and electrical conductivity, for example, do not then depend on Lorentz forces and Ohmic heat.) The reduced magnetohydrodynamic system treated in this paper is then akin to the "kinematic dynamo" problem, although there are additional approximations that can be made because the background main magnetic field is largely determined by processes other than the ones considered and therefore it can also be prescribed.

The scope in this paper is primarily directed at large and global scale processes. This creates challenges, as well as opportunities for implementing useful approximations. Challenges include the need to recognize the spherical geometry (while calculations are typically much easier in a Cartesian domain), and the need to include within the domain extremely strong contrasts in parameters. The contrast in electrical conductivity between land and ocean, for example, can lead to instability in some numerical algorithms and can also require high spatial resolution to preserve important electrical connections through ocean straits. Focus on the larger scales can simplify calculations by eliminating the need to simultaneously include various small-scale processes, and

because the expected geometric attenuation of electromagnetic fields away from their sources provides a basis for aspect-ratio approximations. The simultaneous need for high resolution and large/global domains means that there is a strong need to seek suitable approximations in the formulations and efficient numerical schemes such that computations become feasible. The computational efficiency in these methods gains even higher priority when extending their use to inverse methods in which forward computations may need to be performed many times to infer physical parameters from observations of the electromagnetic fields.

The primary goal of this paper is then to address formulations and solution methods that are as simplified and efficient as needed to realistically capture the important physical processes. Even overly simplistic approaches can be useful if it is clear what component process is missing and/or if the solutions represent an intelligible end-member or limiting case. A useful alternative goal (not considered here) might be to seek feasible (if not necessarily fast) general solution approaches where less prerequisite care is required in examining the applicability of the method and fewer caveats may come in interpreting the solutions. (A general solution method developed by this author for higher-frequency applications (where the displacment current must be included) in the marine environment is described in Tyler et al. (2004); a comparison of other modern modeling approaches that include the realistic global ocean are described in Kelbert et al. (2014).)

The scope of this paper focuses on the mathematical formulations, suitable approximations, and solution methodologies. Applications enter primarily for illustration and evaluation of the methods. The methods are directed at cases where the surface shell may have highly inhomogeneous electrical properties, the shell may be a fluid in motion, and one need not make advance assumptions about the relative importance of induction, motional induction, and magnetic diffusion. Though not the focus, a variety of simplified formulations and methods where less generality is required is described in Appendix F. The appendices also include other topics and details that would be a distraction from the focus in the main text. An outline of the material is provided by the Table of Contents.

1.2 Background on development of formulations

Simplified forms of the equations governing electrodynamics have been sought in applications involving the near-surface global Earth. Schuster and Lamb (1889) for example, used a formulation by Lamb (1883) for an assumed uniformly conducting sphere in his attempt to infer the electrical conductivity of the Earth from analyses of the variations in the observed geomagnetic field. Modern applications involve a variety of numerical modeling approaches that may show much less restrictive assumptions in the formulation, but bring new approximations implicit in the numerical discretization and resolution.

These formulations have typically been based in the Maxwell (or pre-Maxwell) equations together with the constitutive relationships describing the electrodynamic response of media, despite the history of complaints appearing in the literature that these equations do not formally apply to the large-scale rotating frame of the Earth (see review in Tyler and Mysak, 1995a). At issue appears to be the erroneous assumption that the Lorentz invariance of Maxwell's equations applies when transferring from an inertial frame to a rotating (accelerating) frame. The source-free Maxwell's equations (i.e. the homogeneous Maxwell's equations involving electromagnetic fields but no material media) indeed retain this invariance but because of the more trivial lack of any reference to the location of any material matter or charge in the Universe. In applications of continuous material media, the Maxwell's equations are sometimes called the "macroscopic" Maxwell equations as they involve averaging of the fields over small-scale processes including those fundamentally occurring at molecular and atomic scales within the material media. In this case, the presence of material media injects a special reference frame (i.e. one where the material is at rest) and the transformation between coordinate systems requires more consideration. While Lorentz invariance (from Special Relativity) does not allow transformation from an inertial frame to a rotating frame, covariance principles (from General Relativity) apply more generally and it has been shown that three of the four Maxwell's equations are retained within good approximation in the rotating frame and expected electrical properties of Earth (Tyler and Mysak, 1995a). Luckily, the so-called "electromagnetic induction equation" used in

many of the relevant geophysical applications is composed from only these three of the four Maxwell's equations and so its use in the rotating frame has remained valid, even if the reason for its validity has been perhaps misunderstood. (Further details on this topic are included in Appendix A.) In the study described below, it shall be assumed that the conventional electromagnetic induction equation applies in the rotating frame of the global Earth and the approximations to be discussed involve considerations beyond those of the transformation of the coordinate system.

The early work of Schuster and Lamb was followed by further studies that treated the Earth as a uniform conductor and it was quickly appreciated that treating the Earth as a uniform conductor was a poor approximation; it appeared that the upper mantle was a relative insulator several hundred kilometers thick with electrical conductivity perhaps three orders of magnitude smaller than that in the surface ocean or in the lower mantle (Chapman, 1919). Once it was appreciated that the upper mantle was resistive and the ocean was the major contributor to the near-surface conductivity, it must have also then been immediately clear that no spherically-symmetric conductivity distribution would adequately represent the Earth's near-surface conductivity.

Price (1949) next provided a thin-sheet induction equation that allowed for non-uniform conductance. Except in the steady-state or low-frequency limits, this two-dimensional equation should be regarded as a boundary equation that must be satisfied while solving (other) equations appropriate for the adjacent three-dimensional regions. While the work by Price (1949) assumed these adjacent domains to be electrically insulating, subsequent work allowed for inductive (though not galvanic) coupling with a mantle having uniform layers of constant conductivity (e.g. Hewson-Browne and Kendall, 1978; Beamish and Hewson-Browne, 1980). Solution methods for induction applications involving radially symmetric conductivity distributions over a sphere have also been described (e.g. Srivastava (1966)). Later developments exploiting thin-shell approximations have primarily followed an approach where the electric and magnetic fields are first decomposed into toroidal/poloidal scalar fields and governing integral equations are solved. A careful review and description of this approach has been provided by Sun and Egbert (2012). These methods were primarily directed at induction applications excited by time-dependent external magnetic fields. The study here includes as an essential component the possibility that the conducting shell is in fluid motion, with associated motional induction effects. While the previous approach may include motional induction sources through simple prescription of an associated imposed current distribution, the approach may not be optimal for maintaining dynamical consistency with the fluid component. For this purpose, a numerical approach might ideally attempt to use the same bases or discretization representation in both the electromagnetic and fluid representations such that conserved properties in both are retained. Additionally, the approach may gain higher accuracy by following the treatment in calculating integrals of products over the ocean depth as described by Sanford (1971) and repeated in other global ocean applications (e.g. Stephenson and Bryan, 1992; Tyler, Sanford, and Oberhuber, 1997). Because the development using toroidal/poloidal bases is well described by Sun and Egbert (2012), we complete this section by focusing on the past studies using alternate bases aimed at applications of motional induction in the global ocean.

Tyler et al. (2003) extended the Price equation to allow for relative motion within a spherical conducting shell. This was needed because in the application of Tyler et al. (2003) it was the relative motion of the ocean fluid (rather than excitation by external time-dependent magnetic fields) that was driving the electric currents in the shell. (Stephenson and Bryan (1992) describe a thin-shell formulation that includes essentially a similar motional modification to the Price formulation but ignores the time dependency such that this approach falls within a larger class of magnetostatic/electrostatic formulations.) Both of these studies included the conductivity-weighted depth averaging as described in Sanford (1971). In Tyler et al. (2003), the adjacent domains were taken to be insulators, while in Sabaka et al. (2015, 2016), the formulation was extended to include either a reflecting lower mantle or an upper mantle with a spherically symmetric distribution of electrical conductivity. Hence, the Tyler approach extends the Price formulation to include motional sources and inductive coupling with neighboring (e.g. mantle) conductors in global, spherical geometry. The approach in Tyler et al. (2003) addressed a previous difficulty in obtaining general solutions with the Price formulation. While the early Price (1949) and early following studies had provided iterative approaches that reached convergence in applications involving domains with either no land or no ocean, the radius of convergence in these methods could not, in general, be maintained below unity.

Frustratingly, with both land and ocean in the domain, convergent methods were available only in applications that avoided the near-diurnal frequencies that were precisely of interest in studying the daily variations in the geomagnetic field. The physical reason behind this convergence problem and the separate behaviors of the equation below and above the near-diurnal frequency is described in Section 5.

2 Mathematical formulations

2.1 General formulation

2.1.1 Induction equation

The starting point in this analysis is the electromagnetic induction equation

$$\partial_t \mathbf{B} = \nabla \times (\mathbf{u} \times \mathbf{B} - K \nabla \times \mathbf{B}), \tag{2.1}$$

where $\mathbf{B}$ (T) is the magnetic field vector, $\mathbf{u}$ (m/s) is the velocity vector, and K (m^2/s) is the magnetic diffusivity (note $K = (\mu_0 \sigma)^{-1}$, where $\mu_0 = 4\pi \times 10^{-7}$ V·s/(A·m) is the permeability of free space, and σ (S/m) is the electrical conductivity of the media.) While $\mathbf{u}$ and K are parameters describing the material media and its relative motion, $\mathbf{B}$ is a field quantity and typically extends beyond the domain of the material media which, by assumption, is a relatively good conductor. Because of this, it should be immediately appreciated that (2.1) may be incomplete and auxiliary equations may be needed to describe the behavior of $\mathbf{B}$ on the material boundaries or in adjacent subdomains where material media is either absent or the assumption of high conductivity breaks down. A related issue is to understand any discontinuities in the applicability of (2.1) to domains containing both good and poor conductors. To understand these additional equations and conditions that must typically be supplied, it is helpful to review the equations from which the induction equation is derived:

The induction equation is constructed from three of the Maxwell's equations (2.2–2.4) and the constitutive Ohm's Law for a moving conductor (2.5):

$$\partial_t \mathbf{B} + \nabla \times \mathbf{E} = 0 \tag{2.2}$$

$$\nabla \times \mathbf{B} = \mu_0 \mathbf{J} \tag{2.3}$$

$$\nabla \cdot \mathbf{B} = 0 \tag{2.4}$$

$$\mathbf{E} + \mathbf{u} \times \mathbf{B} = \mathbf{J}/\sigma \tag{2.5}$$

where $\mathbf{E}$ (V/m) is the electric field and $\mathbf{J}$ (A/m^2) is the electric current density. Written in this way, the electromagnetic fields ($\mathbf{E}$, $\mathbf{B}$) and referential velocities ($\mathbf{u}$) are on the left side of the equations while the material densities $\mathbf{J}$ and material properties σ, μ_0 are on the right.

The induction equation (2.1) is a vector equation and therefore provides three equations in terms of seven parameter components of $\mathbf{B}$ $\mathbf{u}$, and K. It does not insure, however, that any choice of the three components can be determined if the other four are known. One can see, for example, that an arbitrary $\mathbf{B}$-parallel component can be added to $\mathbf{u}$ and (2.1) is left unchanged. A solution $\mathbf{u}$ obtained from known $\mathbf{B}$ and K using (2.1) is evidently non-unique and other conditions are required to select the physically correct solution. Moreover, the domain over which solutions must be considered depends on which of the seven components are treated as solution variables and which are treated as prescribed/observed parameters. An application involving prescribed $\mathbf{B}$ may require a domain comprising only material media, while one where components of $\mathbf{B}$ are treated as solution variables may require a domain extending into regions where no material media is present and the applicability of (2.1) may be questioned. Let us then discuss the auxiliary conditions and equations that may be added in typical applications:

2.1.2 Formulation for electrically insulating region

Equations (2.2–2.4) are better referred to as "pre-Maxwell" equations because the displacement current (the key contribution by Maxwell) is not included. Moreover, other forms of electric current (e.g. advection of spatial charge density) are also ignored and $\mathbf{J}$ is regarded as specifically a conduction current which can take place only in material media having non-vanishing electrical conductivity σ.

In a region in which $\mathbf{J}$ =0, (2.3, 2.4) require that $\mathbf{B}$ is both curl-free and divergence-free. From Helmholtz theorems it can be shown that $\mathbf{B}$ can be uniquely obtained from a potential field driven by boundary values. That is, not only does $\mathbf{B}$ obey Laplace's equation (i.e. $\nabla^2\mathbf{B} = 0$, which can be obtained from (2.3), with $\mathbf{J} = 0$, and (2.4)) but more fundamentally $\mathbf{B} = \nabla\mathfrak{B}$, where $\mathfrak{B}$ is a potential field satisfying $\nabla^2\mathfrak{B} = 0$.

In the appropriate limit of $\sigma \to 0$, the induction equation (2.1) reduces to $\nabla \times \nabla \times \mathbf{B} \to 0$, which together with (2.4) and vector identities provides $\nabla^2\mathbf{B} = 0$. Use of (2.1) is then expected to be consistent even when very small values of σ are prescribed to reflect insulating regions. Care must be taken, however, to insure that $\nabla \times \mathbf{B} = 0$ and $\nabla \cdot \mathbf{B} = 0$ are respected. Alternatively, one can apply the governing equation

$$\nabla^2\mathfrak{B} = 0 \tag{2.6}$$

in the insulating regions and the lower order relationships $\nabla \times \mathbf{B} = 0$ and $\nabla \cdot \mathbf{B} = 0$ are then automatically satisfied.

In summary, the induction equation (2.1) can be applied to domains containing both good and poor conductors but an advance assumption is that the electric currents $\mathbf{J}$ are specifically due to the conduction of charge through a medium that is either stationary, electrically neutral, or moving with low enough relative velocity such that the products of spatial charge density and velocity do not contribute appreciably as electric current (note that the assumption of non-relativistic speeds is an additional and independent assumption.) These fundamental assumptions are required even for the validity of the transformation of the induction equation to the rotating frame.

2.1.3 Boundary conditions

It is assumed that in all applications to be considered the natural boundary conditions of boundedness and containment for $\mathbf{u}$ and $\mathbf{B}$ are obeyed, such that only solutions with finite values in a limited domain of the Universe are accepted. Because different equations (e.g. 2.1 and 2.6) may be applied in different subdomains, one must consider matching conditions connecting solutions for $\mathbf{B}$ at the interface of these subdomains.

From examination of (2.2–2.4) and assumed boundedness of $\mathbf{J}$, continuity across the interface between media can be expected for all components of $\mathbf{B}$ as well as $\partial_r B_r$, where here "r" can initially be taken to be an axis normal to the interface.

2.2 Projections of the induction equation onto smooth surfaces

2.2.1 Induction equation on arbitrary smooth surfaces

Toward tractability in finding solutions using the induction equation (2.1), observed or expected symmetries and/or geometric aspect ratios implicit in some of the parameter fields $\mathbf{B}$, $\mathbf{u}$, and K may be used to uncouple one or more of the induction equation components. Let us define a vector $\mathbf{g} = -\nabla\mathfrak{G}$ where $\mathfrak{G}$ is initially an arbitrarily chosen scalar field. Taking the dot product of $\mathbf{g}$ with (2.1) and using standard vector identities we write

$$\mathbf{g} \cdot \partial_t\mathbf{B} = \nabla \cdot (\{\mathbf{u} \times \mathbf{B}\} \times \mathbf{g} - K\{\nabla \times \mathbf{B}\} \times \mathbf{g}), \tag{2.7}$$

which is an expression describing generation of the magnetic vector component perpendicular to $\mathfrak{G}$ = constant surfaces. With further use of algebra and vector identities, (2.7) can be written

$$\mathbf{g}\cdot\partial_t\mathbf{B} = \nabla\cdot\left(\left[\mathbf{g}\cdot\mathbf{u}\right]\mathbf{B}_H - \left[\mathbf{g}\cdot\mathbf{B}\right]\mathbf{u}_H + K\nabla_H\left[\mathbf{g}\cdot\mathbf{B}\right] - K\left[\mathbf{g}\cdot\nabla\right]\mathbf{B}_H - \left(\hat{\mathbf{g}}\cdot\mathbf{B}\right)\hat{\mathbf{g}}\cdot\nabla|\mathbf{g}| - K\left[\mathbf{B}\cdot\nabla\right]\mathbf{g}\right), \quad (2.8)$$

where $\hat{\mathbf{g}} = \mathbf{g}/|\mathbf{g}|$. When we assume $\mathbf{g}$ is temporally constant, the term on the left of (2.8) may be written $\partial_t\left[\mathbf{g}\cdot\mathbf{B}\right]$ and (2.8) becomes

$$\partial_t B_z + \nabla_H\cdot\left(B_z\mathbf{u}_H\right) - \nabla_H\cdot\left(K\nabla_H B_z\right) = \nabla_H\cdot\left(u_z\mathbf{B}_H\right) - \nabla_H\cdot\left(K\left[\mathbf{g}\cdot\nabla\right]\mathbf{B}_H\right) - \nabla_H\cdot\left(K\left[\mathbf{B}\cdot\nabla\right]\mathbf{g}\right) \quad (2.9)$$

where $B_z = \mathbf{g}\cdot\mathbf{B}$, $u_z = \mathbf{g}\cdot\mathbf{u}$, and subscript H refers to the tangential components as above. When $\mathfrak{G}$ is chosen such that $\mathbf{g}$ has unit amplitude, B_z and u_z clearly represent the vector components of $\mathbf{B}$ and $\mathbf{u}$ normal to the constant-$\mathfrak{G}$ surface, but other choices for $\mathbf{g}$ can be convenient in some applications involving the conservation of magnetic flux or fluid material quantities. Note that the left side of (2.9) involves only B_z and all spatial differentiation is tangent to the constant-$\mathfrak{G}$ surface. The terms on the left side describe a two-dimensional advection-diffusion process where B_z is advected along the surface by flow $\mathbf{u}_H$ and diffuses laterally at a rate controlled by the diffusion coefficient K and the gradients/curvature in the field B_z. The terms on the right side still involve the other components $\mathbf{B}_H$, and the last two terms may involve differentiation ∂_z perpendicular to the constant-$\mathfrak{G}$ surface. As respective consequences, this scalar equation controlling the behavior of B_z is still coupled to the other magnetic vector components, and a computational domain consisting of only a two-dimensional surface is not possible outside of highly idealized cases where much of the behavior of $\mathbf{B}$ can be prescribed.

Although the freedom in choosing $\mathfrak{G}$ is not generally sufficient to isolate an uncoupled, two-dimensional component of the induction equation, a judicious choice of $\mathfrak{G}$ may reduce the complexity of coupling between the induction equations on stacked $\mathfrak{G}$ surfaces filling a domain. A few examples of such choices are described next.

2.2.2 Induction equation on radially symmetric surfaces

Consider here the case $\mathfrak{G} = r$, where r is the radius in a spherical coordinate system. In this case, the constant-$\mathfrak{G}$ surfaces are radially symmetric, and $\mathbf{g} = \hat{\mathbf{r}}$ is simply the radial unit vector. In spherical coordinates θ, φ, r (colatitude, longitude, radius), we may apply the vector identity

$$\left[\mathbf{B}\cdot\nabla\right]\mathbf{g} = \left(\mathcal{L}_{\mathbf{B}}g_r - r^{-1}\left(B_\theta g_\theta + B_\varphi g_\varphi\right)\right)\hat{\mathbf{r}} + \left(\mathcal{L}_{\mathbf{B}}g_\theta + r^{-1}\left(B_\theta g_r - B_\varphi g_\varphi\cot\theta\right)\right)\hat{\theta} + \left(\mathcal{L}_{\mathbf{B}}g_\varphi + r^{-1}\left(B_\varphi g_r + B_\varphi g_\theta\cot\theta\right)\right)\hat{\varphi}, \quad (2.10)$$

where $\mathcal{L}_{\mathbf{B}} = \left[B_r\partial_r + B_\theta r^{-1}\partial_\theta + B_\varphi\left(r\sin\theta\right)^{-1}\partial_\varphi\right]$, together with standard identities and $\mathbf{g} = \hat{\mathbf{r}}$, to find that in this case $\left[\mathbf{B}\cdot\nabla\right]\mathbf{g} = \mathbf{B}_H/r$ and we write (2.9) as

$$\partial_t B_r + \nabla_H\cdot\left(B_r\mathbf{u}_H\right) - \nabla_H\cdot\left(K\nabla_H B_r\right) = \nabla_H\cdot\left(u_r\mathbf{B}_H\right) - \nabla_H\cdot\left(K\partial_r\mathbf{B}_H\right) - \nabla_H\cdot\left(Kr^{-1}\mathbf{B}_H\right), \quad (2.11)$$

or, equivalently,

$$\partial_t B_r + \nabla_H\cdot\left(B_r\mathbf{u}_H\right) - \nabla_H\cdot\left(K\nabla_H B_r\right) = \nabla_H\cdot\left(u_r\mathbf{B}_H\right) - \nabla_H\cdot\left(Kr^{-1}\partial_r\left(r\mathbf{B}_H\right)\right). \quad (2.12)$$

2.2.3 Induction equation on geopotential surfaces

Typical large-scale geophysical flows are in hydrostatic balance to first order, meaning the fluid momentum equations with only the most important terms retained would express simply a balance between pressure gradient forces and effective gravity. The flow (then a higher-order effect) is predominantly along geopotential surfaces,

and it becomes interesting to consider the case where $\mathfrak{G}$ is taken to be the geopotential surface $\mathcal{G}$. In this case, one may neglect the first term on the right of (2.8). In many applications, assumed slow variation in the geopotential allows one to also neglect the last term in (2.8).

If $\delta\mathcal{G}$ is the difference in geopotential between two constant-$\mathcal{G}$ surfaces separated by a small distance δz, then we may write $\mathbf{g} \approx \hat{\mathbf{z}}\delta\mathcal{G}/\delta z$ When considering integration or averaging over a layer bound by geopotential surfaces, $\delta\mathcal{G}$ is uniform and the variations of $\mathbf{g}$ are due to variations in the geopotential thickness δz. This representation is similar to the geopotential "height" used in atmospheric studies and the approach described here can form the basis for transforming equations to a system with geopotential height as the vertical coordinate.

Note that the hydrostatic assumption is often a reasonable approximation for describing the shape of rotating bodies composed of "solid" material that is not conventionally regarded as a fluid. The surface of such a body falls, to a better approximation, on a geopotential surface rather than a spherical surface. This suggests that improved accuracy may be obtained using an induction equation cast onto these surfaces or with geopotential height as a coordinate. When there are significant bathymetric variations, one should note that the lowest surface following this bathymetry does not conform to a geopotential surface except in the large-scale average. Consideration of the induction equation terms when cast on this surface may at the least provide a description of the errors involved when assuming simpler projections (e.g. spherical) involving fluids in near hydrostatic balance.

2.2.4 Induction equation on fluid material surfaces

In the last three subsections, the induction equation was projected onto various smooth surfaces in preparation for simplifications allowing the uncoupling of the vector induction equation components. Here we describe an approach that, while more abstract, is also more general and immediately includes the previous projections as special cases. This approach has been described in Tyler and Mysak (1995b). A general derivation is shown using Lie derivatives along space-time 4-vector trajectories (Palmer, 1988), and Hide (1983) has described a specific example in magnetohydrodynamics.

When we specify the vector $\mathbf{g}$ to be the gradient of an arbitrary scalar field (i.e. $\mathbf{g} = -\nabla\mathfrak{G}$), standard vector identities allow us to write the induction equation (2.1) as

$$\partial_t (\mathbf{g}\cdot\mathbf{B}) + \nabla\cdot((\mathbf{g}\cdot\mathbf{B})\,\mathbf{u}) = -\mathbf{B}\cdot(-\partial_t\mathbf{g} - \nabla(\mathbf{g}\cdot\mathbf{u})) - \nabla\cdot(K\{\nabla\times\mathbf{B}\}\times\mathbf{g}). \tag{2.13}$$

Let us further assume that the field $\mathfrak{G}$ is a material property of the fluid medium:

$$D_t\mathfrak{G} = \partial_t\mathfrak{G} + \mathbf{u}\cdot\nabla\mathfrak{G} = \Psi_{\mathfrak{G}}, \tag{2.14}$$

where the notation $D_t = \partial_t + \mathbf{u}\cdot\nabla$ refers to the material derivative and $\Psi_{\mathfrak{G}}$ is the source/sink term for $\mathfrak{G}$. Using (2.14), (2.13) becomes

$$\partial_t (\mathbf{g}\cdot\mathbf{B}) + \nabla\cdot((\mathbf{g}\cdot\mathbf{B})\,\mathbf{u}) = -\mathbf{B}\cdot\nabla\Psi_{\mathfrak{G}} - \nabla\cdot(K\{\nabla\times\mathbf{B}\}\times\mathbf{g}), \tag{2.15}$$

or, using $\nabla\cdot\mathbf{u} = 0$,

$$D_t (\mathbf{g}\cdot\mathbf{B}) = -\mathbf{B}\cdot\nabla\Psi_{\mathfrak{G}} - \nabla\cdot(K\{\nabla\times\mathbf{B}\}\times\mathbf{g}), \tag{2.16}$$

which, with $\mathbf{g} = -\nabla\mathfrak{G}$ (as well as $\nabla\cdot\mathbf{B} = 0$, $\nabla\cdot\mathbf{u} = 0$), can be written in the forms

$$D_t (\mathbf{B}\cdot\nabla\mathfrak{G}) = \mathbf{B}\cdot\nabla\Psi_{\mathfrak{G}} - \nabla\cdot(K\{\nabla\times\mathbf{B}\}\times\nabla\mathfrak{G}), \tag{2.17}$$

$$D_t\nabla\cdot(\mathfrak{G}\mathbf{B}) = \nabla\cdot(\Psi_{\mathfrak{G}}\mathbf{B}) - \nabla\cdot(K\{\nabla\times\mathbf{B}\}\times\nabla\mathfrak{G}), \tag{2.18}$$

$$\partial_t\nabla\cdot(\mathfrak{G}\mathbf{B}) + \nabla\cdot(\nabla\cdot(\mathfrak{G}\mathbf{B})\,\mathbf{u}) = \nabla\cdot(\Psi_{\mathfrak{G}}\mathbf{B}) - \nabla\cdot(K\{\nabla\times\mathbf{B}\}\times\nabla\mathfrak{G}). \tag{2.19}$$

The appropriate form of induction equation depends on the application or intuition sought. Generally, the forms involving the material derivative may help when adopting a Lagragian (i.e. moving with the flow) perspective, while the forms involving the divergence of terms are easily integrated over volumes to obtain bulk behavior and conservation principles.

While the previous projections of the last three subsections can be derived from these forms, they do not demonstrate the power of this formulation because the incorporation of material properties is somewhat trivialized. A very simple example that does use these properties is as follows. Consider $\mathfrak{G}$ to be the fractional height in the water column subjected to horizontal laminar flow. One may view this as $\mathfrak{G} = z/h$, where z is the depth below a flat fluid surface and h is the thickness of the fluid layer that we shall assume here also varies spatially. While the values of z and h vary following a fluid parcel, the ratio (i.e. z/h) should remain the same if the fluid is conserved (i.e. $\Psi_{\mathfrak{G}} = 0$). More generally we may have fluid sources and sinks (i.e. $\Psi_{\mathfrak{G}} \neq 0$). Assuming the surfaces $\mathfrak{G}$ vary only on scales much larger than h (the thin-shell assumption), $\nabla\mathfrak{G} \approx \frac{1}{h}\hat{\mathbf{z}}$, where $\hat{z}$ is a unit vector normal to the $\mathfrak{G}$ surface, and (2.17) becomes

$$D_t \frac{B_z}{h} = \mathbf{B} \cdot \nabla\Psi_{\mathfrak{G}} - \nabla \cdot (K\{\nabla \times \mathbf{B}\} \times \nabla\mathfrak{G}). \tag{2.20}$$

In the limiting case where the terms on the right side of (2.20) vanish, $D_t \frac{B_z}{h} = 0$ expressing a conservation of "potential magnetism" following the flow. This is directly analogous to the concept of "potential vorticity" used in geophysical fluid dynamics. Here it expresses the effect of contraction and dilation of the fluid column as it flows over (e.g. topographic) variations in h. The component B_z varies individually because the contraction/dilation of the water column leads to a similar contraction/dilation of the magnetic field lines. In this case, although B_z is not conserved following the flow, the ratio $\frac{B_z}{h}$ is.

2.3 Thin-shell induction equation

2.3.1 Formulation

Let us consider the electrodynamics in a thin, spherical shell of electrically conducting fluid material which may be in fluid motion. The exterior regions immediately adjacent to the shell are assumed to be electrical insulators such that there is no electric charge transfer between the shell and these regions. While this assumes the thin shell is galvanically isolated, it is not inductively isolated because electromagnetic fields due to time-dependent electric currents can pass out of the shell, through the adjacent insulators, and into other conductors where they may excite electric currents (and associated electromagnetic fields that may return to induce further electric currents in the shell). Because the adjacent insulating layers may be chosen to be arbitrarily thin, one need not envision the thin conductive shell as embedded in insulators. In the application below treating a conductive shell comprising the ocean and sediments at the Earth's surface, we may include a conductive mantle so long as it is separated from the shell by an arbitrarily thin insulating upper mantle. In this case, the ocean and mantle are inductively coupled through the time variable poloidal magnetic field but they are galvanically isolated—meaning there are no poloidal electric currents connecting the two. The thin shell confines material matter and charge but not electromagnetic fields. These are multiple ways of describing the same fundamental assumption that makes the thin-shell approach convenient.

Let us now distinguish a component $\mathbf{b}$ driven by electric currents in the shell, and a component $\mathbf{F}$ that is due to electric currents elsewhere. The field $\mathbf{F}$ may include prescribed components representing the main geomagnetic field or fluctuations due to prescribed external sources. It can also include components due to electric currents (elsewhere than within the conducting thin shell) that are ultimately excited by $\mathbf{b}$. (In which case, the sources may still be described as "prescribed" but with the understanding that we are focusing consideration on one component in a coupled system.) The total magnetic field is then $\mathbf{B} = \mathbf{F} + \mathbf{b}$. Note that because $\mathbf{F}$ has no sources in the thin shell it independently satisfies $\nabla \times \mathbf{F} = 0$ and therefore in examining the initial induction

equation (2.1) it is clear that the magnetic diffusion terms in (2.1) and subsequent forms do not involve $\mathbf{F}$. We may then write (2.11) as

$$\partial_t b_r + \nabla_H \cdot (b_r \mathbf{u}_H - u_r \mathbf{b}_H) - \nabla_H \cdot (K \nabla_H b_r) + \nabla_H \cdot \left(K \partial_r \mathbf{b}_H + K r^{-1} \mathbf{b}_H \right) = -\partial_t F_r - \nabla_H \cdot (F_r \mathbf{u}_H - u_r \mathbf{F}_H) , \quad (2.21)$$

where we see now prescribed ("forcing") terms on the right side of the equation. Note that (2.21) is so far just one component of the induction equation rewritten in a form that anticipates subsequent simplification and uncoupling of the magnetic vector components.

The distinguishing element of the thin shell which is exploited in simplifying the governing equations is essentially just the assumption of small aspect ratios describing the flow of mass (i.e. the fluid flow) and the flow of electrical charge (i. e. the electric current). For the purpose of discussion, let us assume the thin conductive shell occupies the region $a - h_0 < r < a$. The parameter h_0 can be chosen to be uniform and as small as possible provided the shell of uniform thickness $a - h_0$ is thick enough to include the thickest part of the conducting shell. The shell is geometrically thin if the aspect ratio $h_0/L_g << 1$, where L_g represents the horizontal geometric length scales of interest. The shell is electromagnetically thin if $h_0/L_e << 1$. Here $L_e = (2K/\omega)^{1/2}$ is the frequency (ω) dependent electromagnetic "skin depth" of the conductive medium of the shell. The skin depth is simultaneously a measure of the wavelength and attenuation length scales for electromagnetic propagation within the conducting shell. In the thin-shell approximation, one assumes both of these aspect ratios are vanishingly small.

The geometric thinness of the shell allows us to immediately approximate (2.21) as

$$\partial_t b_r + \nabla_H \cdot (b_r \mathbf{u}_H - u_r \mathbf{b}_H) + \nabla_H \cdot (K \partial_r \mathbf{b}_H) = -\partial_t F_r - \nabla_H \cdot (F_r \mathbf{u}_H - u_r \mathbf{F}_H) . \quad (2.22)$$

Within the fluid dynamics in the shell, the geometric thinness also gives the expectation $|u_r| << |\mathbf{u}_H|$ and because $|b_r| \sim |\mathbf{b}_H|$ we may neglect the term in (2.22) involving $u_r \mathbf{b}_H$. Similarly, one may usually neglect the term involving $u_r \mathbf{F}_H$ but because $\mathbf{F}$ is prescribed it should be retained in applications (presumably involving non-global domains) where $|F_r| << |\mathbf{F}_H|$.

The electromagnetic thinness of the shell allows us to conveniently replace some of the variables and parameters in the thin shell with their depth-averaged values (see Appendix D). When the shell is electromagnetically thin both b_r and $\mathbf{E}_H$ are to a very good approximation uniform with depth in the shell.

The uniformity of b_r within the thin layer ($a - h_0 < r < a$) together with the required continuity of b_r at the interfaces allows us to assume

$$b_r(r = a - h_0) = b_r(r = a) = \bar{b}_r, \quad (2.23)$$

where the over bar represents the operation of averaging over the shell depth:

$$\overline{(\cdot)} = \frac{\int_{a-h_0}^{a} (\cdot) dr}{\int_{a-h_0}^{a} dr}. \quad (2.24)$$

The uniformity of $\mathbf{E}_H$ can be exploited to create higher accuracy when depth averaging the terms involving products (Sanford, 1971). (If one of the factors is known to be uniform with depth, the depth average of the product of two factors is clearly the product of the depth averaged factors; by contrast, in the general case there is an additional term that depends on the correlation of the departures of the factors from their means.) When treating all terms except $\partial_t b_r$ and $\partial_t F_r$, we replace the simple depth average $\overline{(\cdot)}$ with the conductivity-weighted depth average $\overline{(\cdot)}^*$ defined by

$$\overline{(\cdot)}^* = \frac{\int_{a-h_0}^{a} (\cdot) \sigma dr}{\int_{a-h_0}^{a} \sigma dr}, \quad (2.25)$$

(see the Appendix D).

Using these aspect-ratio approximations and previous definitions, we may write (2.22) as

$$\partial_t \overline{b_r} + \nabla_H \cdot \left(\overline{b_r} \overline{\mathbf{u}_H}^* \right) + \nabla_H \cdot \left(c_d \frac{\delta \mathbf{b}_H}{2} \right) = -\partial_t \overline{F_r} - \nabla_H \cdot \overline{\left(F_r \mathbf{u}_H - u_r \mathbf{F}_H \right)}^*, \tag{2.26}$$

where

$$\delta \mathbf{b}_H = \mathbf{b}_H(r = a) - \mathbf{b}_H(r = a - h_0), \tag{2.27}$$

$$c_d = \frac{2}{\mu_0 \Sigma} \tag{2.28}$$

is the lateral magnetic diffusion speed (Tyler, 2005), and

$$\Sigma = \int_{a-h_0}^{a} \sigma dr \tag{2.29}$$

is the layer conductance.

Now let us consider the adjacent coupled domains. Because the regions immediately above and below the thin shell are assumed to be electrical insulators, the magnetic fields may be written as $\mathbf{b} = \nabla \mathfrak{B}$ for the insulating region above the thin shell and similarly $\mathbf{b} = \nabla \mathfrak{B}^{(-)}$ for the insulating region below the thin shell, where $\mathfrak{B}$ and $\mathfrak{B}^{(-)}$ represent the associated magnetic potentials in the insulating upper and lower regions (see Section 2.1.2). We may write the governing equations explicitly as

$$\nabla^2 \mathfrak{B} = 0, \tag{2.30}$$

for region $a \leq r < a_2$, and

$$\nabla^2 \mathfrak{B}^{(-)} = 0, \tag{2.31}$$

for region $a_1 < r \leq a - h_0$.

We require that $\mathbf{b}$ remains continuous across the interfaces of the thin shell and neighboring insulators. This allows us to write the following conditions:

$$\mathbf{b}_H \left(r = a \right) = \nabla_H \mathfrak{B}|_{r=a} \tag{2.32}$$

$$b_r(r = a) = \partial_r \mathfrak{B}|_{r=a} \tag{2.33}$$

$$\mathbf{b}_H \left(r = a - h_0 \right) = \nabla_H \mathfrak{B}^{(-)}|_{r=a-h_0} \tag{2.34}$$

$$b_r(r = a - h_0) = \partial_r \mathfrak{B}^{(-)}|_{r=a-h_0} \tag{2.35}$$

Using (2.23, 2.32, 2.33, 2.34) to substitute for the components of $\mathbf{b}$, we may write the thin-shell induction equation as

$$\partial_t \partial_r \mathfrak{B}|_{r=a} + \nabla_H \cdot \left(\partial_r \mathfrak{B}|_{r=a} \overline{\mathbf{u}_H}^* \right) + \nabla_H \cdot \left(c_d \nabla_H \left(\frac{\mathfrak{B}(r = a) - \mathfrak{B}^{(-)}(r = a - h_0)}{2} \right) \right) = -\partial_t \overline{F_r} - \nabla_H \cdot \overline{\left(F_r \mathbf{u}_H - u_r \mathbf{F}_H \right)}^*, \tag{2.36}$$

and by combining (2.23) with (2.33, 2.35) we obtain

$$\partial_r \mathfrak{B}|_{r=a} = \partial_r \mathfrak{B}^{(-)}|_{r=a-h_0}. \tag{2.37}$$

Equations (2.36, 2.37) are boundary equations/conditions that must be solved with (2.30, 2.31) to obtain solutions for the variables $\mathfrak{B}$ and $\mathfrak{B}^{(-)}$. As (2.30, 2.31) are second-order equations, there are two further conditions that must be imposed before unique solutions can be obtained. These two missing conditions describe the behavior of $\mathfrak{B}^{(-)}$ at $r = a_1$ and $\mathfrak{B}$ at $r = a_2$. In the approach in this study where $\mathfrak{B}$ and $\mathfrak{B}^{(-)}$ are regarded as due solely to electric currents within the shell considered, we may take for consistency the missing conditions to describe boundedness at $r = a_1 = 0$ and $r = a_2 \to +\infty$. If no other conductors other than the thin shell are present, then the equations above provide a closed set from which general solutions can be obtained. If other conductors are present (e.g. a conductive lower mantle), then the magnetic fields generated by electric currents in the shell may induce electric currents in these additional conductors. Associated with this are additional components to the total magnetic field. We may keep the formulation above as it is by allowing the "forcing" term $\partial_t F_r$ to include a component representing the field due to electric currents in the additional conductors. This component of $\partial_t F_r$ may, however, depend on the solution rather than being a prescribed parameter. The system is then not closed until additional equations and conditions are specified. Methods for coupling the thin-shell equations with the equations describing other conductors are then postponed to Section (2.4).

Returning to the thin-shell formulation above, note that with the conditions for boundedness described in the last paragraph, the solutions to (2.30, 2.31) that satisfy these conditions are

$$\mathfrak{B} = \sum_{n,s} \mathfrak{B}_{[n,s]} S_n^s \left(\frac{r}{a}\right)^{-(n+1)}, \tag{2.38}$$

$$\mathfrak{B}^{(-)} = \sum_{n,s} \mathfrak{B}^{(-)}_{[n,s]} S_n^s \left(\frac{r}{a-h_0}\right)^{n} \tag{2.39}$$

where $\sum_{n,s}$ represents an appropriate summation over the complete set of spherical harmonics and $\mathfrak{B}_{[n,s]}$, $\mathfrak{B}^{(-)}_{[n,s]}$ represent the associated coefficients of degree n and order s. Taking the radial derivative of (2.38) and (2.39) and applying (2.37) the following relationship between the coefficients is obtained:

$$\mathfrak{B}^{(-)}_{[n,s]} = -\left(1+\frac{1}{n}\right)\left(1-\frac{h_0}{a}\right)\mathfrak{B}_{[n,s]} \simeq -\left(1+\frac{1}{n}\right)\mathfrak{B}_{[n,s]}. \tag{2.40}$$

For all but the lowest degrees n, (2.40) shows that the coefficients for the potential above and below the shell are approximately equal in amplitude and opposite in sign (note that because there are no magnetic monopoles, there are not $n = 0$ coefficients and therefore $1/n$ remains bounded in (2.40)).

Further, let us define

$$M = \frac{\mathfrak{B}(r=a) - \mathfrak{B}^{(-)}(r=a-h_0)}{2}, \tag{2.41}$$

and let $M_{[n,s]}$ represent a spectral coefficient. We may combine this with (2.40) to obtain the following relationship between the spectral coefficients

$$M_{[n,s]} = (1+\frac{1}{2n})\mathfrak{B}_{[n,s]}. \tag{2.42}$$

Using (2.42), we may write (2.36) as

$$\partial_t \mathcal{L}_a[M] + \nabla_H \cdot \left(\mathcal{L}_a[M]\,\overline{\mathbf{u}_H}^*\right) + \nabla_H \cdot (c_d \nabla_H M) = -\partial_t \overline{F_r} - \nabla_H \cdot \overline{\left(F_r \mathbf{u}_H - u_r \mathbf{F}_H\right)}^*, \tag{2.43}$$

where $\mathcal{L}_a[\cdot]$ is an operator that provides

$$\mathcal{L}_a[M] = \partial_r \mathfrak{B}|_{r=a}, \tag{2.44}$$

and is expected to have an inverse. Using (2.38) and (2.42), we may specify

$$\mathcal{L}_a[M] = \sum_{n,s} \left(-\frac{n+1}{a}\right)\left(1+\frac{1}{2n}\right)^{-1} M_{[n,s]} S_n^s. \tag{2.45}$$

In summary, the three-dimensional coupled domain thin-shell formulation in several variables has been reduced to a two-dimensional governing equation (2.43) in one variable M and involving summation over the spectral components. We see by summation of spectral components while using (2.42) that M is approximately equal to the lower boundary value of the magnetic potential $\mathfrak{B}$ (i.e. $\mathfrak{B}(r=a)$). A small difference due to sphericity appears only for the lowest degree (n) components. The inverse relationship can be described as

$$\mathfrak{B}(a \leq r) = \sum_{n,s} (1 + \frac{1}{2n})^{-1} M_{[n,s]} S_n^s \left(\frac{r}{a}\right)^{-(n+1)}. \tag{2.46}$$

One may then solve (2.43) for M. From the associated coefficients, the magnetic potential $\mathfrak{B}$ may be obtained using (2.46). Similarly, using (2.40) and (2.42) in (2.39), $\mathfrak{B}^{(-)}$ is

$$\mathfrak{B}^{(-)}(r \leq a - h_0) = \sum_{n,s} - \left(1 - \frac{h_0}{a}\right) \left(\frac{n+1}{n+\frac{1}{2}}\right) M_{[n,s]} S_n^s \left(\frac{r}{a-h_0}\right)^n. \tag{2.47}$$

The magnetic fields are obtained as the gradients of these fields. The radial derivative is easily applied to the spherical-harmonic expansion terms in (2.46, 2.47) to obtain

$$b_r(a \leq r) = \sum_{n,s} \left(-\frac{n+1}{a}\right) \left(1 + \frac{1}{2n}\right)^{-1} M_{[n,s]} S_n^s \left(\frac{r}{a}\right)^{-(n+2)}, \tag{2.48}$$

$$b_r(r \leq a - h_0) = \sum_{n,s} \left(\frac{n}{a}\right) \left(-\frac{n+1}{n+\frac{1}{2}}\right) M_{[n,s]} S_n^s \left(\frac{r}{a-h_0}\right)^{n-1}. \tag{2.49}$$

One may verify using these expressions that indeed $b_r(r = a - h_0) = b_r(r = a)$, as required by (2.23). The product of the first two factors in parenthesis in each of (2.48, 2.49) are in fact equivalent. The different forms here are helpful in showing a separated factor (the first in parenthesis) that is due to the derivative operation.

2.3.2 Non-dimensional form

Non-dimensionalization of the system of governing equations can be useful for several reasons: 1) The number of parameters in the equations may be consolidated into a smaller number of degenerate combinations; 2) The relative amplitudes of various terms in the equations may be easier to estimate; 3) The equations may gain greater stability in the numerical implementation of solutions. An extended goal here is to choose a non-dimensionalization approach that leaves the equations and notation nearly identical to that in the dimensional form such that translation between the two forms is simple or trivial. Although in this case the number of parameters is not formally reduced, one or more of the non-dimensionalized parameters may gain an amplitude of unity.

Let us introduce the following non-dimensional operators, parameters, and variables: $\tilde{\partial}_t = (1/|\omega_F|)\partial_t$, $\tilde{\mathcal{L}}_a = a\mathcal{L}_a$, $\tilde{\nabla}_H = a\nabla_H$, $\tilde{h}_0 = h_0/a$, $\tilde{c}_d = c_d/(a|\omega_F|)$, $\tilde{\mathfrak{B}} = \mathfrak{B}/(a|\mathcal{F}|/|\omega_F|)$, $\tilde{\mathfrak{B}}^{(-)} = \mathfrak{B}^{(-)}/(a|\mathcal{F}|/|\omega_F|)$, $\tilde{M} = M/(a|\mathcal{F}|/|\omega_F|)$, $\tilde{\mathcal{F}} = \mathcal{F}/|\mathcal{F}|$, (where $\mathcal{F} = -\partial_t \overline{F_r} - \nabla_H \cdot \overline{(F_r \mathbf{u}_H - u_r \mathbf{F}_H)}^*$), and $\tilde{\mathbf{u}}_H = \mathbf{u}_H/(a|\omega_F|)$. The scaling parameters used here include the arbitrary length scale a (for spherical geometry, we prescribe this to be the radius of the spherical shell), the radial component of the prescribed part of the magnetic field F_r, and the characteristic frequency ω_F. In frequency-domain applications ω_F may typically represent the frequency (a positive or negative value) of the forcing $\mathcal{F}$. In time-domain applications, ω_F may be taken to represent a chosen inverse time scale.

The thin-shell induction equation (2.43) can then be written as

$$\tilde{\partial}_t \tilde{\mathcal{L}}_a \left[\tilde{M}\right] + \tilde{\nabla}_H \cdot \left(\tilde{\mathcal{L}}_a \left[\tilde{M}\right] \overline{\tilde{\mathbf{u}}_H}^*\right) + \tilde{\nabla}_H \cdot \left(\tilde{c}_d \tilde{\nabla}_H \tilde{M}\right) = \mathcal{F}, \tag{2.50}$$

where

$$\tilde{\mathcal{L}}_a \left[\tilde{M}\right] = \sum_{n,s} - (n+1) \left(1 + \frac{1}{2n}\right)^{-1} \tilde{M}_{[n,s]} S_n^s \tag{2.51}$$

and the solution for the magnetic potential satisfying

$$\nabla^2 \tilde{\mathfrak{B}} = 0, \tag{2.52}$$

is related to $\tilde{M}$ by

$$\tilde{\mathfrak{B}}(a \leq r) = \sum_{n,s} (1 + \frac{1}{2n})^{-1} \tilde{M}_{[n,s]} S_n^s \left(\frac{r}{a}\right)^{-(n+1)}. \tag{2.53}$$

2.3.3 Scaling estimates and further approximations

Consider now the relative scaling amplitudes of terms in (2.50). To satisfy (2.52), the spatial scales for the radial and horizontal variations of $\tilde{\mathfrak{B}}$ must be similar (a monopole solution is excluded here). Let us write this symbolically as $|\tilde{\partial}_r| \sim |\tilde{\nabla}_H|$, where these gradient components inside the modulus bars represents the appropriate wavenumber or inverse spatial scale components. The largest spatial scales are limited by a and, to retain consistency with the thin-shell assumption, the smallest scales are limited by h_0. Therefore, both $1 \lesssim |\tilde{\nabla}_H| \leq 1/\tilde{h}_0$ and $1 \lesssim |\tilde{\partial}_r| \leq 1/\tilde{h}_0$.

The scaling ratio of the second term to the first is $|\tilde{\mathbf{u}}_H|/(|\tilde{\partial}_t|/|\tilde{\nabla}_H|)$. In applications involving fluid wave phenomena, the ratio $|\tilde{\partial}_t|/|\tilde{\nabla}_H|$ can be associated with the phase propagation which is typically much larger than the flow speed for large-scale linear wave phenomena. In this case, the second term in (2.50) may be neglected relative to the first. An additional situation where the second term may be neglected involves the typical case where it is expected that $|b_r| << |F_r|$. If this allows one to assume $|\nabla_H \cdot (b_r \mathbf{u}_H)| << |\nabla_H \cdot (F_r \mathbf{u}_H)|$, then the second term is negligible relative to $\tilde{\mathcal{F}}$. Some care must be taken, however, in validating this assumption as it should be noted that while F_r is prescribed, $\mathcal{L}_a M = \partial_r \mathfrak{B}|_{r=a} = b_r$ is a solution variable.

When the additional approximations described in this subsection are suitable, the thin-shell induction system gains the simplified form

$$\tilde{\partial}_t \tilde{\mathcal{L}}_a \left[\tilde{M}\right] + \tilde{\nabla}_H \cdot \left(\tilde{c}_d \tilde{\nabla}_H \tilde{M}\right) = \tilde{\mathcal{F}}, \tag{2.54}$$

The two terms remaining on the left side of (2.54) can, in their order of appearance, be associated with self induction and magnetic diffusion, respectively. The relative importance of magnetic diffusion to self induction is then of fundamental importance and is given by the ratio $\tilde{c}_d |\tilde{\nabla}_H||\tilde{\nabla}_H|/(|\tilde{\partial}_t||\tilde{\partial}_r|) \approx \tilde{c}_d/(|\tilde{\partial}_t|/|\tilde{\nabla}_H|)$. Again, for wave phenomena the ratio $|\tilde{\partial}_t|/|\tilde{\nabla}_H|$ may be associated with the non-dimensionalized phase velocity of the wave. In this case, we see that the importance of magnetic diffusion depends on the ratio of $\tilde{c}_d$ to this phase speed. Because the same parameters are used to non-dimensionalize both of these speeds, the significance of this ratio is the same when dimensional speeds are used.

We may regard c_d as the speed of diffusive adjustment of the magnetic field. Recalling the definition $\tilde{c}_d = c_d/(a|\omega_F|)$, and noting that $1/a$ is at the small-end limit of the wavenumber (or inverse spatial scale) that can fit on the globe, we can interpret the meaning of the non-dimensionalized $\tilde{c}_d$. The factor $(a|\omega_F|)$ is an estimate of the maximum phase speed expected and so cases where $\tilde{c}_d \gtrsim 1$ are cases where magnetic diffusion generally dominates over self induction and quasi-static approximations apply. Conversely, $\tilde{c}_d << 1$ does not, however, immediately imply that self-induction dominates magnetic diffusion. Such a determination is application dependent and can be determined from the ratio of speeds using the minimum phase speed expected.

2.3.4 Formulations for re-expressing the motional-induction source

On the right side of the thin-shell induction equation (2.43), one may consider the terms $-\partial_t \overline{F_r} - \nabla_H \cdot \overline{(F_r \mathbf{u}_H - u_r \mathbf{F}_H)}^*$ as "sources" for electric current in the thin shell. We refer to the first term as an induction source and the second as a motional-induction source. Here we impose constraints from geophysical fluid dynamics for the purpose of re-expressing the motional induction term. Re-expressing the motional induction term can be useful for implicitly including dynamical flow constraints. Of course it is already expected that the

prescribed flow is indeed dynamically consistent and that appropriate care is taken in any analytical and numerical approximations to preserve this consistency. But rewriting the term can provide intuition on the relationships between electromagnetic and fluid variables. Alternate expressions can also be useful in replacing the flow vector with other variables that are more directly measurable.

The thin-shell approximations expect $|u_r| << |\mathbf{u}_H|$ but this cannot be used to immediately disregard the term involving u_r in the motional-induction source because the relative amplitudes of the radial and horizontal components of $\mathbf{F}$ have not been specified. For global problems, one expects these amplitudes may be comparable and so one expects that the term involving u_r can typically be disregarded. Indeed, outside of flow restricted to the magnetic equator, it is difficult to imagine cases where this term must be retained. While this term is included in the formulation for completeness, in this study we shall not consider such cases nor an evaluation of this term.

The motional-induction term on the right side of the thin-shell induction equation is then just $-\nabla_H \cdot \overline{(F_r \mathbf{u}_H)}^*$. We note that a term $\nabla_H \cdot \overline{(b_r \mathbf{u}_H)}^*$ appears on the left side of the thin-shell induction equation (2.25), as b_r is a dynamical variable. For the purposes of this section, we can provide a more comprehensive discussion by first re-combining (using $B_r = F_r + b_r$) these into the single term $-\nabla_H \cdot \overline{(B_r \mathbf{u}_H)}^*$. In this section we seek to remove the flow velocity from the induction equation by re-expression in terms of other dynamical variables.

While baroclinic flow can be very efficient at generating toroidal magnetic fields that stay inside of the ocean, barotropic flow is more efficient at generating the (poloidal) component of the magnetic field reaching outside of the ocean. The barotropic component of the flow can be understood here to be simply the depth average $\bar{\mathbf{u}}$. Focusing our consideration on barotropic flow and using (2.25), we then expect

$$\bar{\mathbf{u}}^* = \frac{\Sigma_{oc}}{\Sigma} \bar{\mathbf{u}}. \tag{2.55}$$

Where most of the shell conductance is due to the ocean layer ($\Sigma \approx \Sigma_{oc}$), we see that $\bar{\mathbf{u}}^*$ reduces to the simple depth-averaged velocity $\bar{\mathbf{u}}$. We may also expect that $B_r = F_r + b_r$ is approximately uniform with depth. The uniformity of b_r with depth is required to meet the assumption made in the formulation that the shell is electrically thin. The uniformity of F_r with depth in the shell is not required in the formulation but it is expected to be typically valid due to the assumption that the shell is geometrically thin. We have then for barotropic flow

$$\overline{(B_r \mathbf{u}_H)}^* \approx B_r \overline{\mathbf{u}_H}^* = B_r \frac{\Sigma_{oc}}{\Sigma} \bar{\mathbf{u}}_H. \tag{2.56}$$

Now let us consider constraints derived from the dynamical equations for the barotropic fluid dynamics. The two governing equations are derived from the principles of conservation of mass and momentum but the forms typically expressed incorporate varying approximations. Mass conservation is usually expressed as the continuity equation

$$\partial_t \eta + \nabla \cdot (h \bar{\mathbf{u}}_H) = 0, \tag{2.57}$$

where η represents the surface displacement of the ocean. Momentum conservation can be represented by the linearized momentum equation

$$\left[\partial_t + \alpha + f \hat{\mathbf{r}} \times\right] \bar{\mathbf{u}}_H = -g \nabla_H \left(\eta - \eta_F\right) + \frac{\boldsymbol{\tau}}{\bar{\rho} h}, \tag{2.58}$$

where the acceleration terms on the left include the Coriolis parameter $f = 2\Omega \cos\theta$ (Ω is the rotation rate and θ is colatitude) and α represents either a Rayleigh drag coefficient or, more generally, an operator describing dissipation/drag. On the right, g is the surface gravity acceleration and $\bar{\rho}$ is the depth-averaged fluid density. The term $-g\nabla\left(\eta - \eta_F\right)$ represents pressure-gradient forces due to the instantaneous departure of the surface η from the equilibrium surface η_F. If the equilibrium surface is steady, then one usually defines η such that $\eta_F = 0$. The equilibrium surface corresponds with a surface of constant gravitational potential which, however, varies in time when tidal forces are considered. In the latter case, η_F is the equilibrium tidal displacement, corresponding to

the surface the ocean would adopt if the ocean could instantaneously dynamically adjust to the changing tidal force. The vector $\boldsymbol{\tau}$ is a force vector due to prescribed sources. We regard the dynamical variables in (2.58) as $\mathbf{u}_H$, η, while other parameters are considered to be prescribed.

We will give two re-expressions for the motional-induction source term—the first incorporating conservation of mass, and the second incorporating conservation of momentum. Using (2.56) and (2.57), we may write

$$-\nabla_H \cdot \overline{(B_r \mathbf{u}_H)}^* = \frac{B_r}{h}\frac{\Sigma_{oc}}{\Sigma}\partial_t \eta - h\bar{\mathbf{u}}_H \cdot \nabla_H \left(\frac{B_r}{h}\frac{\Sigma_{oc}}{\Sigma}\right). \tag{2.59}$$

We see that this expression involves both the surface displacement η and the flow velocity $\bar{\mathbf{u}}_H$. In applications where the gradients of $\frac{B_r}{h}\frac{\Sigma_{oc}}{\Sigma}$ can be ignored, the term involving $\bar{\mathbf{u}}_H$ vanishes. Even where both terms remain, this re-expression can be useful because $\bar{\mathbf{u}}_H$ no longer appears in the divergence operation and the motional-induction source may then be less susceptible to interpolation errors.

In the second example we incorporate (2.58). We expect that for a wide range of applications and assumptions, the operator

$$\mathcal{L}_u = \partial_t + \alpha + f\hat{\mathbf{r}}\times \tag{2.60}$$

can be inverted such that one can solve (2.58) for $\mathbf{u}_H$ to obtain

$$\bar{\mathbf{u}}_H = \mathcal{L}_u^{-1}\left[-g\nabla_H(\eta - \eta_F) + \frac{\boldsymbol{\tau}}{\rho h}\right]. \tag{2.61}$$

In such cases, we can then combine (2.56, 2.61) to write

$$-\nabla_H \cdot \overline{(B_r \mathbf{u}_H)}^* = -\nabla_H \cdot \left(B_r \frac{\Sigma_{oc}}{\Sigma}\mathcal{L}_u^{-1}\left[-g\nabla_H(\eta - \eta_F) + \frac{\boldsymbol{\tau}}{\rho h}\right]\right) \tag{2.62}$$

An important specific example where $\mathcal{L}_u$ can be easily inverted is where the time dependence is repre sented parametrically such that the operator ∂_t can be regarded simply as a symbol representing a coefficient, and α is independent of time. In this case, we can discover $\mathcal{L}_u^{-1}$ by performing the operation $[\partial_t + \alpha - f\hat{\mathbf{r}}\times]$ on (2.58) and rearranging to obtain

$$\mathcal{L}_u^{-1} = \gamma\left(\frac{\partial_t + \alpha}{2\Omega} - \frac{f}{2\Omega}\hat{\mathbf{r}}\times\right), \tag{2.63}$$

where

$$\gamma = \frac{2\Omega}{(\partial_t + \alpha)^2 + f^2}. \tag{2.64}$$

The operator $\mathcal{L}_u$ may also be easily inverted in applications where the frequencies (or inverse time scales) considered are much smaller in amplitude than f. In global applications, $|f/(2\Omega)| \leq 1$ and we may write this criterion as $|\partial_t/(2\Omega)| << 1$. In this case, $\mathcal{L}_u \approx \alpha + f\hat{\mathbf{r}}\times$ is easily inverted to obtain $\mathcal{L}_u^{-1} = \gamma\left(\frac{\alpha}{2\Omega} - \frac{f}{2\Omega}\hat{\mathbf{r}}\times\right)$. An alternative argument leading to the same approximations is the assumption $|\partial_t| << |\alpha|$. Note that when this condition applies, and additionally $\alpha = 0$, the flow is geostrophic (see Section 2.3.5).

In this subsection, we have shown that the motional-induction source term, usually involving the flow velocity vector $\mathbf{u}_H$, can be re-expressed in terms of the surface displacement η and forces on the ocean. The surface displacement is a scalar rather than a vector, and it may also be measured remotely. The forces on the ocean may include wind stress and atmospheric pressure that are also measured. By contrast, the barotropic flow velocity is less observable directly and so this replacement with observables can provide benefit.

2.3.5 Geostrophic flow in dipole magnetic field

On time scales much larger than the rotation period, geophysical flows are often geostrophically balanced, at least to the first order of approximation. In the case of the flow described in the last section, $\mathcal{L}_u^{-1}$ (from (2.63) is then $\mathcal{L}_u^{-1} \approx -\frac{1}{f}\hat{\mathbf{r}}\times$ and

$$\bar{\mathbf{u}}_H = -\frac{g}{f}\nabla_H \eta \times \hat{\mathbf{r}}, \tag{2.65}$$

while in the more general case of geostrophic flow in response to an arbitrary pressure field P,

$$\bar{\mathbf{u}}_H = -\frac{1}{\rho f}\nabla_H P \times \hat{\mathbf{r}}, \tag{2.66}$$

where ρ is the fluid density.

An interesting feature of geostrophic flow is that the motional induction source term is then

$$-\nabla_H \cdot \overline{(B_r \mathbf{u}_H)}^* = \nabla_H \cdot \left(B_r \frac{\Sigma_{oc}}{\Sigma} \frac{1}{\rho f} \nabla_H P \times \hat{\mathbf{r}} \right) = \nabla_H \left(\frac{\Sigma_{oc}}{\Sigma} \frac{B_r}{\rho f} \right) \cdot \left(\nabla_H P \times \hat{\mathbf{r}} \right). \tag{2.67}$$

Where, as a first approximation, $\Sigma_{oc}/(\Sigma\rho)$ may be treated as uniform, we see that magnetic field generation requires then that B_r/f be non uniform; magnetic fields are motional induced by flow across the contours of B_r/f . Note, however, that when B_r is an axis aligned dipole, this ratio is uniform over the globe. Geostrophic flow does not interact with the axis dipole component of the main magnetic field to generate electric currents and associated magnetic fields. This provides an important example where the first-order source term to the induction equation cancels by symmetry. One must then take precautions with interpolating parameters so that interpolation errors do not corrupt the second-order source term remaining.

2.4 Coupling thin shell with exterior conducting regions (e.g. mantle)

If conducting regions other than the thin shell are included, an appropriate induction equation for these regions (or prescribed values on the boundaries) is required. Electric currents in these conductors may be excited by their own motional-induction sources or they may be excited by induction sources external to the conductor. Of special interest is the case where the induction source is due to electric currents in the thin shell considered and is therefore a solution variable rather than prescribed parameter. Let us explicitly write $\partial_t F_r = \partial_t F_r^{(p)} + \partial_t F_r^{(d)}$ to distinguish these prescribed ('p') and solution-dependent dynamic ('d') components.

2.4.1 Concentric conducting shells

An example that is immediate, because the governing equations and boundary conditions are similar to those already described, is the inclusion of another thin conducting layer that is concentric with the first (i.e. both shells have uniform radii within the same coordinate system). For that matter, one may consider any number N of additional shells. The equation for each of the thin shells gains contributions to $\partial_t F_r$ describing the radial derivative of all the other magnetic potentials generated by the other layers. We may write this as follows. In order of increasing radius, let layer i, be located between shells $1...i-1$ and $i+1...N$. The thin shell equation for layer i then gains the coupling term

$$\partial_t F^{(d)}_{r,(i)} = \sum_{1}^{i-1} \partial_t \partial_r \mathfrak{B}_{(i)} + \sum_{i+1}^{N} \partial_t \partial_r \mathfrak{B}^{(-)}_{(i)}. \tag{2.68}$$

The total magnetic field (or magnetic potential) at any point is of course due to the sum over the N components.

2.4.2 Perfectly conducting layer

A second simple example is the assumption of a perfectly conducting layer at uniform radius. In this case one may assume that the radial component of the total magnetic field vanishes at the interface with the perfect conductor.

Consider the case where the highly conducting lower mantle is represented as a perfect conductor. The top surface of the perfect conductor is located at radius r_m concentrically below the thin shell. The condition at the

interface requires that we find $F_r^{(d)}$ such that $F_r^{(d)}(r = r_m) = -b_r(r = r_m)$, where $b_r(r < a - h_0)$ is given by (2.49). The solution is

$$F_r^{(d)}(r_m \leq r) = \sum_{n,s} \left\{ \frac{n}{a} \left(\frac{n+1}{n+\frac{1}{2}} \right) M_{[n,s]} S_n^s \left(\frac{r_m}{a - h_0} \right)^{n-1} \right\} \left(\frac{r_m}{r} \right)^{n+2}, \tag{2.69}$$

where the term in curly brackets represents the coefficients for -$b_r(r = r_m)$ and the factor $\left(\frac{r_m}{r}\right)^{n+2}$ gives the geometric attenuation with radius away from the internal source. Depth-averaging (2.52) over the shell thickness h_0 and noting $b_r(r = a - h_0) = b_r(r = a)$ we have

$$\overline{F_r^{(d)}} = \sum_{n,s} \left\{ \frac{n}{a} \left(\frac{n+1}{n+\frac{1}{2}} \right) M_{[n,s]} S_n^s \right\} \left(\frac{r_m}{a} \right)^{2n+1} \left\{ \left(1 - \frac{h_0}{a} \right)^{-(n-1)} \left(\left(1 - \frac{h_0}{a} \right)^{-(n-1)} - 1 \right) \right\}, \tag{2.70}$$

which, within the thin shell assumption $a/n >> h_0$, can be written as

$$\overline{F_r^{(d)}} = \mathcal{L}_{pcl}\,[M] = \sum_{n,s} \left\{ \left(\frac{n+1}{a} \right) (1 + \frac{1}{2n})^{-1} M_{[n,s]} S_n^s \right\} \left(\frac{r_m}{a} \right)^{2n+1}, \tag{2.71}$$

where the term in curly brackets is, by (2.48), equal to $-b_r(r = a)$ and we have defined the operator $\mathcal{L}_{pcl}$ for the perfectly conducting lower ('pcl') layer.

Similarly, an operator describing the field $\overline{F_r^{(d)}}$ reflected off a perfectly conducting upper ('pcu') layer located at $r = r_e$ is

$$\overline{F_r^{(d)}} = \mathcal{L}_{pcu}\,[M] = \sum_{n,s} \left\{ \left(\frac{n+1}{a} \right) (1 + \frac{1}{2n})^{-1} M_{[n,s]} S_n^s \right\} \left(\frac{r_e}{a} \right)^{2n+1}. \tag{2.72}$$

2.4.3 Radially symmetric conductor

More generally, one expects that an appropriate induction equation is required to represent the additional conducting region. The most versatile form is (2.1) but this retains the complication of the coupled vector form that the thin-shell formulation is designed to simplify. As described in earlier sections, simplification of the induction equation requires a symmetry in the spatial distribution of the electrical parameters and/or the expected electromagnetic fields. A useful simplification for representing the conductivity of the mantle, for example, is to assume that it varies only radially. (In some models, the largely radial dependence of pressure may also justify an expected radial dependence for conductivity.) In this case, the induction equation (2.1) simplifies to the following:

$$\partial_t \mathbf{B} - K\nabla^2 \mathbf{B} + \partial_r K \hat{\mathbf{r}} \times \nabla \times \mathbf{B} = \nabla \times (\mathbf{u} \times \mathbf{B}) \tag{2.73}$$

Applied to the presumed-stationary mantle ($\mathbf{u} = 0$), and observing (2.4) with vector identities one can extract an equation for the uncoupled radial component

$$\partial_t B_r - K\nabla^2 B_r = 0. \tag{2.74}$$

To provide more generality with little more computational burden, we may assume instead

$$\partial_t B_r - K\nabla^2 B_r = \mathcal{G}, \tag{2.75}$$

where $\mathcal{G} = \hat{\mathbf{r}} \cdot \nabla \times (\mathbf{u} \times \mathbf{F})$ represents a prescribed component. Note that even in the typical case where $\mathcal{G} = 0$, (2.75) may be set up as either a homogenous equation driven by inhomogeneous boundary conditions or an inhomogeneous equation with homogenous boundary conditions. The latter arrives if one breaks B_r into components ($B_r = F_r^{(p)} + F_r^{(d)} + b_r$) and observes that $F_r^{(p)}$ and b_r independently satisfy Laplace's equation within this domain because their source electric currents are, by definition, elsewhere than in the shell. In this case, one has as an alternative to solve the inhomogeneous equation

$$\partial_t F_r^{(d)} - K\nabla^2 F_r^{(d)} = -\partial_t b_r \tag{2.76}$$

with simpler boundary conditions.

Because the insulating layer between the thin shell and the conducting region considered here (e.g. a conducting mantle below the thin shell) can be taken to be arbitrarily small, we may assume it vanishes and apply the continuity conditions for the radial magnetic field directly between the conducting mantle and the thin shell. Although the insulating region is then absent, the assumption that the thin shell is galvanically isolated is, however, retained. Note that this formulation permits the conductivity to approach zero and so there are no restrictions imposed on the extent of insulating regions. Indeed, this formulation is more general than the approaches in Section 2.4.2 that assume insulators with perfectly conducting boundaries.

One has then to solve (2.75) assuming $K = K(r) = (\mu_0\sigma(r))^{-1}$. At the interfaces of this conductor with other regions, continuity of B_r is required. Continuity of B_H together with (2.44) require also that $\partial_r B_r$ is continuous across the interface. We have further the requirement of bounded solutions.

Applying a separation of variables and spherical-harmonic expansion,

$$\mathcal{G} = \sum_{n,s} Q_{[n]}(r)\mathcal{G}_{[n,s]}(t)S_n^s, \tag{2.77}$$

$$B_r = \sum_{n,s} R_{[n]}(r)B_{[n,s]}(t)S_n^s \tag{2.78}$$

and using these in (2.75) we find that for each degree n the following equation must be satisfied

$$R_{[n]}\partial_t B_{[n,s]} - K\frac{1}{r^2}\partial_r\left(r^2\partial_r R_{[n]}\right)B_{[n,s]} + K\frac{n(n+1)}{a^2}R_{[n]}B_{[n,s]} = Q_{[n]}\mathcal{G}_{[n,s]}. \tag{2.79}$$

Finally, let us describe more specifically the boundary conditions as they could be applied in the example of the underlying conductive mantle (with vanishing insulator between the two) where $\mathcal{G} = 0$ and all electric currents in the mantle are ultimately induced by the fields from the electric currents in the overlying thin shell. In this case, within the mantle $B_r = F_r^{(d)} + b_r$ (where $b_r = \partial_r\mathfrak{B}^{(-)}$). Because $F_r^{(d)}$and b_r are respectively due to sources below and above the interface $r = a - h_0$, we may write the following expansions for bounded solutions

$$F_r^{(d)}(a - h_0 \le r) = \sum_{n,s} F_{[n,s]}(t)\left(\frac{r}{a-h_0}\right)^{-(n+1)} S_n^s, \tag{2.80}$$

$$b_r(r \le a - h_0) = \sum_{n,s} b_{[n,s]}(t)\left(\frac{r}{a-h_0}\right)^{n} S_n^s. \tag{2.81}$$

Equating terms of each harmonic in $B_r = F_r^{(d)} + b_r$, we may write

$$R(r = a - h_0)B_{[n,s]} = F_{[n,s]} + b_{[n,s]}. \tag{2.82}$$

Continuity of $\partial_r B_r$ at $r = a - h_0$ requires

$$\partial_r B_r|_{r=a-h_0} = \partial_r F_r^{(d)}|_{r=a-h_0} + \partial_r b_r|_{r=a-h_0}. \tag{2.83}$$

Taking the radial derivatives in (2.80, 2.81) and combining with (2.82), we have the following boundary condition

$$\left(\partial_r R_{[n]}|_{r=a-h_0} + \frac{(n+1)}{a-h_0}R_{[n]}(r = a - h_0)\right)B_{[n,s]} = \frac{2n+1}{a-h_0}b_{[n,s]} \tag{2.84}$$

which must be solved together with (2.79) and a second condition (e.g. boundedness or vanishing values on the low-r end of the domain).

The solution in (2.78) involves only the product of $B_{[n,s]}$ and $R_{[n]}$and so one must specify an additional condition if these are to be described uniquely. In some applications (e.g. cases where the temporal dependence is represented parametrically), one may interpret the solution variable as this product and a unique description of $B_{[n,s]}$ and $R_{[n]}$ is not needed. In more general applications (e.g. one with explicit time dependence), a convenient condition to specify is

$$R_{[n]}(r = a - h_0) = 1 \tag{2.85}$$

as one can see by (2.82) that $B_{[n,s]}$ is then the value of B_r at $r = a - h_0$.

2.5 Summary of the coupled thin-shell formulation

As described above, the thin-shell induction equation is a boundary equation in two dimensions that must generally be solved simultaneously with appropriate equations in three dimensions for the behavior of fields and currents in the adjacent insulators and conductors. In the special case where these three-dimensional regions are either insulators or the conductivity is a function only of spherical radius, a spherical-harmonic expansion provides analytical solutions in the three-dimensional regions and the system in three dimensions reduces to solving a two-dimensional thin-shell induction equation with terms involving spherical-harmonic transformations.

Replacing a multivariate system in three dimensions by this reduced-dimension system involving one variable should show strong computational advantages. But note that in the derivations above the system of the thin-shell coupled with external conductors reduced to a closed two-dimensional equation only in the examples where $F_r^{(d)}$ could be related to M. At the risk of repetition, we shall attempt here to consolidate and summarize these formulations.

The thin-shell induction equation is

$$\partial_t \mathcal{L}_a[M] + \nabla_H \cdot \left(\mathcal{L}_a[M]\,\overline{\mathbf{u}_H}^*\right) + \nabla_H \cdot (c_d \nabla_H M) = -\partial_t \overline{F_r} - \nabla_H \cdot \overline{(F_r \mathbf{u}_H - u_r \mathbf{F}_H)}^*, \tag{2.86}$$

where the operator $\mathcal{L}_a$ is defined by (2.44). This equation involves the variable M (the difference in magnetic potential between the upper and lower surfaces (2.41)), the horizontal and radial components of the flow velocity $\mathbf{u}$ and associated averaging operators described by the overbar and star operations (2.24, 2.25), the lateral magnetic diffusion speed c_d (2.28), and a magnetic field component $\mathbf{F}$ due to electric currents elsewhere than within the thin shell. Because F_r may include dynamical components $F_r^{(d)}$ that ultimately depend on M, (2.86) must, in general, be solved together with the equations governing $F_r^{(d)}$. Solving these equations "together" means that they are solved either simultaneously or, alternatively, that they are solved sequentially in a convergent iterative approach. In the latter, a component $F_r^{(d)}$ contributing to F_r may be treated as a correction term that can be regarded as a prescribed term during an iteration in which (2.86) is solved.

The simultaneous solution approach includes numerical methods in which coefficient matrices for the coupled systems are inverted simultaneously. It also includes examples we have shown of analytical combination where the base solutions for $F_r^{(d)}$ are incorporated into the thin-shell equation which then becomes closed (i.e. uncoupled from other equations). These examples of analytical combination were possible in the case where $F_r^{(d)}$ is the magnetic field associated with response electric currents in external conductors, and assuming these external conductors have radial symmetry. These cases can here be summarized as being governed by the thin-shell equation

$$\partial_t \mathcal{L}[M] + \nabla_H \cdot \left(\mathcal{L}[M]\,\overline{\mathbf{u}_H}^*\right) + \nabla_H \cdot (c_d \nabla_H M) = -\partial_t \overline{F_r^{(p)}} - \nabla_H \cdot \overline{\left(F_r^{(p)} \mathbf{u}_H - u_r \mathbf{F}_H\right)}^*, \tag{2.87}$$

where $\mathcal{L} = \mathcal{L}_a + \mathcal{L}_d$, the operator $\mathcal{L}_d$ provides

$$\mathcal{L}_d[M] = \overline{F_r^{(d)}}, \tag{2.88}$$

and F_r on the right side has been replaced with $F_r^{(p)}$ to emphasize that it now strictly includes only a prescribed component that is independent of M. In the case of a perfectly conducting external layer (Section 2.4.2), $\mathcal{L}_d$ represents either $\mathcal{L}_{pcl}$ (as defined in (2.71)) or $\mathcal{L}_{pcu}$ (as defined in (2.72)). In the case of a conducting mantle with radial symmetry, see (2.4.3).

In nearly every application one would consider, it is consistent with the thin-shell assumptions to ignore the component involving u_r on the right of (2.87). It is retained to allow the somewhat contrived application where the only sources are flow, and the only flow is at the magnetic equator. Outside of that isolated application, the component involving u_r is ignored and we see the right side of (2.87) includes only prescribed terms. In typical cases for Earth where the magnetic field associated with electric currents in the shell is much weaker than the background (main) magnetic field (i.e. $|\mathbf{b}| << |\mathbf{F}^{(p)}|$), we may also ignore the second term on the left of (2.87). As will be seen below, the latter approximation can be useful in seeking analytical solutions, or numerical solutions following the fixed-point iterative method, but this approximation is not needed (nor necessarily helpful) in the primary solution method proposed below in which Krylov sub-space methods are used (the Krylov methods used to solve linear systems require only a procedure for calculating the matrix-vector product, and so simplifications that help construct the explicit coefficient matrix can lose relevance).

The remaining terms on the right of (2.87) include the induction source $-\partial_t \overline{F_r^{(p)}}$. Important examples include the fluctuating magnetic field due to external electric currents in the ionosphere and magnetosphere, or fluctuating magnetic fields due the magnetic field of a neighboring planetary body under rotation (e.g. the case of Jupiter's field projected onto the Galilean satellites.) In the approximations above, it is important to note that while $|b_r| << |F_r^{(p)}|$, it is not assumed that $|\partial_t b_r| << |\partial_t F_r^{(p)}|$. In the case of Earth, $F_r^{(p)}$ primarily represents the quasi-steady main field with source currents in the core, while $\partial_t F_r^{(p)}$ may be dominated by fluctuating sources in the ionosphere and magnetosphere.

Also included on the right of (2.87) is the motional induction source $-\nabla_H \cdot \overline{\left(F_r^{(p)} \mathbf{u}_H\right)}^*$ which is due to the interaction of the flow with the background main magnetic field $F_r^{(p)}$. As described in Section 2.3.4, the equations for the fluid dynamics can be used to remove the flow velocity from this term and re-express it in terms of the dynamical surface displacement of the fluid and/or the external forces on the flow such as the tidal potential, wind stress, and atmospheric surface pressure. These re-expressions can be useful for imposing implicit fluid-dynamical constraints, and for expressing the source in terms of other remotely observable quantities such as the surface displacement.

3 Analytical solutions

Here we describe fundamental analytical solutions of the thin-shell induction formulation under idealized conditions.

3.1 Eigenfunction analyses of thin-shell formulation (free-decay time scales)

Here we consider the homogeneous version of (2.87) with coupling representing a perfectly conducting layer at radius r_m below the thin shell. (This includes the case without the conducting layer as a limiting case.) Assuming $|F_r| >> |b_r|$, we also ignore the self-advection term (second term on left). In this case $\mathcal{L} = \mathcal{L}_a + \mathcal{L}_{pcl}$ (with $\mathcal{L}_a$ defined by (2.44) and $\mathcal{L}_{pcl}$ defined in (2.71)) and (2.87) becomes

$$\partial_t \left\{\mathcal{L}_a + \mathcal{L}_{pcl}\right\}[M] + \nabla_H \cdot (c_d \nabla_H M) = 0. \tag{3.1}$$

When, additionally, we assume that c_d is uniform, the eigenfunctions of (3.1) are simply the spherical-harmonic functions and we may investigate the nature of the associated eigenvalues. Associated with each spherical-harmonic degree n, we treat here the symbol $\partial_{t,[n]}$ as describing a real, negative valued inverse time scale

describing the exponential free decay of the electric currents in the shell and their associated electric and magnetic fields. Performing a spherical-harmonic expansion of (3.1), the algebraic equations for the eigenvalues are solved to give

$$\partial_{t,[n]} = -\left(\frac{1+\frac{1}{2n}}{1-\left(\frac{r_m}{a}\right)^{2n+1}}\right)\frac{nc_d}{a}. \tag{3.2}$$

The case of an isolated thin shell is obtained by letting $r_m \to 0$, in which case the inverse decay time scale is $\partial_{t,[n]} = -(1+\frac{1}{2n})\frac{nc_d}{a}$. For all but the very lowest degrees, $\partial_{t,[n]} \approx -\frac{nc_d}{a}$, which can be interpreted as follows. The length-scale/inverse wavenumber is given by a/n and so the decay time scale is simply set by the amount of time it takes for the lateral diffusive adjustment speed c_d to span this length scale. The parameter c_d, introduced in Cartesian-coordinate studies (Tyler, 2005) is then seen to extend to the spherical geometry with the same physical interpretation. The additional factor $(1+\frac{1}{2n})$ is a small adjustment due to sphericity.

We see in the denominator of the term in parenthesis in (3.2) that the effect of a perfectly conducting layer below the shell is to increase the amplitude of the inverse decay time scale (i.e. the amplitude of the decay time scale increases.) In the limiting case of a perfectly conducting layer immediately below the thin shell ($r_m \approx a$), $\partial_{t,[n]} \to -\infty$ and the decay time scale vanishes. In this limiting case, b_r generated by electric currents in the shell is immediately cancelled by $F_r^{(d)}$ due to electric currents in the perfectly conducting layer immediately below.

3.2 Response function analyses of thin-shell formulation

Consider now the inhomogeneous version of (2.87), again with the self advection term ignored and again assuming a lower perfectly conducting layer. We have

$$\partial_t \left\{\mathcal{L}_a + \mathcal{L}_{pcl}\right\}[M] + \nabla_H \cdot (c_d \nabla_H M) = \mathcal{F}, \tag{3.3}$$

where $\mathcal{F}$ represents here an arbitrary prescribed source with associated spherical-harmonic coefficients $\mathcal{F}_{[n,s]}$. With a prescription of the temporal dependence of $\mathcal{F}$ one may perform a spherical-harmonic expansion and temporally integrate (3.3) to obtain the solution for each $M_{[n,s]}$. Here we shall assume that ∂_t is a symbol representing the parametric temporal dependence. In this case, an algebraic (rather than differential) equation is presented for each degree n and one may immediately solve for $M_{[n,s]}$. We further apply (2.48) to present the solution in terms of $b_{r,[n,s]}$:

$$b_{r,[n,s]}(r=a) = \left(\frac{\left(\frac{a}{n}\partial_t\right)}{\left(\frac{a}{n}\partial_t\right)+(1+\frac{1}{2n})c_d}\right)\left(\frac{\left(\frac{a}{n}\partial_t\right)+(1+\frac{1}{2n})c_d}{\left(1-\left(\frac{r_m}{a}\right)^{2n+1}\right)\left(\frac{a}{n}\partial_t\right)+(1+\frac{1}{2n})c_d}\right)\left(\frac{\mathcal{F}_{[n,s]}}{\partial_t}\right). \tag{3.4}$$

The second factor in parenthesis on the right of (3.4) describes a factor due to the perflectly conducting layer. One sees that as the layer vanishes ($\frac{r_m}{a} \to 0$), this factor becomes unity. The first factor in parenthesis describes the response function in the absence of the perflectly conducting layer.

When taking the periodic dependence to be specifically sinusoidal (e.g. $\partial_t \to -i\omega$, where ω is the frequency and the real part of complex solution variables correspond to physical variables), we may write (3.4) as

$$b_{r,[n,s]}(r=a) = \left(\frac{c_p}{c_s}\right)\left(\frac{1}{1-\left(\frac{r_m}{a}\right)^{2n+1}\frac{c_p}{c_s}}\right)\left(\frac{\mathcal{F}_{[n,s]}}{\partial_{t,[n]}}\right) \tag{3.5}$$

where $c_p = i\frac{a}{n}\partial_t$ may be associated with a phase speed and $c_s = c_p + (1+\frac{1}{2n})ic_d$ is a complex scaling speed (identical to that defined in (Tyler, 2005) with the exception of the factor $(1+\frac{1}{2n})$ due to sphericity). Similarly, the first factor in parenthesis on the right of (3.4) is the response function identical to that in (Tyler, 2005).

The second factor in parenthesis on the right side of (3.5) is due to the reflecting layer. We see that this factor is generally a complex number with amplitude less than or equal to one. Hence, in periodic applications,

the reflecting layer decreases the amplitude of b_r and may also change the phase. In the absence of the reflecting layer (i.e. $r_m \to 0$), this term is unity and (3.5) shows that the response depends simply on the ratio c_p/c_s.

The term "response function" used above becomes most clear for the case of induction. When $\mathcal{F} = -\partial_t F_r^{(p)}$, representing an inductive external field, (3.5) becomes

$$\frac{b_{r,[n,s]}(r=a)}{F^{(p)}_{r,[n,s]}} = -\left(\frac{c_p}{c_s}\right)\left(\frac{1}{1-\left(\frac{r_m}{a}\right)^{2n+1}\frac{c_p}{c_s}}\right), \tag{3.6}$$

which shows that the fractional amplitude of the magnetic field associated with electric currents induced in the thin shell is fully described by the response factors on the right side of the equation. The total observed response will be the combination $b_r + F_r^{(d)}$. Using (2.71) with (3.6) we may write

$$\frac{b_{r,[n,s]}(r=a) + F^{(d)}_{r,[n,s]}(r=a)}{F^{(p)}_{r,[n,s]}} = -\left(\frac{c_p}{c_s}\right)\left(\frac{1-\left(\frac{r_m}{a}\right)^{2n+1}}{1-\left(\frac{r_m}{a}\right)^{2n+1}\frac{c_p}{c_s}}\right), \tag{3.7}$$

from which we see that when magnetic diffusion is relatively weak ($c_d << c_p$), and the reflecting layer is not present ($r_m \to 0$, and $F_r^{(d)} = 0$), $\frac{b_r(r=a)}{F_r^{(p)}} \approx -1$. In this case, the thin shell acts like a perfectly conducting layer. When magnetic diffusion dominates ($c_d >> c_p$) and the reflecting layer is not present, $\frac{b_r(r=a)}{F_r^{(p)}}$ is imaginary (therefore b_r is 90 degrees out of phase with $F_r^{(p)}$) and the amplitude is less than one.

When the reflecting layer is included, we must consider the second factor in parenthesis on the right in (3.7) as it is no longer necessarily unity as in the case where the layer vanishes ($r_m \to 0$). First note that because $\left(\frac{r_m}{a}\right)^{2n+1} \leq 1$, and because $\frac{c_p}{c_s}$ has a positive real comonent and amplitude $|\frac{c_p}{c_s}| \leq 1$, the second factor in parenthesis in (3.7) has an amplitude less than or equal to unity. In the limit of the layer being raised to the shell radius ($r_m \to a$), the right side of (3.7) vanishes and $b_r = -F_r^{(d)}$. This is true so long as c_s retains an imaginary component (i.e. a non-vanishing c_d). When $c_d << c_p$, $\frac{b_r(r=a)+F_r^{(d)}(r=a)}{F_r^{(p)}} \approx -1$, indicating that some combination of b_r and $F_r^{(d)}$ together cancel $F_r^{(p)}$.

When considering motional-induction sources, we may replace (3.6) with

$$\frac{\partial_t b_{r,[n,s]}(r=a)}{-\nabla_H \cdot \overline{\left(F_r^{(p)}\mathbf{u}_H - u_r \mathbf{F}_H\right)}^*} = \left(\frac{c_p}{c_s}\right)\left(\frac{1}{1-\left(\frac{r_m}{a}\right)^{2n+1}\frac{c_p}{c_s}}\right), \tag{3.8}$$

and (3.7) with

$$\frac{\partial_t b_{r,[n,s]}(r=a) + \partial_t F^{(d)}_{r,[n,s]}(r=a)}{-\nabla_H \cdot \overline{\left(F_r^{(p)}\mathbf{u}_H - u_r \mathbf{F}_H\right)}^*} = \left(\frac{c_p}{c_s}\right)\left(\frac{1-\left(\frac{r_m}{a}\right)^{2n+1}}{1-\left(\frac{r_m}{a}\right)^{2n+1}\frac{c_p}{c_s}}\right). \tag{3.9}$$

In this case, the response functions on the right side of the equations may be more appropriately understood as functions describing the efficiency at which the background field $F_r^{(p)}$ is advected by the flow and/or strengthened through bundling of field lines by flow convergence (or weakened by flow divergence).

3.3 Using dispersion relationships from fluid dynamics as constraints

In the last sections, a parameter c_p was introduced and termed a "phase speed" though it is initially just a combination of parameters having units of speed. This terminology follows (Tyler, 2005) and anticipates situations where the length and time scales of the flow phenomenon considered are not independently prescribed but rather are related through the dynamics. For various wave phenomena in geophysical fluid dynamics, there is a dispersion relationship, often described as $\omega = \omega(\kappa)$, where ω is the frequency and κ is the wavenumber. One may similarly write the phase speed $c_p = \omega/\kappa$ as $c_p = c_p(\kappa)$. When the space and time scales are those associated with a dynamical fluid process, the form (3.5) can be useful because constraints may be more easily applied to c_p than to the space and time scale parameters taken individually.

Interestingly, there are important examples where the wave propagation is not dispersive (i.e. c_p does not depend on κ) and the dispersion relationship is simply a statement that c_p is determined by environmental parameters. In the case of the class of shallow-water gravity waves (swell, tsunamis, and to an approximate degree tides are examples) we have $c_p = (gh)^{1/2}$, where g is the surface gravity acceleration and h is the water depth. Rossby waves in the long wavelength limit are another example of nondispersive waves with a phase speed set by environmental parameters. For dispersive wave classes, $c_p = c_p(\kappa)$ may be regarded in the spherical domain as $c_p = c_p(n)$. In all cases, we see that explicit reference to the frequency or time scale is removed from the first two factors in (3.5). This amounts to applying the constraint that the fluid process considered corresponds to the wave class of the dispersion relationship assumed.

3.4 Relationship between electrodynamics and fluid sources

There are cases where the magnetic field generated by motional induction shows simple or intuitive relationships with flow parameters and variables. A well known example is an extension of the frozen-flux theorem. If magnetic diffusion can be ignored, the thin-shell electrodynamics shows

$$\partial_t B_r - \nabla_H \cdot \left(B_r \bar{\mathbf{u}}^*_H \right) = 0 \tag{3.10}$$

and can be interpreted as the situation where B_r is conserved by the conductivity-weighted flow. Writing (3.10) as

$$\partial_t B_r = -\bar{\mathbf{u}}^* \cdot \nabla_H B_r - B_r \nabla_H \cdot \bar{\mathbf{u}}^*_H = 0 \tag{3.11}$$

we see more explicitly that B_r changes in time due to advection by the flow and by bundling of the field lines by divergences/convergences in the flow. The result is that in the thin-shell scenario, the induction and continuity equations can be combined to show that in the absence of magnetic diffusion B_r/h is approximately a constant (i.e. invariant in time) from a Lagrangian perspective following a fluid parcel.

A second example is provided where we also usefully impose as a constraint mass conservation, expressed here as the continuity equation

$$\partial_t \eta + \nabla \cdot (h \mathbf{u}_H) = 0, \tag{3.12}$$

where η is the surface displacement. In cases where we may assume

$$\mathcal{F} = -\nabla_H \cdot \left(F_r \mathbf{u}^*_H \right) = -\nabla_H \cdot \left(F_r \frac{(\Sigma_{oc}/h)}{\Sigma} h \mathbf{u}_H \right) \approx -F_r \frac{(\Sigma_{oc}/h)}{\Sigma} \nabla_H \cdot (h \mathbf{u}_H) \,,$$

we can use the continuity equation to write (3.5) as

$$\frac{b_r(r=a)}{F_r(r=a)} = \left(\frac{c_p}{c_s} \right) \left(\frac{1}{1 + \frac{n+1}{n} \frac{c_p}{c_s} \left(\frac{r_m}{a} \right)^{2n+1}} \right) \frac{\Sigma_{oc}}{\Sigma} \left(\frac{\eta}{h} \right) \tag{3.13}$$

Ignoring sediment conductance and the reflecting layer, this is more simply

$$\frac{b_r(r=a)}{F_r(r=a)} = \left(\frac{c_p}{c_s} \right) \frac{\eta}{h}, \tag{3.14}$$

from which we see that the fractional amplitude of the magnetic field is proportional to the fractional amplitude of the sea-surface displacement, as in (Tyler, 2005). The complex proportionality constant is given by the important ratio of speeds c_p/c_s.

3.5 Estimates of missing galvanic currents

As described in previous sections, the thin-shell induction equation does not include galvanic contact with neighboring regions. While an insulating lower atmosphere may strongly justify the lack of galvanic contact between a conducting surface shell and conducting upper atmosphere, the galvanic insulation between a surface shell and the mantle may be more questionable. Here we attempt to estimate the effect of the missing galvanic currents.

To start, we expect that for otherwise similar surface sources, galvanic penetration is strongest for a steady (rather than oscillating) source because sufficient time has been allowed for the electric currents to penetrate more deeply and use a greater volume of the mantle, thereby providing less resistance to the currents. We expect then that estimates based on the simple quasi-static electropotential formulation described in Appendix F can provide conservative estimates of the length scales/degree at which the galvanic currents become important. For this application we may rewrite the thin-shell electropotential equation (F.5) as

$$\Sigma \nabla_H^2 \phi + j_r(r = a - h_0) = \mathcal{F} \tag{3.15}$$

where Σ is assumed uniform, $j_r(r = a) = 0$ because galvanic contact with the poorly conducting domain above the shell is ignored, and $\mathcal{F}$ represents an abitrary source. The term $j_r(r = a - h_0) = 0$, representing electric currents passing between the thin shell and conductive mantle, couples (3.15) with (F.6) such that these equations must be solved simultaneously. More explicitly, the coupling occurs as $j_r(r = a - h_0) = -\sigma_m(r = a - h_0)\partial_r \phi_m|_{r=a-h_0}$ is required for continuity of electric current crossing the interface. For the purposes here, we may consider two alternative descriptions for the mantle conductivity that allow us to analytically combine the equations to provide the desired estimates.

First, note that for uniform mantle conductivity σ_m, (F.6) reduces to $\nabla^2 \phi_m = 0$ which must be solved together with the continuity condition $\phi_m(r = a - h_0) = \phi$, and boundedness as $r \to 0$. Through spherical-harmonic expansion, an immediate solution for the mantle domain that satisfies these equations and conditions is then

$$\phi_m = \sum_{n,s} \phi_{[n,s]} \left(\frac{r}{a - h_0} \right)^n S_n^s, \tag{3.16}$$

where $\phi_{[n,s]}$ is a spherical harmonic coefficient of ϕ, the potential in the thin shell. We then perform a similar expansion of (3.15), while substituting using (3.16) and including standard results for the derivatives of spherical harmonics (evaluated at $r = a - h_0$), to obtain the analytical solution

$$\phi = \sum_{n,s} \phi_{[n,s]} S_n^s = -\sum_{n,s} \left(\frac{n(n+1)}{(a - h_0)^2} \Sigma + \frac{n}{a - h_0} \sigma_m \right)^{-1} \mathcal{F}_{[n,s]}. \tag{3.17}$$

From this solution we see that for each spherical-harmonic component, the effect of the conducting mantle is to reduce the potential by a factor $\left(1 + \frac{a-h_0}{n+1} \frac{\sigma_m}{\Sigma}\right)^{-1}$. Evidently, when $\frac{a-h_0}{n+1} \frac{\sigma_m}{\Sigma}$ is small this factor approaches unity, indicating that galvanic contact with the mantle is unimportant.

4 Numerical solution method

In the following subsections below, we first describe the requirements and important considerations for designing a numerical solution method for the thin-shell induction equation. This primarily involves choices for discretization and representation that set up a linear system of equations to be solved. We then describe two methods for solving the system of linear equations. The first, fixed-point iteration, has predictable convergence properties. Perhaps more importantly, the derivation of this method provides important suggestions for designing a preconditioner for use in much faster Krylov-subspace solution methods. While Krylov methods such as *bicgstab* and *gmres* can produce much faster convergence rates (compared to convergence rates in the fixed-point method), for most thin-shell applications one will find that the Krylov methods do not converge unless a very good preconditioner is applied. Success in the Krylov-space approach is then contingent on finding an appropriate preconditioner.

4.1 Initial considerations

In this section we describe an efficient and accurate numerical approach for solving (2.87). The choice in approach follows from a number of considerations. First, we expect that we cannot make any advance assumptions on the relative importance of self induction and magnetic diffusion. Hence, we cannot follow previous numerical approaches that essentially iterate from a solution obtained where one of these processes can be assumed to dominate. We assume that the electrical parameter c_d in the thin shell is inhogeneous with an extremely large range of values. We therefore shall not seek methods that iterate from a solution involving homogeneous c_d. We assume that the method must allow simultaneously for both global coverage and high spatial resolution. Because the driving sources can include ocean dynamical flow, we do not want the method to involve interpolation or other transforms in which important dynamically conserved properties are sacrificed in the process of bringing the flow-dependent terms into the numerical method. To provide support for extensions into inverse modeling, we want the method to be not just computational feasible but fast. Finally, we want the method to provide the potential for solving the equations to high accuracy.

Note that spherical-harmonic decomposition is probaby the best approach when considering the domains of the insulators or regions where K is radially symmetric. The reason is that fast spherical-harmonic numerical transforms are available, and solutions in these domains can be calculated analytically or through integration of an ordinary differential equation, thereby reducing the dimensionality of the problem.

There are, however, strong disadvantages of spherical-harmonic methods applied to the inhomogeneous thin shell. One can consider that while numerical methods using spherical-harmonic bases have been popular in atmospheric dynamics, they have not been common in oceanography. The reason is the non-local nature of the spherical-harmonic functions presents difficulties in representing regional subdomains, boundaries, and sharp transitions in parameters. Finite-difference/volume/element methods have been more popular in oceanography because the local discretization allows one to check or adjust the local representation of elements. One may wish, for example, to ensure that the total cross section of an ocean strait is correctly represented and this is possible with the locally discretized methods. With spherical harmonics, the representation is no longer local and harder to check or control. These checks and controls are also difficult when representing oceanographic dynamical flow components. Finite-difference models are most commonly used in ocean models. These methods commonly involve flux-conservation to preserve dynamical conservation principles and so they can be considered as finite-volume models.

The method we follow is a hybrid that combines the best elements of both approaches. We use finite-difference/volume discretization within the thin shell and spherical-harmonic methods in the other domains. Where the source terms are given from a numerical ocean model, the method anticipates the thin shell being discretized using the same native grid from the ocean model. In this way full dynamical consistency in the ocean dynamics is retained when represented in the electrodynamic model. Sacrificing this consistency can produce errors even at lowest order (though typically spreading only through a local stencil of grid points). As a quick example, note that the flow sources of the thin-shell induction equation can be expanded to include leading terms proportional to either $\nabla\cdot(h\mathbf{u}_H)$ or $\nabla\cdot(\mathbf{u}_H)$. There are, however, flow applications (e.g. steady flow, geostrophic flow) where either or both of these divergences vanish. If these divergences are calculated from interpolated ocean parameters they may primarily represent interpolation errors rather than dynamics.

The method we seek shall treat the temporal dependence only parametrically such that the symbol ∂_t, where it appears, can be treated as a uniform, potentially complex coefficient. Although this is not strictly limiting as more general cases with time dependence may be treated, for example, through summation of Fourier components, the details of such are not included in the scope of this paper.

4.2 Fixed-point iteration method

We see by (2.46) that for all but the lowest degrees n, $M_{[n,s]} \approx \mathfrak{B}_{[n,s]}$ and we may therefore expect as an approximation $M \approx \mathfrak{B}(r=a)$. Let us rewrite (4.1) as

$$\partial_t \partial_r \mathfrak{B}|_{r=a} + \nabla_H \cdot \left(\partial_r \mathfrak{B}|_{r=a} \overline{\mathbf{u}_H}^* \right) + \nabla_H \cdot \left(c_d \nabla_H \mathfrak{B}|_{r=a} \right) = \mathcal{F}^{(d)} + \mathcal{F}^{(p)}, \tag{4.1}$$

where the right side includes the prescribed terms

$$\mathcal{F}^{(p)} = -\partial_t \overline{F_r^{(p)}} - \nabla_H \cdot \overline{\left(F_r^{(p)} \mathbf{u}_H - u_r \mathbf{F}_H^{(p)} \right)}^* \tag{4.2}$$

as well as dynamic (solution-dependent) terms

$$\mathcal{F}^{(d)} = -\partial_t \overline{F_r^{(d)}} - \nabla_H \cdot \overline{\left(-u_r \left(\nabla_H \mathfrak{B}|_{r=a} + \mathbf{F}_H^{(d)} \right) \right)}^* + \mathcal{Q}, \tag{4.3}$$

where

$$\mathcal{Q} = \partial_t \left(\partial_r \mathfrak{B}|_{r=a} - \mathcal{L}_a M \right) + \nabla_H \cdot \left(\left(\partial_r \mathfrak{B}|_{r=a} - \mathcal{L}_a M \right) \overline{\mathbf{u}_H}^* \right) + \nabla_H \cdot \left(c_d \nabla_H \left(\mathfrak{B}|_{r=a} - M \right) \right) \tag{4.4}$$

is an expectedly small correction term due to the small inequality between M and $\mathfrak{B}(r=a)$. Following thin-shell approximations previously discussed and the expectation that $\mathbf{F}^{(d)}$ represents a presumably secondary field with smaller amplitude than the inducing primary, the first and second terms in (4.3) can be regarded as correction terms that are weak relative to terms retained on the left side of (4.1).

Now note that the term $\partial_r \mathfrak{B}|_{r=a}$ can be represented by the simple first-order, forward-step, finite-difference approximation

$$\partial_r \mathfrak{B}|_{r=a} = \frac{\mathfrak{B}\left(r = a + \Delta r\right) - \mathfrak{B}\left(r = a\right)}{\Delta r}, \tag{4.5}$$

although in what follows we shall use the second-order approximation

$$\partial_r \mathfrak{B}|_{r=a} = \frac{-\frac{1}{2}\mathfrak{B}\left(r = a + 2\Delta r\right) + 2\mathfrak{B}\left(r = a + \Delta r\right) - \frac{3}{2}\mathfrak{B}\left(r = a\right)}{\Delta r} \tag{4.6}$$

to retain consistency with the second-order approximation available for other terms. In these finite-difference approximations, one expects accuracy to increase with smaller choices of the radial step Δr. There are, of course, limits to this improved accuracy with smaller Δr. An immediate one is set by the thin-shell assumption. As Δr becomes comparable to the thickness of the thin shell, the limits of the thin-shell approximation are reached.

Let us define the operators

$$\mathcal{L}_1 \left[\cdot \right] = \nabla_H \cdot \left[c_d \nabla_H \left[\cdot \right] \right], \tag{4.7}$$

$$\mathcal{L}_2 \left[\cdot \right] = -\frac{1}{\Delta r} \left(\partial_t \left[\cdot \right] + \nabla_H \cdot \left[\left[\cdot \right] \overline{\mathbf{u}_H}^* \right] \right). \tag{4.8}$$

Applying (4.6–4.8) to (4.1), we write

$$\mathcal{L}_3 \left[\mathfrak{B}\left(r = a\right) \right] = \mathfrak{F}, \tag{4.9}$$

where

$$\mathcal{L}_3 = \mathcal{L}_1 + \frac{3}{2}\mathcal{L}_2 \tag{4.10}$$

and

$$\mathfrak{F} = \left\{ 2\mathcal{L}_2 \left[\mathfrak{B}\left(r = a + \Delta r\right) \right] - \frac{1}{2}\mathcal{L}_2 \left[\mathfrak{B}\left(r = a + 2\Delta r\right) \right] \right\} + \mathcal{F}^{(d)} + \mathcal{F}^{(p)}. \tag{4.11}$$

Observe that the left side of the equation (4.9) involves operation only on the boundary value ($\mathfrak{B}(r=a)$) of the variable. The right side gains a new component (in curly brackets) which, because of geometric attenuation

($|\mathfrak{B}(r=a)|$ is larger in amplitude than $|\mathfrak{B}(r>a)|$), is weaker than the term $\mathcal{L}_3\mathfrak{B}\,(r=a)$ retained on the left side.

Let us assume that for given $\mathfrak{F}$ there is an analytical or numerical procedure available to solve (4.9), obtaining a solution which we describe symbolically as $\mathfrak{B}\,(r=a)=\mathcal{L}_3^{-1}\mathfrak{F}$. We now consider the fixed-point iteration

$$\mathfrak{B}^{(k+1)}\,(r=a)=\mathcal{L}_3^{-1}\mathfrak{F}^k, \tag{4.12}$$

where $\mathfrak{B}^{(k+1)}$ is the solution at iteration $k+1$, and $\mathfrak{F}^{(k)}$ is evaluated from (4.11) assuming $\mathfrak{B}=\mathfrak{B}^{(k)}$. (The components in $\mathfrak{F}^{(k)}$ involving $\mathfrak{B}(r>a)$ as well as $\mathcal{F}^{(d)}$ can be calculated following spherical-harmonic expansion methods described in previous sections.) Independent of the specific analytical or numerical method chosen for solving (4.12), it is expected that the iterative scheme (4.12,) converges to the correct solution as k increases.

4.3 Krylov-space iteration method

The fixed-point iteration method has the advantage of a predictable convergence but other methods are available that may converge more quickly. Krylov sub-space solvers are highly efficient at solving large, sparse linear systems provided a suitable preconditioner can be designed. In solving the linear system $\mathbf{Ax}=\mathbf{b}$ for $\mathbf{x}$, where $\mathbf{A}$ is square matrix and $\mathbf{x}$, $\mathbf{b}$ are vectors, Krylov methods have an additional advantage in that one need not directly specify $\mathbf{A}$. Rather, one need only specify a procedure for producing the matrix-vector product $\mathbf{Ax}_g$, where $\mathbf{x}_g$ is presumably a trial solution vector during an iteration.

Specific Krylov-space methods that can be applied to the non-symmetric matrices expected include *gmres* and *bicgstab*. In a variety of applications to the realistic global Earth, we have found that use of either of these methods converges quickly when the method is first preconditioned using a matrix representing the discretized operator $\mathcal{L}_3$ (or approximated versions) described in (4.2). Contrarily, experiments with either a simplistic or no preconditioner assigned fail to converge.

Because in the Krylov method only a procedure for producing the matrix-vector product is required, one may solve (2.87) without moving solution-dependent correction terms over to the right side of the equation. The reason why this was done in the fixed-point method in the last section is partially due to the difficulty in building the coefficient matrix in this hybrid case involving both finite-difference and spherical-harmonic discretizations.

The procedure for building the matrix-vector product on the left side of (2.87) is as follows:

1. Select a grid for the two-dimensional global surface. It is advisable to adopt the native grid on which the ocean parameters are available. On the staggered Arakawa C grid in spherical coordinates, for example, define M on the cell center grid points and c_d on the cell face points.
2. Perform a spherical-harmonic expansion of M; apply the operator $\mathcal{L}$, and then perform an inverse transform (i.e. sum over the harmonic components) to bring $\mathcal{L}M$ back onto the grid.
3. Construct flux-conserving finite volumes around each grid point (as this is in two-dimensions, one can interpret the "volume" to include a unit radial height.)
4. Integrate (2.87) over each volume and apply Gauss' theorem to replace divergence operations with flux summation over the faces of the volume.
5. The volume integrated equations retain terms with $\hat{\mathbf{n}}\cdot\nabla M$ (where $\hat{\mathbf{n}}$ is the outward unit vector normal to the volume face) that must be evaluated at the volume faces. Evaluated as simple first-order differences between neighboring grid points, the diffusion operator is represented with second-order accuracy. The parameter c_d is needed only at the volume faces (not at the center of the volume) and should be taken from the ocean model, where possible, rather than through interpolation. (Typical ocean models involve staggered grids where, aside from the grid points for the centers of the volumes, there are also grids associated with the location of the faces. To obtain the ocean conductance at the faces (needed for c_d), one should not calculate the conductance at the center points and interpolate to the face points. Rather, one should interpolate only the depth-average conductivity and multiply this by the depths that are usually also provided at the face grid points in the ocean model.)

6. The calculation of a preconditioner matrix should follow steps consistent with those above (see also Section 4.2).

To build the forcing terms on the right side of (2.87), the procedure also follows some of the steps above. When motional (flow) sources are involved, special care should be taken with element (5.) to ensure that dynamical consistency is retained. We provide here a specific demonstration. In typical cases one may assume

$$-\nabla_H \cdot \overline{\left(F_r^{(p)}\mathbf{u}_H - u_r\mathbf{F}_H\right)}^* \approx -\nabla_H \cdot \left(F_r^{(p)}\bar{\mathbf{u}}_H^*\right).$$

In computing this from ocean model data, it is better to first rewrite this term as

$$-\nabla_H \cdot \left(F_r^{(p)}\bar{\mathbf{u}}_H^*\right) = -\nabla_H \cdot \left(c_d\frac{\mu_0}{2}F_r^{(p)}\mathbf{T}_\sigma\right), \tag{4.13}$$

where $\mathbf{T}_\sigma = \int_h \sigma\mathbf{u}_H dr$ is the conductivity transport (calculated in a manner that is dynamically consistent with other weighted transports in the ocean model). In evaluating this term in the steps above, one then specifies c_d at the volume faces precisely as done for the diffusion term. Similarly, one should rewrite and consider the second term in (2.87) as

$$\nabla_H \cdot \left(c_d\frac{\mu_0}{2}\mathcal{L}[M]\mathbf{T}_\sigma\right). \tag{4.14}$$

With these careful steps, one may then retain the full dynamical consistency with the fluid dynamics as calculated in the ocean model. Contrary examples where interpolation is applied unnecessarily or inconsistently can produce errors in the forcing terms even at lowest order of approximation. The reason these errors can reach the lowest order is ultimately due to the fact that in geophysical fluid dynamics there are many important examples where the horizontal flow and/or transport vectors are approximately non-divergent. This means that components of the forcing can happen to have lowest-order terms that vanish due to the dynamics. The next order terms in an approximation series then lead, and could even predominantly represent interpolation errors.

If the ocean model data is given on a grid that is of much higher resolution than what one wishes to retain in the grid for the electrodynamics, or for any other reason that the native ocean model grid cannot be adopted for the thin shell electrodynamic model, one should first complete the divergence calculations on the native grid and interpolate the whole forcing term rather than interpolating components within the divergence operator. To understand why this is important, consider that interpolation of the divergence of a vector can be far more accurate than the divergence of an interpolated vector. As a clear example, consider a divergence free vector field. If one calculates the divergence and then interpolates, one retains the vanishing divergence on the new grid. If, however, one interpolates the vector field to the new grid and then calculates the divergence, the result need not vanish and is highly sensitive to the interpolation scheme chosen.

Because this numerical approach is sparse and efficient, it should be easily feasible to adopt even the highest resolution global grids used in oceanography. Any reason for not using the native ocean grid will probably not come from poor computational performance on the native grid. Even if one does not need the high spatial resolution in the ocean model for the electrodynamics, it is advisable to nonetheless adopt the native grid. While the steps above assume that the ocean model uses a finite difference/volume approach, the instructions can be easily adapted to finite-element and other ocean-model approaches. Basically, the operators that must be discretized for the thin-shell electrodynamics are included within the selection of operators that must be formulated for the ocean dynamical models. So one should generally be able to retain dynamical consistency provided the numerical operators for the electrodynamics in the thin shell are composed in the same way as in the ocean model from which the ocean parameters and flow are taken.

Finally, some comments on the details of the step for the spherical-harmonic transform are needed. A number of methods are available to perform the transform. The one used by this author (based in Gaussian-Legendre quadrature and written in Matlab) is very fast and allows very high truncation degree. But it involves an interpolation step that should not be confused as vulnerable to the important concerns described above. The transform is fast but requires that the data to be transformed be provided on a grid representing the Gaussian-Legendre

nodes required for Gaussian quadrature integration over the sphere. Because this grid does not necessarily coincide with the native grid of the ocean model, interpolation is required. But note that this step involves only interpolation of the magnetic potential, and one is interpolating onto a grid with a resolution that can be adjusted by the selection of the spherical-harmonic truncation degree chosen. One may then limit the interpolation errors by increasing the truncation degree.

In selecting the truncation degree of the spherical harmonic expansion, the safest approach is to match or exceed the truncation degree that provides spatial resolution similar to the grid spacing used. The correspondence is not exact because it depends on the form of fields one wishes to represent, and because the longitudinal resolution of the grid is not uniform over the globe but rather increases poleward. One may, however, consider here a correspondence drawn from the highest wave numbers that can be represented in each. With the finite-difference/volume approach, the highest wave number that can be represented is $\kappa_{FD} = \frac{2\pi}{N_{FD}} \frac{1}{a\Delta\theta}$, where $\Delta\theta$ is the largest angular step (in radians) between adjacent grid points, and N_{FD} is the number of grid points one expects are needed to accurately resolve a wavelength. In the spherical-harmonic representation, one may draw from the form of the Laplacian of a degree-n harmonic, to propose the wave number $\left(\frac{n(n+1)}{a^2}\right)^{1/2}$. The highest wavenumber resolved is then $\kappa_{SH} = \left(\frac{N(N+1)}{a^2}\right)^{1/2}$, where N is the truncation degree. The truncation degree N needed to resolve (with N_{FD} grid points) the highest wavenumber representable on the grid (with angular spacing $\Delta\theta$) is then obtained by equating the two wavenumber formulae. We have

$$N = \frac{1}{2}\left(-1 \pm \left(1 + 4\left(\frac{2\pi}{N_{FD}\Delta\theta}\right)^2\right)^{1/2}\right), \tag{4.15}$$

which, assuming $N >> 1$, is approximately

$$N \approx \left(\frac{2\pi}{N_{FD}\Delta\theta}\right). \tag{4.16}$$

One should expect that $N_{FD} \geq 2$ even in the most poorly resolved cases, and accurate descriptions probably require $N_{FD} \geq 10$. One may safely assume then that by taking $N \geq \frac{\pi}{\Delta\theta}$ the spherical-harmonic representation has at least as good resolution as the grid.

4.4 Validation with analytical solutions

Here we compare solutions obtained using the numerical approach of Section 4.3 with analytical solutions derived in Section 3. Specifically, we use the *gmres* solver (Saad, 1995) restarted every 10 iterations and with a preconditioner described by the matrix inverted in the initial iteration of the fixed-point method, as described in Section 4.2. The discretization is coded in *Matlab* using sparse arrays, and elements are accessed through vectorized calls (rather than *for*-loops) such that memory use is efficient and the processing is implicitly parallel. The tolerance for satisfying the (preconditioned) system is set to 10^{-12}. The domain of the shell is represented on a 1/6-degree longitude by 1/6-degree latitude global grid. The domains outside of the shell are represented with a spherical-harmonic truncation degree of $N = 1200$ (exeeding the $N = 1080$ that would be required using (4.16) with $N_{GP} = 2$).

For the configuration, we consider uniform conductance of $\Sigma = 1.5 \times 10^4$ S over a sphere of radius $a = 6371$ km. The conducting shell is assumed to occupy a vanishgly thin layer of thickness h_0 (to remain consistent within the error of the horizontal spatial resolution chosen below, one should assume $h_0 \leq 10$ km). The uniform conductivity within the shell is then $\sigma = \Sigma/h_0$. We assume domains outside of the shell are insulators although we consider cases first without and then with a perfectly reflecting layer at a depth $r = a - 500$ km.

We evaluate the numerical solution for the radial component of the magnetic field at $r = a$ due to a simple prescribed source:

$$\mathbf{u} \times \mathbf{F} = \mathcal{R}\left\{ \frac{-a^2}{n(n+1)} \nabla_H \Psi_{[n,s]} \times \hat{\mathbf{r}} \right\} = \frac{-a^2}{n(n+1)} \nabla_H \left(P_n^s \cos(s\phi + \omega t) \right) \times \hat{\mathbf{r}}, \tag{4.17}$$

where the spherical harmonic $\Psi_{[n,s]} = P_n^s e^{i(s\phi+\omega t)}$, P_n^s is the schmidt-normalized associated legendre function of degree n, order s, ϕ is eastward longitude, and ω is the frequency of the M_2 principal lunar semi-diurnal tide having a period of 12.42 hours. This reflects a westardly propagating source at the M_2 period (which, for this conductance value, is ideal for testing as it is located between frozen-flux and diffusive regimes). Note that in this case the source in the thin-shell induction equation is simply $-\nabla_H \cdot \overline{\left(F_r^{(p)} \mathbf{u}_H - u_r \mathbf{F}_H \right)}^* = \nabla \cdot ([\mathbf{u} \times \mathbf{F}] \times \hat{\mathbf{r}}) = -\nabla \cdot (F_r \mathbf{u}) = \Psi_{[n,s]}$.

We evaluate the numerical solution by comparing it to the analytical expressions (3.8, 3.9). We expect

$$\frac{\partial_t b_{r,[n,s]}(r=a) + \partial_t F^{(d)}_{r,[n,s]}(r=a)}{\Psi_{[n,s]}} = \left(\frac{c_p}{c_s} \right) \left(\frac{1 - \left(\frac{r_m}{a}\right)^{2n+1}}{1 - \left(\frac{r_m}{a}\right)^{2n+1} \frac{c_p}{c_s}} \right), \tag{4.18}$$

where the left side is the time rate of change of the total radial magnetic field (divided by $\Psi_{[n,s]}$) and the right side describes the essential response function. The case with no reflecting mantle is included by letting $r_m/a \to 0$.

We first consider the case with no reflecting lower layer and $n = 5$, $s = 5$ (the matching of degree/order is a good choice because it places the anomaly near the equator where the model resolution is lowest). Plots of the numerical and analytical solution appear identical. The fractional misfit error (as represented by the root-mean-square of the differences divided by the root-mean-square of the analytical field itself) is 1.07×10^{-5}, which is well within the expected grid resolution error of 5.29×10^{-5} following (4.16). Recall that the latter error does not describe inaccuracy in model perfomance (because the grid resolution can be increased) but rather sets a benchmark for validation. Model errors within this value then indicate that the model is working correctly to within an accuracy that can be expected given the grid resolution.

A second case, identical to the first but with the reflecting layer included shows similarly small errors. The choice of $n = 5$ was made to provide comparable amplitudes in the magnetic fields from the shell and from the reflecting layer (that from the reflecting layer is about half that from the shell). The fractional misfit error in the total radial magnetic field is 1.45×10^{-5}, while that of the parts from the shell and reflecting layer separately are 2.42×10^{-5} and 9.77×10^{-6}, respectively. (The fractional error in the part due to just the shell can be larger than that of the total fractional error because the reflecting mantle reduces the total amplitudes.) Again, these errors are with the value of 5.29×10^{-5} following (4.16).

To test the performance of the model in the expected high-resolution limit, we repeat the cases above but with $n = 200$ and $s = 200$. With the grid resolution described, it is expected that the model should indeed be able to produce solutions to within the grid-resolution error described by (4.16). Indeed, for the case without a reflecting layer, we find a fractional error of 0.0284, which falls within the 0.0846 expected from (4.16). For the case with a reflecting layer, the errors are 0.0284, 0.0284, and 2.13×10^{-6} for the total, shell, and reflecting layer parts, respectively. Again, these errors are within the 0.0846 expected from (4.16).

5 Application to Earth

The formulations presented are relevant to a wide variety of applications involving electrodynamics near the surface of the Earth. The scope in this study does not include a survey of these applications or associated phenomena. Rather, examples are chosen only for the purposes of illustration and for evaluating some of the approximations made in the thin-shell formulation.

5.1 Basic electrical parameter values

The surface water and hydrology on Earth create a shell near the surface with relatively high electrical conductivity when compared to that of the lower atmosphere or upper mantle. The higher conductivity primarily comes from the disassociated ions (dissolved salts) arising from contact of water with rock. This contact may take place in the sediments below water bodies, from water running over land, and from water permeating the subsurface. The result is an expected near-spherical shell at the surface with relatively high conductivity.

The thin-shell formulation assumes that the shell is both geometrically and electrically thin, with the result that it is only the depth integral of conductivity (i.e. conductance, Σ) that is the fundamental electrical parameter describing this shell. The conductivity of seawater depends on temperature, salinity, and to a small degree pressure. A three-dimensional, globally gridded data set of ocean conductivity has recently been created from an exhaustive objective analyses of observations (Tyler et al., 2016). The associated ocean conductance is shown in Figure 1 (top panel). Also described in Tyler et al. (2016), the temporal/seasonal variability in the conductance is relatively small and so this data set is expected to provide an accurate description of the ocean conductance. The sediment conductance (shown in Figure 1, middle panel) estimates the water content from age-dependent porosity and the sediment thickness from seismology. The accuracy of the sediment conductance estimates is expected to be much less than that of the ocean conductance. Finally a rather negligible contribution to the conductance is allowed for by the conductivity within the igneous rock. These combine to give the total conductance of the surface shell shown in Figure 1 (bottom panel).

From the point of describing the electrodynamics in the shell, we found that the lateral adjustment speed for the magnetic diffusion $c_d = \frac{2}{\mu_o \Sigma}$ is what is relevant. This parameter is shown in Figure 2 (top panel). We see that over the open ocean c_d shows values of the order of hundreds of meters per second and the values quickly increase in shallow regions. This should immediately indicate that magnetic diffusion is relatively fast when considering most motionally-induced phenomena as phase speeds associated with the fluid dynamics are often much smaller. But an important exception is the class of long gravity waves (and potentially long Rossby waves). These "long" waves are more often referred to as "shallow-water" waves in terrestrial applications. But familiar examples are found for both deep-water (e.g. tsunami) and shallow-water (e.g. swell) regions. This class of waves simply involves wavelengths much larger than the ocean depth, and gravity as the primary restoring force. These waves are of fundamental importance in the dynamical adjustment of a wide variety of fluid-dynamical processes because they travel relatively fast. Exceptions, notably acoustic waves, may travel faster but have an incomplete dynamical sensitivity to the process or frequency range considered. When considering a wide range of geophysical dynamics, one may loosely regard the shallow-water wave speed as the maximum speed at which dynamical information can propagate.

The shallow-water wave speed $c_g = (gh)^{1/2}$ for Earth's ocean is shown in Figure 2 (bottom panel). The phase speeds of order 100 m/s, are comparable to c_d in the open ocean, though typically about twice the amplitude. In this case, the terrestrial ocean expresses open-ocean waves for which the electrodynamic process is roughly situated between the frozen-flux and diffusive regimes. Inductive external sources with apparent propagation due to the Earth's rotation will also have associated phase speeds comparable to that of the open-ocean value of c_d. Hence, there are important examples where calculations of the electrodynamics near the surface of the Earth can use neither frozen-flux approximations nor quasi-static approximations. There are examples (e.g. shallow water and/or lower frequency sources) where the processes fall in the diffusive regime and quasi-static assumptions apply. But cases where a strong frozen flux assumption can be applied are less apparent. In the electrodynamics near the surface of the Earth, one expects then that magnetic diffusion is always important while self-induction is important in some cases involving phase speeds comparable to the speed of c_d.

5.2 Criteria for electrically thin ocean

The thin-shell formulation presumes that the shell is electrically thin. This subsection uses values for the conductivity of Earth's ocean to describe the specific criteria for validating this assumption.

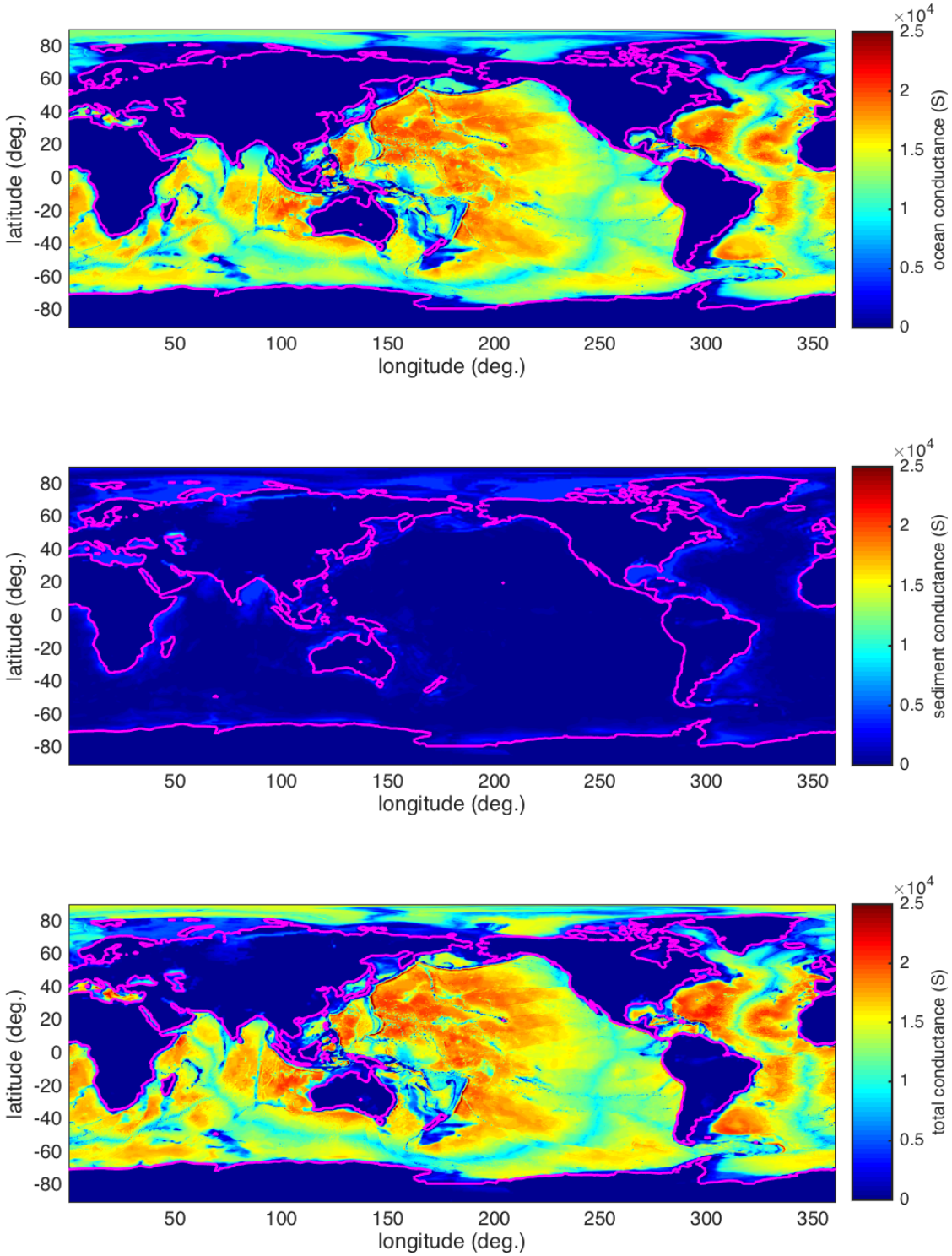

Fig. 1 The electrical conductance of Earth's surface shell (bottom panel) is primarily due to the ocean (top panel) and, to a much lesser degree, wet sediment (mid panel) components of the hydrosphere.

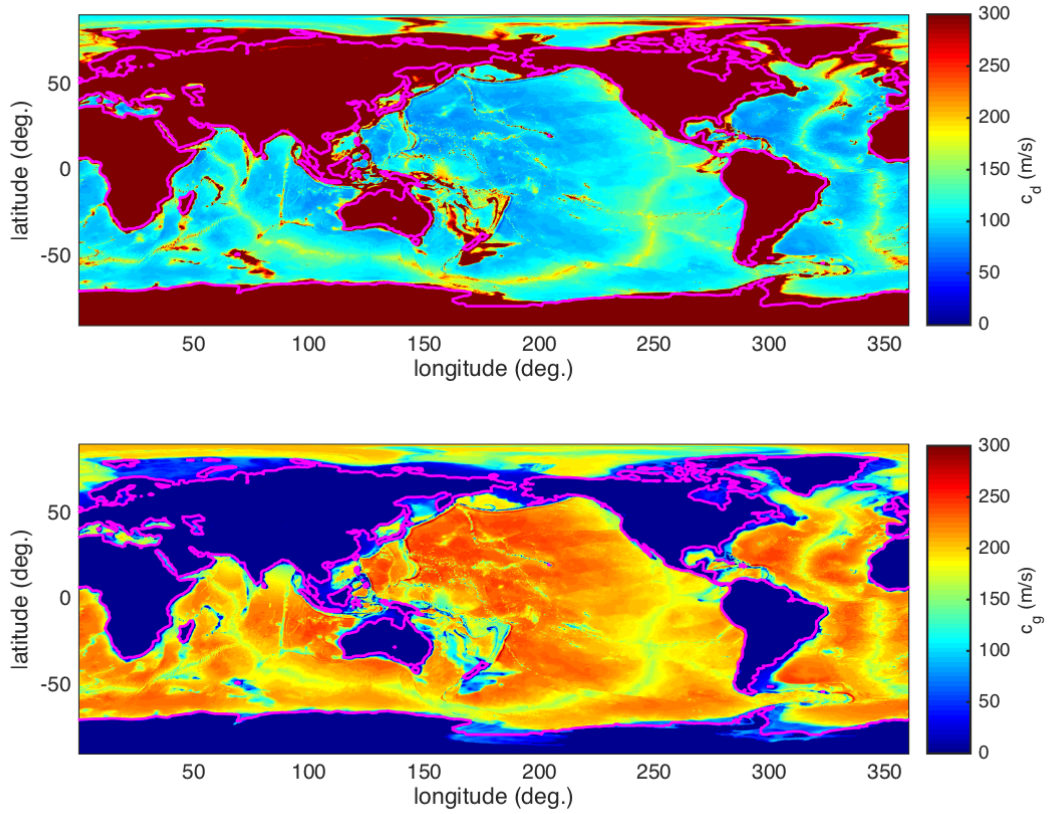

Fig. 2 Top panel: Lateral adjustment speed c_d (m/s) for magnetic diffusion. Bottom panel: shallow-water wave speed c_g (m/s).

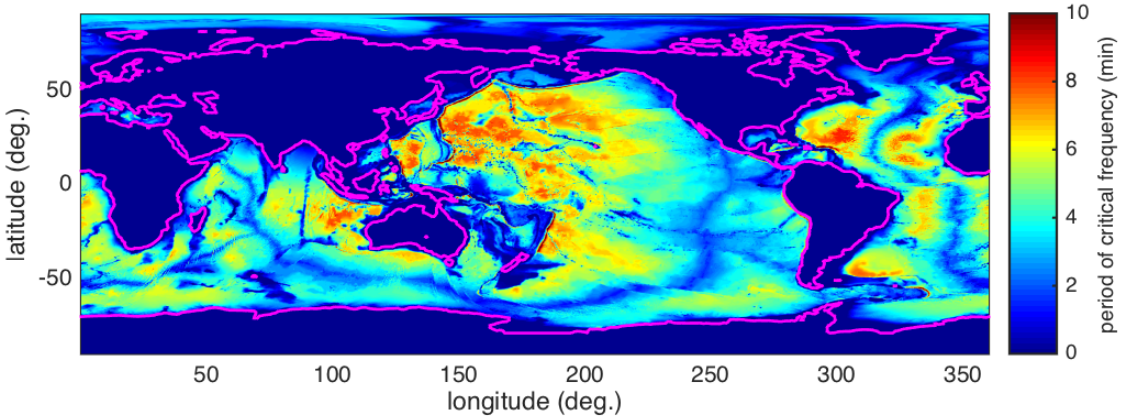

Fig. 3 Critical period τ_c (min). When considering periods/time-scales much larger than τ_c , the ocean layer is electrically thin (i.e. the electromagnetic skin depth is much larger than the geometric depth).

As described in the last subsection, most of the conductance of the thin shell is due to the conductance of the ocean, which is known accurately, and the estimate of the smaller component due to sediments is less reliable. We shall therefore make the next estimates based on just the ocean layer.

The ocean layer is electrically thin if the frequency-dependent skin depth $L_e = (2K/\omega)^{1/2}$ is much larger than the physical thickness h. Assuming depth averages, we can write this criterion as $\tau >> \tau_c$, where τ is the period/time-scale considered and

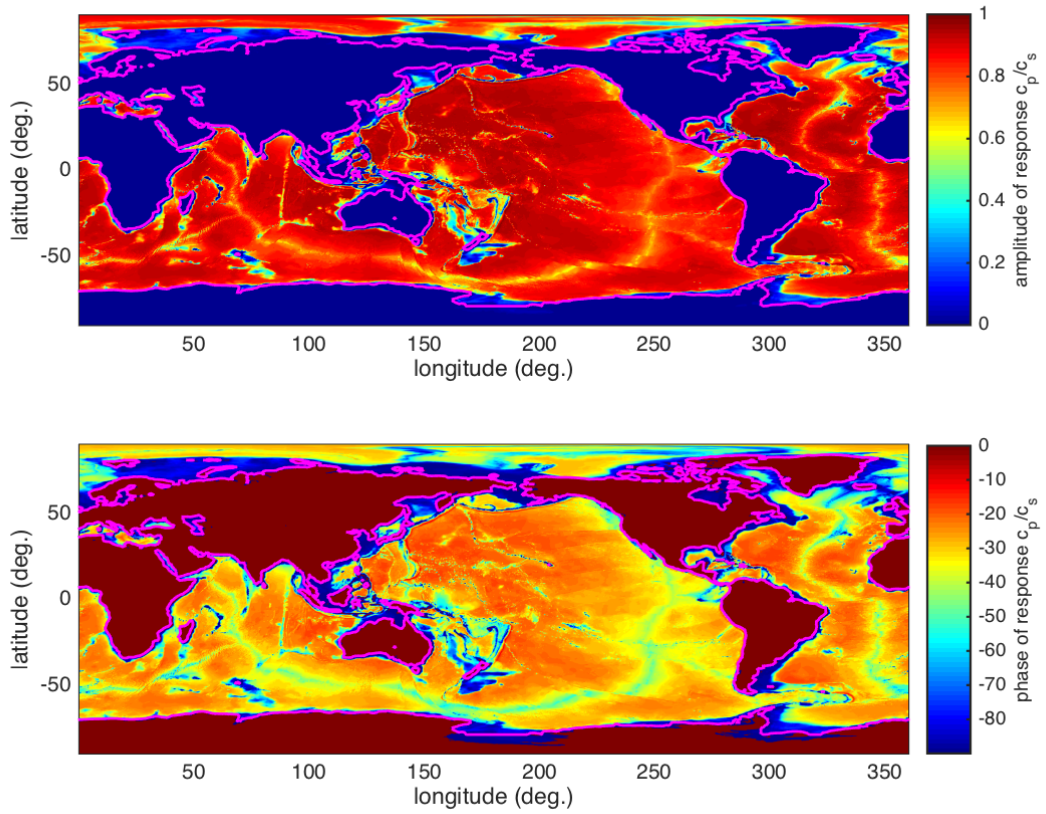

Fig. 4 Amplitude (top panel) and phase (bottom) of the ratio c_p/c_s for processes mediated by long gravity waves (in which case the phase speed is $c_p = c_g = (gh)^{1/2}$. An interesting aspect of the terrestrial case is that the amplitude of the ratio is close to unity over most of the ocean—indicating that for this important class of flow, self induction and magnetic diffusion are equally important.

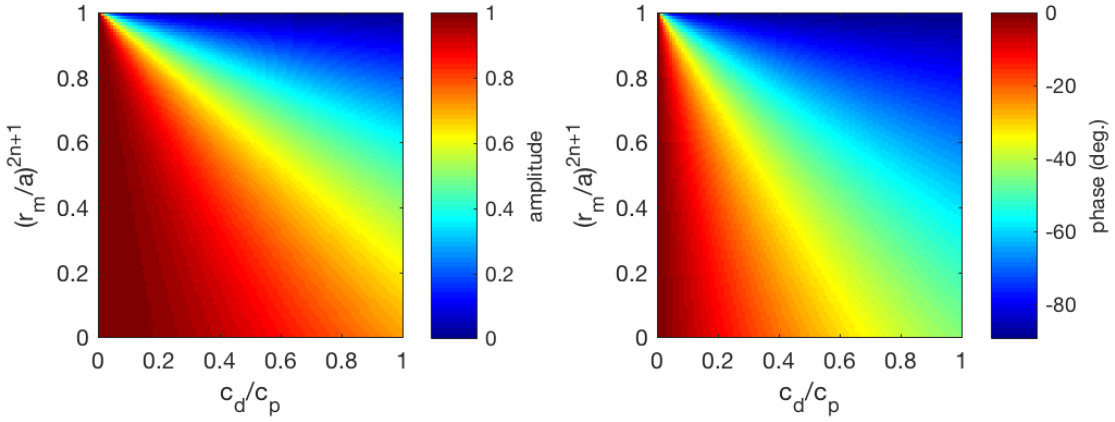

Fig. 5 Amplitude and phase of the approximate response function as a function of the ratio c_d/c_p (in this case, $c_p = c_g = (gh)^{1/2}$) and fractional radius of a perfectly reflecting layer representing the lower mantle. One expects that r_m/a may be as high as ≈ 0.9 for some applications. Most of the applications on Earth are expected to fall in the lower sections of these diagrams. It is clear, however, that inductive coupling with the mantle is important when considering the largest spatial scales.

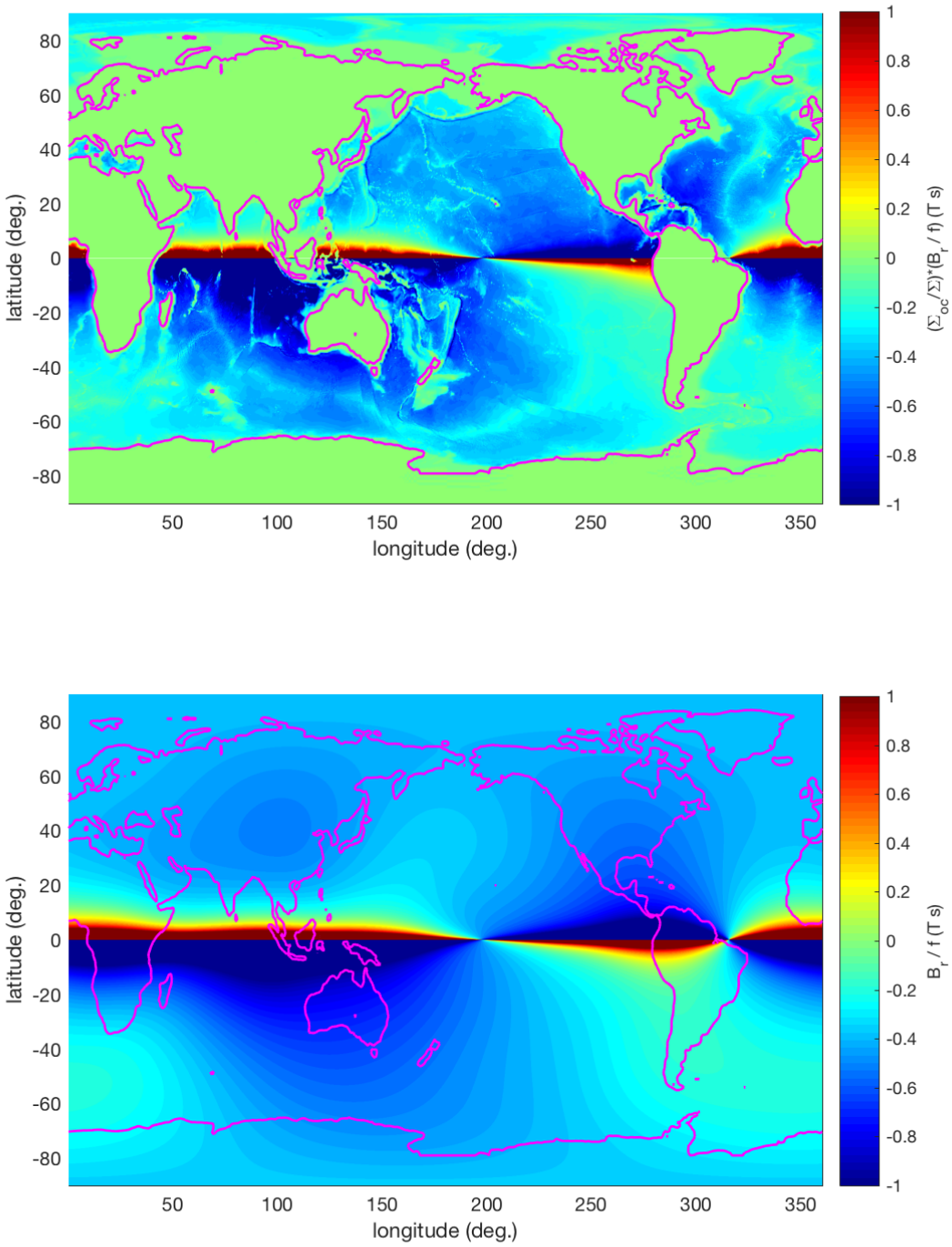

Fig. 6 To first order, geostrophic flow in Earth's ocean does not interact with the main magnetic field. Induction occurs only as a second-order effect where flow crosses contours of $\frac{\Sigma_{oc}}{\Sigma}\frac{B_r}{f}$ (top panel). The factor $\frac{\Sigma_{oc}}{\Sigma}$ includes an uncertain component due to sediment conductance, although it is expected that this ratio is near unity over most of the deep ocean. In this case, the relevant contours are of $\frac{B_r}{f}$ (bottom panel).

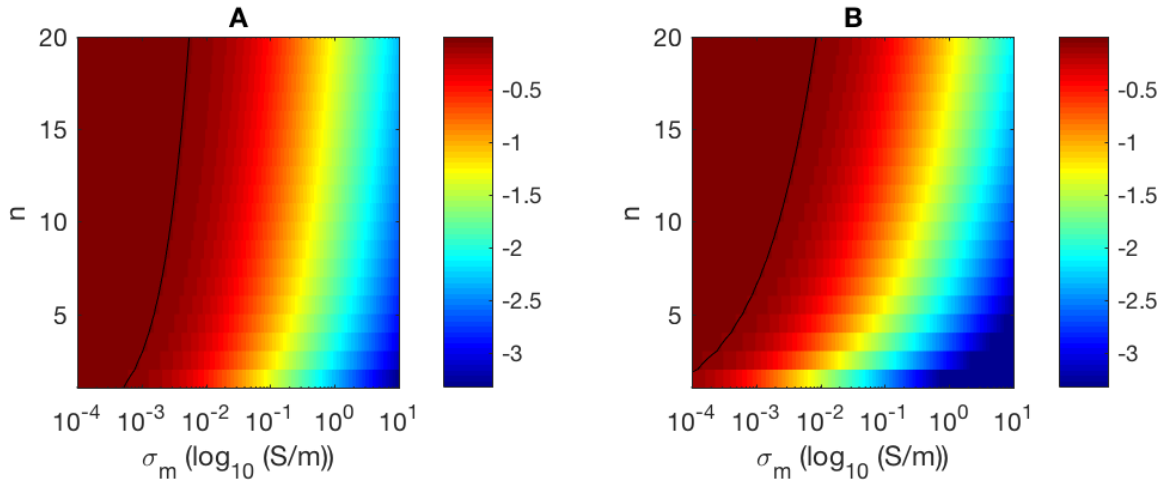

Fig. 7 Reduction factor on electric potential due to galvanic electric currents in the mantle. An expected underestimate is presented by the reduction factor $\left(1+\frac{a-h_0}{n+1}\frac{\sigma_m}{\Sigma}\right)^{-1}$ in frame A, while an expected overestimate is presented by the reduction factor $\left(1+\frac{(a-h_0)^2}{n(n+1)}\frac{\sigma_m}{d\Sigma}\right)^{-1}$ in frame B. The black curve shows the value 0.9 separating the region on the left where reduction is less than 10 percent from the region on the right where reduction is greater. The effects of unmodeled lateral inhomogeneities in the mantle introduce uncertainties that may be at least 10 percent and so a deficiency in the thin-shell approach appears only for combinations of assumed σ_m and n to the right of the black curves.

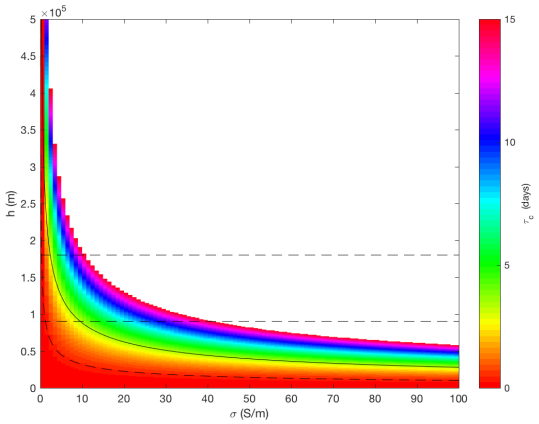

Fig. 8 Critical period (days) as a function of ocean depth-averaged conductivity and geometric thickness (values run off scale above 15 days). The satellite oceans are electrically thin if the ocean thickness is thin and/or the conductivity is low. Europa's ocean thickness falls within the horizontal dashed lines, and the solid curve describes the 85.2 hr period of the primary induction signal due to Jupiter's rotating field. The 11.1 orbital period of Europa is shown with the dashed curve.

$$\tau_c = \pi\mu_0 h\Sigma_{oc} \tag{5.1}$$

is the critical period at which $L_e = h$. A map of τ_c, shown in Figure 3, shows that for processes with periods/time-scales above about 10 minutes, the global ocean is indeed electrically thin. In exclusively shallower regions, this criteria can be met with shorter periods.

An important result for the application of Earth is then that for time scales longer than about ten minutes, one can efficiently replace the 3-D computational domain of the ocean with a 2-D domain involving depth-averaged variables.

5.3 Motional induction constrained by fluid dynamics

As described, magnetic diffusion is important when c_d becomes comparable to or larger in amplitude than the phase speed of the process. While the phase speed can be set by space and time scales associated with prescribed forcing or parameter variations, an interesting case is one where the phase speed is set by the fluid dynamics. This was discussed in Tyler (2005) where the electrodynamic response is set by the ratio c_p/c_s and c_p is constrained by a dispersion relationship for the fluid dynamic wave process considered. In Section 3.2, $c_s = c_p + (1 + \frac{1}{2n})ic_d$ gains a small dependence n due to sphericity. For simplicity, we shall here ignore the small dependence on n and treat $c_s = c_p + ic_d$, as in the initial Cartesian derivation (Tyler, 2005). In this case, the response function is specifically c_p/c_s.

As an example, we consider here the important class of long gravity waves for which we may take $c_p = c_g = (gh)^{1/2}$. The response function c_p/c_s is then an environmental parameter that applies for all cases of long-gravity wave dynamics in Earth's ocean. The amplitude and phase (i.e. argument) of the complex ratio (c_g/c_s) is plotted in Figure 4.

The long gravity wave speed should probably be regarded as a maximum phase speed for ocean fluid wave dynamics. The maximum phase speed of long dispersionless Rossby waves converge with this limit and a large suite of other wave classes have slower wave speeds. It should be expected then that in Earth's ocean, all electrodynamics associated with wave phenomena appreciably involve magnetic diffusion and that magnetic diffusion even dominates for all cases with lower phase speed than the long gravity wave limit. In these latter cases where $c_p << c_d$, the response function c_p/c_s is then imaginary, indicating that the response is 90 degrees out of phase with the forcing.

When a reflecting lower layer (representing the conductive lower mantle) is included the response function of the ocean/mantle system (see Section 3.2) is instead

$$\left(\frac{c_p}{c_s}\right)\left(\frac{1-\left(\frac{r_m}{a}\right)^{2n+1}}{1-\left(\frac{r_m}{a}\right)^{2n+1}\frac{c_p}{c_s}}\right).$$

The additional factor, representing a reduction in the amplitude of the response due to reflection by the lower layer, contains a dependence on the degree n and therefore the length scales in the application considered. Even when c_p is fully prescribed, as in the example of the long gravity waves above, the dependence of this second factor on n means that the response function is no longer an environmental parameter prescribable for the general flow class considered. Of course for wave classes without the trivial dispersion relationship as above, we should expect $c_p = c_p(n)$. So in general we should expect that the response function depends on environmental parameters and the dynamical parameter n. One might use the appropriate dispersion relationship to replace the need to specify n (the spatial frequency) with the parameter describing the temporal frequency. The important point here is that both parameters need not and, for dynamical consistency, should not be chosen independently.

Despite the dependence on n of the response function described in the last paragraph, one may consider some limiting cases to evaluate the effect of the reflecting lower layer. Of course for $r_m/a \to 0$ (no reflecting layer), an effect is absent and the response function remains as c_p/c_s. For $r_m/a \approx 1$ (the situation where the reflecting layer is very close to the surface shell), $b_r = -F_r^{(d)}$. The behavior between these limits can always be found by inserting parameter values in the response function above. Aside from the end members associated with the limits in r_m/a, a third limiting case is described in Figure 5. In choosing this case, we first note that the factor due to sphericity $(1 + \frac{1}{2n}) \approx 1$ for all but the smallest n choices. Ignoring the n-dependent sphericity factor, the behavior of the response function is plotted as a function of the real parameters c_d/c_p and $\left(\frac{r_m}{a}\right)^{2n+1}$ in Figure 5. Additionally, the continents break up the largest scales such that realistically there is expected to be a sharp drop in energy below $n \approx 5$. From these considerations and others, one expects that applications for Earth to typically fall in the lower section of these diagrams. Inductive coupling with a lower mantle is clearly important for the largest spatial scales possible.

5.4 Non-dynamo action of geostrophic flow

As described in Section 2.3.5, geostrophic flow does not efficiently generate radial magnetic field components when the background magnetic field is predominantly an axis aligned dipole. Specifically, induction by geostrophic flow is a second-order process (i.e. the first-order terms vanish both because of symmetries between the background main field and the Coriolis parameter, and because of the approximate non-divergent nature of geostrophic flow.) Motional induction by geostrophic flow occurs only where flow crosses contours of the parameter $\frac{\Sigma_{oc}}{\Sigma}\frac{B_r}{\rho f}$.

The Earth's main magnetic field is primarily an axis aligned dipole, and flow varying on time scales longer than a day is primarily geostrophic. An important and immediate result is that much of the flow in Earth's ocean does not efficiently interact with the main magnetic field to generate horizontal electric currents and (poloidal) magnetic fields reaching outside of the ocean.

While $\frac{\Sigma_{oc}}{\Sigma}\frac{B_r}{\rho f}$ is approximately uniform in the case of Earth, the departures are informative for understanding the motional induction process in Earth's ocean. In Figure 6 the contours for both $\frac{B_r}{f}$ and $\frac{\Sigma_{oc}}{\Sigma}\frac{B_r}{f}$ are shown.

5.5 Galvanic currents

The thin-shell induction equation can include excitation of electric currents in the mantle through inductive coupling but galvanic coupling is omitted. The purpose of this section is to estimate the error associated with this approximation using typical parameters describing the surface conducting layer of the Earth.

Because the thin-shell conductance includes the conductance of both the ocean and sediment layers, galvanic electric currents circulating within the ocean and sediment layers are implicitly included. But galvanic electric currents penetrating deeper into the mantle are not included in the thin-shell formulation. The basis for an approximation that ignores the deeper galvanic currents is that estimates of the conductivity of the upper mantle are typically two to four orders of magnitude smaller than that in the ocean or wet sediments. Still, for extremely large-scale (low spherical-harmonic degree n) processes, penetration of substantial galvanic electric currents may take place due to the very large surface areal cross section as noted in the study of Stephenson and Bryan (1992) (where galvanic connection with the mantle was also omitted).

To estimate this reduction factor using typical parameters, we first make a few remarks:

1. We do not expect sources at the surface to produce monopole electric potentials (i.e. $n \neq 0$), and for very high degree (e.g. $n > 2000$) the small spatial scales described must become inconsistent with the thin shell assumptions; but otherwise n has a very large expected range.
2. Away from very shallow regions and land, the surface conductance Σ is primarily due to the conductance Σ_{oc} of the layer of seawater, with a relatively smaller contribution to Σ from the conductance of sediments.
3. While Σ shows a large range over the ocean (see 1) primarily due to the large variation in ocean depth, regions with small Σ are not of very large spatial scale (therefore an assumption of both small n and small Σ is unrealistic) and we therefore take a mid-ocean value of $\Sigma = 1.5 \times 10^4$ (S) as representive.
4. The value for σ_m is uncertain and, as with n, we should consider a range.
5. For the analyses here, $a - h_0 \approx a \approx 6.371 \times 10^6$(m).

With these values, we plot the electric potential reduction factor $\left(1 + \frac{a-h_0}{n+1}\frac{\sigma_m}{\Sigma}\right)^{-1}$, as derived in Section 3.5, in Fig 7 (A) as a function of σ_m and n. If we assume a typical value for the upper mantle $\sigma_m = 10^{-3}$ (S/m), then we see that the effect of the galvanic currents is to reduce the potential by no more than 10 percent even for the lowest degrees. If we assume the effects of the unmodeled and largely unknown lateral inhomogeneities in the mantle conductivity are probably more important and so one could conclude that there is not yet added realism in simulations that include the galvanic contact. But note that while lateral inhomogeneties might lead to non-systemmatic errors, the ommission of galvanic currents is systemmatically to reduce the total energy of electric currents in the surface layer. From this latter point, it might be argued that higher realism is indeed included with models that include galvanic currents, even when these models do not include the lateral inhomogeneities in the mantle.

The last estimate may be misleading because mantle conductivity is expected to increase with depth and use of the upper-mantle value may be inappropriate when also considering low n (global spatial scales) where electric currents may travel deep into the mantle. The result is that the last estimate may underestimate the reduction factor. Let us then consider a different simple model of mantle conductivity that is likely to over-estimate the reduction factor. The second model is identical to the first except that below a depth $d_m = 5\times10^5$ (m) we assume the conductivity is infinite and therefore ϕ vanishes. Given the relatively thin layer of mantle that remains, we also simplify by assuming that electric currents in the mantle flow only radially following the electric potential drop between $\phi_m = \phi$ at the surface and $\phi_m = 0$ at $r = d_m$. We then have $j_r(r = a - h_0) = -\sigma_m\phi_m/d_m$ and following an approach similar to the last case, we find a galvanic reduction factor of $\left(1 + \frac{(a-h_0)^2}{n(n+1)}\frac{\sigma_m}{d\Sigma}\right)^{-1}$ which we plot in Fig 7 B. In contrast to the last case, this estimate suggests (assuming again $\sigma_m = 10^{-3}$ S/m) important galvanic currents for degrees 6 and below. Both cases show that increasing σ_m quickly increases the importance of the galvanic currents and so both estimates are sensitive to the assumptions of upper mantle conductivity.

6 Application to oceans on icy satellites

6.1 Introduction

There is growing evidence that many bodies in the Solar System may have global oceans under a shell of ice (see Nimmo and Pappalardo (2016) for a recent review, and Tyler (2014) for a description of potential scenarios allowing vigorous tidal flow.) In no case so far, however, have the dynamical state or electrical parameters been well constrained from observations or theory. One might then expect to complete this section with simply the statement that the mathematical formulations and methods described may apply to these bodies as well but few details can yet be extended. There are, however, a few common elements in these oceans that motivate a specialized discussion:

1. A reasonable provisional assumption is that these oceans are global and typically thicker than Earth's ocean.
2. It may typically be the case that the ocean is exposed to rock and electrical conductivity is elevated due to dissolved salts.
3. The most initially-plausible large-scale flow that can be discussed is tidal flow.
4. All the satellites with suspected oceans rotate synchronously with their orbit.
5. The oceans are covered with ice shells.

Because of items 1.) and 2.), we may anticipate that the conductance of the surface shell comprising the ocean is typically higher than that for Earth. Conductance depends on the integral over the shell thickness, and so from this consideration conductance increases for thicker oceans. But it also depends on conductivity which, it may be argued, does not have as large a potential range as one might naively assume. Distilled water has a conductivity of order 10^{-4} S/m, which is several orders of magnitude lower than Earth's ocean (which has an average conductivity of 3.2 S/m (Tyler et al., 2016)). Freshwater streams have conductivities about two orders of magnitude higher than distilled water, indicating that contact with rock and other impurities quickly generates conductive charge carriers. The satellite oceans that have contact with a rocky seafloor then likely have conductivies much higher than that of distilled water. (One should note that in the deepest oceans on the largest satellites, pressure may be great enough to form dense phases of ice that would sink and form the seafloor. While there could still be contact of water and rock through subfloor hydrothermal circulation (Vance et al., 2007) this is not as assured as the case with rock seafloor.) There are also limitations on the maximum conductivities that can be obtained because the amount of salt that water can hold reaches a saturation value. Indeed, one might expect that because there has been much time to reach an equlibrium that the salinity is near the saturation value. (The situation on Earth is different as there are hydrological processes (rain, runoff) that add salt and geological processes (subduction, evaporites) that remove it such that salinity varies regionally and does not typically reach a saturation value.) Estimates of the conductivity at saturation level have been made (Hand and Chyba, 2007) and, while uncertain

because they depend on the composition of the salts involved and local conditions, we see a range much closer to the value of Earth's ocean than what one might initially expect given the large potential range of the conductivity of water. Perhaps a summary anticipation is that conductivity in these oceans is comparable to or higher than Earth's ocean because the satellite oceans have had more time to saturate (while the temperature of the water may be similar to that in ice-covered oceans on Earth.)

With higher conductance, the assumption of electrical thinness of the ocean as required in the thin shell formulation is harder to meet. Also, if the oceans are global, as in 1.) or if at least we yet know no better, then one need not include the complications of the inhomogeneous conductance in the formulations we have discussed. These considerations indicate that the thin-shell formulation discussed may not be the most appropriate for these extraterrestrial cases. Indeed, without the inhomogeneities in the conductance, simpler formulations having spherical harmonics as eigenfunctions are available, as shown in the analytical solutions in Sections 3 as well as the discussion of electrical currents in the mantle (in which radial symmetry of conductivity was always assumed).

Because of items 3.) and 4.), the most important motional induction studies for all satellites involve flow that has force components that are identical (to within scaling factors) if not necessarily similar responses. Properly non-dimensionalized, the available tidal forces are few and the same for all satellites. The frequency of the tidal forcing and therefore tidal flow is also commensurate with the rotation rates such that these frequencies, when nondimensionalized by the rotation rate, are also the same for all satellites. For similar reasons, one can be assured that any resulting tidal flow will show rotation and inertial acceleration as equivalent in dynamical importance. From these considerations, the flow on the satellites fall into a subclass of the much larger range of potential scenarios. But while the tidal force constituents are similar for all of the satellite oceans, the ocean tidal response depends on the ocean parameters and need not be commenurate with the forces. Seemingly small differences in ocean parameters can change the eigenmodes of the ocean such that the ocean tidal response may even be dominated by a subtidal constituent that happens to excite the ocean with a spatial/temporal pattern corresponding to one of the ocean's eigenmodes. As an example, even if the predominant tidal forces on Europa are due to eccentricty, the predominant ocean tidal response may be a resonant response to one of the sub-dominant tidal force constituents due to obliquity (Tyler, 2008). As a related example of resonant tides, consider that the equilibrium ocean tidal height for Earth's ocean is only of order 0.1 m; regions we refer to as having large tides are a result of regional ocean parameters leading to a resonant response, rather than differences in the force constituents. In brief, the predominant flow in all of the satellite oceans may be the response to similar tidal forces but the range of responses depends sensitively on the ocean parameters and is not simply commensurate with or predicted by the amplitudes of the force constituents for the specific case.

Because of item 5.) we should expect that there is little potential for directly measuring the flow velocity and so the formulations of the induction equation with velocity removed (see Section 2.3.4) may be highly relevant.

6.2 Are oceans electrically thin?

The oceans can be considered to be electrically thin if the ratio of the geometric depth (h) to the frequency-dependent electromagnetic skin depth ($2K/\omega$) is much less than unity. This condition can be expressed as a critical period $\tau_c = \pi\mu_0 h\Sigma$. When the dynamical period considered is much larger than τ_c, then the ocean is electrically thin. The periods we must consider for motional induction are those of the tides (which is the period of rotation/orbit in these cases of tides on satellites in synchronous rotation). The periods for induction are less well constrained. The dominant induction signal on Europa comes from the time variations in Jupiter's magnetic field as it spins relative to the orbiting satellite. The period of this dominant signal is about 11 hours, while the spectrum of sub-dominant induction sources includes the 85.2 hour orbit and longer periods. The orbital periods of the other satellites with suspected oceans range from about 1 to 15 days. The geometric thickness of these oceans may reach hundreds of kilometers.

Considering a range of 0 to 100 (S/m) for the depth-averaged conductivity, the expected range for the critical period of these satellite oceans is shown in Figure 8. For comparison, the ocean geometric thickness for Europa

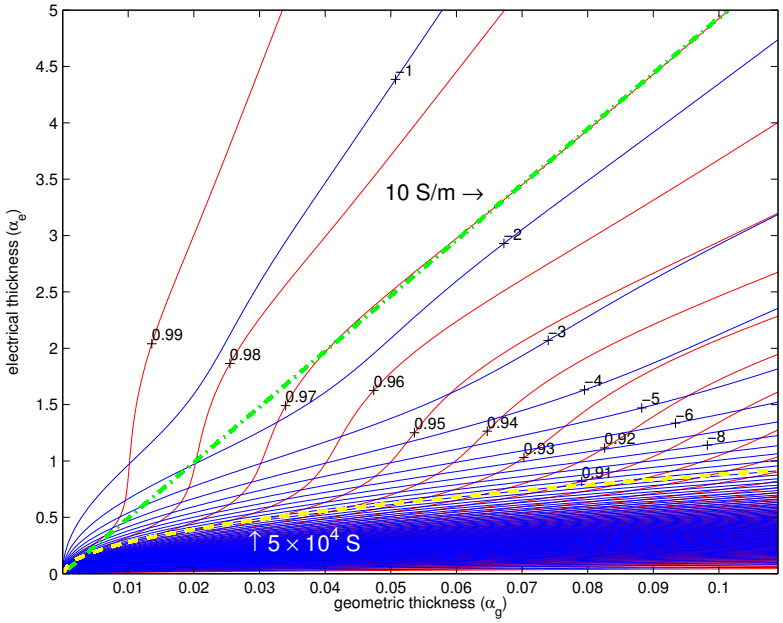

Fig. 9 Within the model assumed, the response of Europa's ocean to a fluctuating external magnetic field depends only on two ocean parameters—it's relative geometric thickness α_g, and it's relative electrical thickness α_e. The two sets of solid curves describe this response; those labeled with negative numbers describe the temporal phase lag (degrees), and the other set describes the relative amplitude. The amplitude inferred from Galileo magnetometers is 0.97, and so it is this curve in the diagram that determines which α_e, α_g pairs are allowed. Physical parameters can be plotted using these same coordinates (α_e, α_g), and we can see that the cited ocean conductance value of 5×10^4 S (dashed curve) indeed aligns with the 0.97 curve, but only below the range $0.04 < \alpha_g < 0.11$ allowed by gravity constraints. The line (dotted-dashed curve) describing an ocean conductivity of 10 S/m, however, agrees very well with the 0.97 curve in the realistic α_g region. Such high conductivity indicates extreme salinity near its saturation value; by weight, Europa's ocean would be about one third salt.

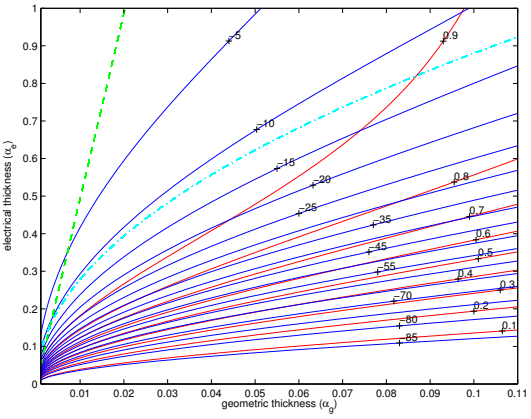

Fig. 10 As in Figure 1 but expanding low α_e region.

has been constrained to fall between the horizontal dashed lines (Anderson et al., 1998). One sees that when considering tidal periods, configurations allowing an electrically thin ocean assumption are reduced to a small subset of parameter coordinates with conductivity much less than 10 S/m. When considering the dominant induction period of 11.1 hours, it seems very likely that Europa's ocean should be regarded as electrically thick. Indeed, this is strongly supported by the magnetic response of Europa as observed by the Galileo spacecraft, as described next.

6.3 Induction

In the vicinity of Europa, magnetometers aboard Galileo reported anomalous magnetic fields that are now thought to be the response of a global ocean to the temporally-varying component of Jupiter's magnetic field as it rotates

once every 11.1 hours (Khurana et al., 1999; Kivelson et al., 2000). Recent attempts to refine the analyses and determine specific properties of the ocean from these magnetic measurements has produced differing results. The electrical conductivity of the ocean is an especially important parameter to determine because this describes the ocean salinity (salt content) which has a major role not only in biological and chemical processes, but also in the dynamics and thermodynamics of the ocean. And yet the two most recent and thorough analyses have produced constraints on the minimum conductivity that differ by two orders of magnitude. A constraint for the minimum conductance (integral of conductivity over ocean depth) implicitly gives an average ocean conductivity of the order of 10^{-1} S/m (Schilling et al., 2007), while other work (Hand and Chyba, 2007) claims that the conductivity must be of order 10^{1} S/m. Reformulating the magnetic response function using dimensionless variables that deconvolve the parameter dependencies, and replacing the basis functions of the formulation such that numerically stable solutions can be plotted throughout the parameter range of interest, we show that the higher conductivity value is the appropriate constraint, while the lower value would be appropriate only in a region of parameter space already excluded by gravity constraints (Anderson et al., 1998). If we admit this higher conductivity estimate, a very important conclusion is that Europa's ocean is very nearly saturated with salt as has been claimed (Hand and Chyba, 2007). A limiting factor in using this result scientifically, however, is that presently there are not suitable estimates for the uncertainties involved in this estimate. The high conductivity result is based on an estimate of the magnetic response of Europa's ocean (Schilling et al., 2007), but only the amplitude and not the phase of the response was estimated from Galileo data. The amplitude A was estimated as $A = 0.97 \pm 0.02$, but the small uncertainty describes only an agreement with the methodology and model assumed (other models might also fit the data) and it is unclear how well this represents the full uncertainty in Europa's observed magnetic response.

Identification of the most appropriate ocean parameter constraints that can be obtained from the magnetic data and which optimally exploit the data depends much on the formulation chosen for the magnetic response function, which gives the amplitude and phase of the ocean's magnetic response in terms of a selection of parameters. Here we formulate this function in terms of only two physically-based dimensionless parameters: The relative electrical thickness α_e is the ratio of the ocean thickness to that of the frequency-dependent "skin depth", it describes the penetration and electrical resistance in the ocean medium; The relative geometric thickness α_g is the ratio of the ocean depth to the length scale for horizontal variation, it controls the geometric attenuation of the magnetic fields away from their electric-current sources. Within the idealizations for the ocean electrodynamic model that have been assumed in the previous work and are continued here, the response of a planetary ocean to a fluctuating external magnetic field depends only on these two free parameters, and so any ocean parameters obtainable from the magnetic data must be derived through ratios of these and known parameters. This consideration forms the base of the analysis here and has lead us to determine that conductivity (and not conductance) is the parameter that can be appropriately constrained in this application of Galileo magnetic data, and that the constrained value (if we ignore consideration of errors) is about 10 S/m. These results are summarized in Figures 9 and 10. We shall describe how we obtain these results after first describing the previous approaches:

The magnetic response function assumed in (Schilling et al., 2004; Hand and Chyba, 2007), and essentially consistent with (Schilling et al., 2007), is

$$Ae^{i\phi} = \left(\frac{r_0}{r_m}\right)^3 \frac{RJ_{5/2}(r_0 k) - J_{-5/2}\left(r_0 k\right)}{RJ_{1/2}(r_0 k) - J_{-1/2}\left(r_0 k\right)} \tag{6.1}$$

where A provides the amplitude of the ocean response (fraction of the imposed jovian magnetic field that is cancelled by the magnetic field due to the electric currents responding in the ocean), ϕ defines the phase lag of the response, J_n is the Bessel function of the first kind,

$$R = \frac{r_1 k J_{-5/2}\left(r_1 k\right)}{3J_{3/2}\left(r_1 k\right) - r_1 k J_{1/2}\left(r_1 k\right)}, \tag{6.2}$$

r_1 is the radius to the seafloor, r_0 is the radius to the sea surface, r_m is the radius to the icy surface of the moon, and $k = (-i\omega/K)^{1/2}$ (where ω is the frequency of the external magnetic field, and the magnetic diffusion coefficient K is a constant inversely proportional to the electrical conductivity).

Despite the spherical geometry of this problem, Bessel (or spherical Bessel) functions are not the best radial basis functions for describing the response of a thin conducting shell surrounded by relative insulators because the response gains physical similarities to that in planar geometry. From the practical point, (6.1) cannot be used to calculate the response over the full range of parameter values of interest because it is numerically unstable; in this form, very similar numbers are subtracted from one another leaving few or no digits to describe the result. An approximate form (Hand and Chyba, 2007) allows stability over part of the parameter range (for the amplitude though not for the phase), and a switch to modified Bessel functions seems to also help the stability. But by recognizing that the electric currents flow in a very thin shell, rather than through a spherical volume, we find a switch to simple and stable trigonometric basis functions once we change to new variables: Here we define $\alpha_g = h\kappa$ (where h is the liquid ocean thickness/depth, and the wavenumber $\kappa = n/r_0$ with the spherical-harmonic degree $n = 1$ for this application), and $\alpha_e = h/\delta$ (where $\delta = (2K/\omega)^{1/2}$ is the electric skin depth). We can then write (6.1) as

$$Ae^{i\phi} = -\left(\frac{r_0}{r_m}\right)^3 \frac{N}{D} \tag{6.3}$$

where

$$\begin{aligned} N &= 3\left(-1+i\right)\alpha_e\alpha_g^2\left(2\alpha_e^2\left(-1+\alpha_g\right)+3i\alpha_g^2\right)\cos\left(\left(1+i\right)\alpha_e\right) \\ &\quad + -4\alpha_e^4\left(-1+\alpha_g\right)^2+9\alpha_g^4-6i\alpha_e^2\alpha_g^2\left(-1+\alpha_g+\alpha_g^2\right)\sin\left(\left(1+i\right)\alpha_e\right), \\ D &= 2\alpha_e^2\left(3\left(1-i\right)\alpha_e\left(-1+\alpha_g\right)\alpha_g\cos\left(\left(1+i\right)\alpha_e\right)+\left(2\alpha_e^2\left(-1+\alpha_g\right)^2+3i\alpha_g^2\right)\sin\left(\left(1+i\right)\alpha_e\right)\right). \end{aligned} \tag{6.4}$$

Note that N/D depends only on two parameters—α_e and α_g. The term $(r_0/r_m)^3$ is not really associated with the ocean's response but rather it's location which is not precisely known for Europa because of the surface layer of ice. This is why the observed response amplitude 0.97 is considered to be only a lower-value constraint; the observations allow just as well for an ocean response near 1.0 but separated from the surface by an ice layer 16 km thick (Hand and Chyba, 2007). Gravity data constrain the total of ice plus liquid water thickness to fall in the range 80 km – 170 km (Anderson et al., 1998). Adding this consideration, we find the constraint for the realistic range of α_g described in the caption of Figure 9. (The latter constraint can also be used to convert the attenuation factor $(r_0/r_m)^3$ in (6.3) into a function of α_g such that the full response, including uncertain ice thickness, is described in α_g, α_e coordinates.)

A version of Figure 9 showing the low α_e region is shown in Figure 10. This is the diffusive regime that a lower-frequency external source will encounter, and in this case conductance rather than conductivity becomes the better constrained variable. But in the case considered here and highlighted in Figure 9, the ocean's electrical resistance is of less importance than the geometric attenuation effects; in this part of the parameter space, the response amplitude (at the satellite surface) is primarily sensitive to the distance to the electric currents which are separated by a layer of ice and center at an effective depth controlled by conductivity. Interestingly, in this part of the parameter space the primary importance of the ocean's conductivity is it's control over the geometry of the electric currents rather than their strength.

If both the amplitude and phase of the magnetic response were known without uncertainty then we would just need to look for the intersection of the correct amplitude and phase in Figure 1, and from this location obtain the parameters α_e, α_g, which are the complete set of ocean parameters that can be determined from perfect magnetic data and within the idealized model assumed. If both the amplitude and phase are known, but each with a specified uncertainty, then a parameter-space patch of possible α_e, α_g are extracted. But as can be seen in Figure 1 the extension of this patch depends much on the location in the parameter space. The optimal position

in the parameter space corresponds to $\alpha_e \approx 1$ where the amplitude and phase lines are most perpendicular. In this region, uncertain amplitude and phase retain the most unique information. In other regions where the amplitude and phase lines are nearly parallel, the two pieces of information about the ocean can be redundant for practical purposes. The region $\alpha_e \approx 1$ describes an ocean with a frequency-dependent electrical depth similar to its physical depth. This is probably not the case for the application we have been considering (an unrealistically thin ocean would be required) but can be designed in a similar analysis using an imposed magnetic field of lower frequency. We do not presently have an estimate for the phase, and the preliminary indication is that with uncertainties the phase information will be largely redundant with the amplitude information. This is because we expect the correct α_e, α_g pair lies in the upper right of Figure 1 where phase and amplitude lines run nearly parallel. Even in this case, the phase information could be usefully applied for confirmation of the information contained by the amplitude, and as a consistency check of the uncertainty calculated. If the amplitude is 0.97, then the phase should be about 1.9 degrees. Confirming this, even if the uncertainties are relatively large, can be used to exclude the low α_g region (involving phase several times greater than 1.9 degrees) which we presently exclude using only the gravity constraint.

At present, we have available only the amplitude estimate and are unsure how to interpret the uncertainties that have been given. In the expected region, the amplitude 0.97 alone can be translated into an estimate of ocean conductivity of 10 S/m because the 0.97 amplitude contour and the 10 S/m conductivity contour are very nearly parallel. The lower value given by the uncertainty is 0.95 and this corresponds to a conductivity of 3.5 S/m. The upper value of 0.99 is not likely the true ocean response because this would fall in the low α_g region forbidden by the gravity data, and this upper value is probably only useful in confirming that there is a layer of ice of maximum thickness 16 km thick (as in Hand and Chyba (2007)) on top of the ocean. An independent estimate for the upper bound on conductivity can be obtained by considering salinity saturation conditions, and the value of 10 S/m appears to be near saturation Hand and Chyba (2007).

An important point that can be seen in Figure 9 is that small uncertainties in the amplitude can lead to much larger uncertainties in the ocean parameter estimated. In the example in the last paragraph, a 2 percent change in the response-amplitude estimate leads to a 300 percent change in the estimate of conductivity. Hence, improvements in the magnetic response estimate can lead to disproportionate improvements in the ocean parameters estimated. But there are limitation that must be considered. The reason why the 0.97 amplitude contour and the 10 S/m contour align in the region of interest is that the 11.1-hour excitation frequency used in this application is too high to have penetrated all but the surface of the ocean; there can be little information in the magnetic data about the total conductance (depth integrated conductivity) or ocean depth. This can be alleviated by using a lower source frequency, and Khurana et al. (2002) have proposed sounding Europa's seafloor with an 85.2-hour orbital-period magnetic source. This can provide information about the ocean depth provided the conductivity is not substantially higher than the guess of 2.75 S/m (similar to Earth's ocean) that they assume, or if the amplitude and phase of the response are both known accurately (as might be obtained from a magnetometer in orbit).

In the best circumstances, melding of a simple spherically symmetric, uniform-conductivity ocean electrodynamical model with remotely-sensed magnetic-field observations can be used to translate two observed quantities (the amplitude and phase of the magnetic response) into two ocean parameters (ocean depth and average electrical conductivity). No further information is possible within the simple dynamics allowed by the model. But in practice one or both of these parameters may be unattainable because of observational errors—the two observed quantities may contain the same information, at least in any retrievable sense.

Other studies of induction in satellite oceans have been described for Ganymede (Kivelson et al., 2002), and a third example (though for a magma ocean) has been described for Io (Khurana et al., 2011).

6.4 Motional induction

The gravitational potential of the primary on a satellite involves a time-dependent, spatially-differential component. Combined with a hydrostatic approximation, this potential is often expressed as the equilibrium tide displacement η_F, the horizontal gradients of which lead to the tidal forces. For all synchronously rotating satellites, the temporal variation in η_F is due to the satellite's obliquity (the angle of tilt of the satellite's rotation axis with respect to its the normal vector of its orbital plane) and orbital eccentricity. Where obliquity and eccentricity are small parameters, a McLauren expansion is performed on the gravitational potential to isolate the leading-order terms comprising η_F.

An important result is that to a very good approximation, η_F on the satellite involves only spherical-harmonic degree 2 (the order/rank may be 0, 1, 2). This suggests that the tidal flow on the satellite will be of very large scale such that the condition for geometric thinness of the ocean shell is met provided the ocean thickness h is much less than the satellite's radius. While this is likely to be reasonable, it should be recognized that it is not, however, assured because of spectral transfer of energy. The governing equations for the dynamics of the fluid tides must include the Coriolis term (because the synchronous orbit requires that the frequency of the tidal force be commensurate with the rotation frequency, as mentioned above). The Coriolis term introduces a dynamical asymmetry in the governing equations such that spherical-harmonic base functions are not eigenfunctions of these equations even at some level of idealization or approximation, as could be the case without the Coriolis term. The physical manifestation of this asymmetry is that momentum propagating in the prograde direction is focused toward the equator while the opposite happens for propagation in the retrograde sense. Mathematically, if spherical harmonics were eigenfunctions of these equations, then tidal forcing at degree two will give an ocean response only at the same degree. With the Coriolis term included, the ocean's response need not be even primarily at the same degree as the forcing and in general will involve a sum of spectral components. Hence, a small ratio of ocean thickness to satellite radius may reasonably suggest that the ocean may be regarded as geometrically thin but this should be checked when specific ocean tidal responses are considered.

While geometric thinness seems likely for the satellite oceans, they may be (even typically) electrically thick when considering tidal periods. As described in the last section, there is evidence that this is the case for Europa. It may also be the case for most of the satellites. When the ocean is electrically thick, induction from external magnetic fields does not penetrate very far into the ocean. Motional induction involves sources within the ocean and so motionally induced fields may penetrate even below the ocean. For electrically thin oceans, the thin-shell formulation cannot be applied except in the case where magnetic diffusion is assumed weak and ignored altogether, in which case the thin-shell formulation reduces to

$$\partial_t B_r = -\nabla_H \cdot (B_r \mathbf{u}_H) \,. \tag{6.5}$$

In this case no depth-averages are implied and so this equation can better be regarded as simply a projection of the induction equation onto a spherical surface.

It may remain unfeasible to directly measure the flow velocity in the satellites and so it is insightful to remove the flow velocity from (6.5) as described in Section 2.3.4. Using (2.61), while assuming $\Sigma = \Sigma_{oc}$, to obtain

$$\partial_t B_r = -\nabla_H \cdot \left(B_r \mathcal{L}_u^{-1} \left[-g \nabla_H \left(\eta - \eta_F \right) + \frac{\boldsymbol{\tau}}{\rho h} \right] \right) . \tag{6.6}$$

While Earth's ocean has momentum fluxes into the ocean from wind stress and other external forces, this is not as clearly the case for the satellite oceans and so there are not obvious examples of other force agents contributing to $\boldsymbol{\tau}$. In this case we can consider

$$\partial_t B_r = -\nabla_H \cdot \left(B_r \mathcal{L}_u^{-1} \left[-g \nabla_H \left(\eta - \eta_F \right) \right] \right) . \tag{6.7}$$

This equation relates the dynamical parameters B_r and η, which are both remotely observable. The other parameters may typically be known, though we may point out exceptions: 1) The tidal equilibrium height is

readily calculated from astronomical and other known parameters except that the very small obliquities of the satellite are not usually known from observations (minimum, forced-component values may be inferred from dynamical expectations (e.g. a Cassini state)); 2) The dissipation parameter/operator α contained in $\mathcal{L}_u^{-1}$ is poorly constrained outside of limiting cases such as boundary layer dissipation where it might be calculated from first principles. In the case of Europa, the dissipation rate is likely to be small and so the latter is not crucial. But on other satellites with very thick ice cover, damping/dissipation rates may be large and knowing α more critical in calculations involving (6.7).

7 Conclusions

This study has presented specialized mathematical formulations appropriate for calculations of electrodynamics near the conductive surface shell of Earth and planetary bodies. It is assumed that the shell may be comprised of fluid in relative motion, and that formulations may gain higher dynamical consistency and accuracy by incorporating conservation principles and/or governing equations for the fluid dynamics. While more general formulations are indeed available, thin-shell formulations exploiting the complete or approximate galvanic isolation of the shell show important advantages as well as restrictions.

The primary advantage is that the thin-shell formulation can be solved numerically with a small fraction of the computational resources needed in more general formulations. The numerical model described in this study is a hybrid approach where the shell is represented with finite differences/volumes and the regions outside of the shell are represented with spherical-harmonic basis functions. The system of coefficients is solved using Krylov subspace methods with a preconditioner matrix obtained from the first iteration of a fixed-point method. The finite difference/volume bases have the advantage of maintaining full dynamical consistency with the ocean models from which parameters are adopted (i.e. we may use the natural grid from the ocean model). The spherical-harmonic bases have the advantage of automatically including the far-field boundary conditions (i.e. the solution domain is effectively reduced). Using this method, high-resolution (e.g. 1/6 by 1/6 degree) global solutions may be obtained very quickly (e.g. on the order of minutes using a standard desktop computer). It is demonstrated that solutions to the equations prescribed are also very accurate. Validation against analytical solutions shows very small errors falling within the theoretical limits of accuracy allowed for a chosen resolution.

The primary disadvantage is that the thin-shell formulation lacks galvanic coupling with conductors outside of the shell. Adjacent thin conducting layers (e.g. due to sediments) can be included by simply extending the shell thickness to accomodate these regions. The neglect of galvanic coupling becomes valid in the limit that the thin shell has electrically insulating regions (even if arbitrarily thin) on both sides. While this is approxiately true for Earth, the low conductivity of the upper mantle can still be galvanically important for the very largest scales (e.g. below spherical-harmonic degree 6) because of the larger cross sectional areas presented for conduction. A method for estimating the error due to the missing galvanic currents is also shown. The thin-shell approach provides then solutions in the limit of no galvanic coupling. Because the galvanic coupling depends on the realism in representing the conductivity in these other conductors (e.g. the upper mantle), the disadvantage described here can become moot in applications where this conductivity is not well known.

Higher realism is not brought by three-dimensional models until the description of the (e.g. upper mantle) conductivity in the galvanically connected region is prescribed accurately. It is arguably the case that such accuracy is not yet available for the Earth's inhomogeneous upper mantle. But it can be important in inverse studies that the three-dimensional models have this representation such that appropriate parameters can be fit using observed data. On the other hand, if three-dimensional models cannot include the high spatial resolution needed to represent the inhomogeneities in the shell, then realism added by galvanic coupling may be overwhelmed by errors due to incomplete spatial resolution. (It is clear from the induction equation with inhomogenous parameters that there is field energy transfer between spatial scales; the reliability of even large-scale features may therefore require high-resolution calculations.)

For applications involving motional induction by dynamical flow, the thin-shell described allows adoption of the native grid on which the dynamical flow calculations were made. This avoids interpolation errors which in some applications could lead to leading order errors. The reason why the errors can reach leading order is because the radial component of the induction equation involves flow-dependent sources that can, for many applications, vanish to leading order. (One can loosely argue that the poloidal component of the ocean flow generated magnetic field is essentially a second-order effect with typical amplitudes an order of magnitude less than that of the toroidal fields.) Errors due to interpolation of ocean parameters can then have a non-comensurate effect on the remaining higher-degree terms. There are, of course, various other advantages of having the electrodynamics calculated on the same grid as that of the oceanographic variables (one should more carefully say the grids are "aligned" when the thin-shell covers a larger domain including land.)

When considering extraterrestrial applications, it may be the case that neither the full induction equation nor thin-shell version are the best formulation with which to start. The reason is that in extraterrestrial cases where the conductivity distribution is highly uncertain, radial conductivity distributions may typically be a reasonable starting assumption. In this case, there is a more immediate uncoupling of the radial vector component of the induction equation from which solutions can be obtained (as in Section 2.4.3). It may also be the case that the oceans in these applications are not electrically thin, as required by the thin-shell formulation.

Some of the ancillary formulations described in this study may be important in both terrestrial and extraterrestrial applications where some parameters (e.g. ocean flow velocity) may be unobservable directly. Forms of the induction equation where these parameters are exchanged for other parameters (e.g. surface displacement) can be a benefit. This study has also reviewed simpler formulations available in the diffusive quasi-static, and frozen-flux limits. Any study should first consider whether one of these simpler formulations is appropriate. In thin shells, the decay time scales and parameter ratios needed for such assessment can be quite different than those more typically described for conducting media because the electromagnetic propagation is not predominantly through the conductor but rather around it. This study provides a detailed description of how to make such assessment in applications of both Earth and planetary oceans.

Acknowledgements The author acknowledges support from the following NASA programs: Earth Surfaces and Interiors, Outer Planets, Planetary Atmospheres. The author extends special thanks to Jakub Velimsky for a careful review of the derivations, Weijia Kuang, Terence Sabaka, and J. Velimsky for helpful comments, and T. Sabaka for software for calculating the spherical harmonic transforms.

References

Anderson, J. D., Schubert, G., Jacobson, R. A., Lau, E. L., Moore, W. B., Sjogren, W. L., 1998. Europa's differentiated internal structure: Inferences from four Galileo encounters. Science 281 (5385), 2019–2022.

Beamish, D., Hewson-Browne, R. C., 1980. Induction in arbitrarily shaped oceans—V. The circulation of Sq-induced currents around land masses. Geophys. J. R. Astr. Soc. 61, 479–488.

Chapman, S., 1919. The Solar and Lunar Diurnal Variations of Terrestrial Magnetism. Philosophical Transactions of the Royal Society of London. Series A, Containing Papers of a Mathematical or Physical Character 218, 1–118.

Chave, A. D., 1983. On the theory of electromagnetic induction in the earth by ocean currents. Journal of Geophysical Research 88, 3531–3542.

Hand, K., Chyba, C., 2007. Empirical constraints on the salinity of the europan ocean and implications for a thin ice shell. Icarus 189 (2), 424–438.

Hewson-Browne, R. C., Kendall, P. C., 1978. Some new ideas on induction in infinitely-conducting oceans of arbitrary shapes. Geophysical Journal International 53 (3), 431–444.

Hide, R., 1983. The magnetic analog of Ertel's potential vorticity theorem. Annales geophysicae 1, 59–60.

Kelbert, A., Kuvshinov, A., Velimsky, J., Koyama, T., Ribaudo, J., Sun, J., Martinec, Z., Weiss, C. J., 2014. Global 3-D electromagnetic forward modelling: a benchmark study. Geophysical Journal International 197 (2), 785–814.

Khurana, K., Jia, X., Kivelson, M., Nimmo, F., Schubert, G., Russell, C., 2011. Evidence of a Global Magma Ocean in Io's Interior. Science 332 (6034), 1186–1187.

Khurana, K. K., Kivelson, M. G., Russell, C., 2002. Searching for liquid water in Europa by using surface observatories. Astrobiology 2, 93–103.

Khurana, K. K., Stevenson, D. J., Kivelson, M. G., Bennet, L., Joy, S., Russel, C. T., Walker, R. J., Zimmer, C., Polanskey, C., 1999. Europa and Callisto: Induced or intrinsic fields in a periodically varying plasma environment. Journal of Geophysical Research 104, 4609–4625.

Kivelson, M., Khurana, K., Russell, C., Volwerk, M., Walker, R., Zimmer, C., 2000. Galileo magnetometer measurements: A stronger case for a subsurface ocean at Europa. Science 289 (5483), 1340.

Kivelson, M., Khurana, K., Volwerk, M., 2002. The permanent and inductive magnetic moments of Ganymede. Icarus 157 (2), 507–522.

Lamb, H., Nov. 1883. Note on the Induction of Electric Currents in a Cylinder placed across the Lines of Magnetic Force. Proceedings of the London Mathematical Society s1-15 (1), 270–275.

Nimmo, F., Pappalardo, R. T., 2016. Ocean worlds in the outer solar system. Journal of Geophysical Research: Planets 121 (8), 1378–1399.

Palmer, T., 1988. Analogues of potential vorticity in electrically-conducting fluids. Geophysical and Astrophysical Fluid Dynamics 40, 133–145.

Price, A. T., 1949. The induction of electric currents in non-uniform thin sheets and shells. The Quarterly Journal of Mechanics and Applied Mathematics 2 (3), 283–310.

Saad, Y., 1995. Preconditioned Krylov subspace methods for CFD applications. Solution Techniques for Large-Scale CFD ....

Sabaka, T. J., Olsen, N., Tyler, R. H., Kuvshinov, A., 2015. CM5, a pre-Swarm comprehensive geomagnetic field model derived from over 12 yr of CHAMP, Orsted, SAC-C and observatory data. Geophysical Journal International 200 (3), 1596–1626.

Sabaka, T. J., Tyler, R. H., Olsen, N., 2016. Extracting ocean-generated tidal magnetic signals from Swarm data through satellite gradiometry. Geophysical Research Letters 43 (7), 3237–3245.

Sanford, T. B., 1971. Motionally induced electric and magnetic fields in the sea. Journal of Geophysical Research 76, 3476–3492.

Schilling, N., Khurana, K., Kivelson, M., 2004. Limits on an intrinsic dipole moment in Europa. Journal of Geophysical Research 109 (E05006).

Schilling, N., Neubauer, F., Saur, J., 2007. Time-varying interaction of Europa with the jovian magnetosphere: Constraints on the conductivity of Europa's subsurface ocean. Icarus 192 (1), 41–55.

Schuster, A., Lamb, H., 1889. The Diurnal Variation of Terrestrial Magnetism. Philosophical Transactions of the Royal Society of London. A 180, 467–518.

Srivastava, S. P., 1966. Theory of the magnetotelluric method for a spherical conductor. Geophysical Journal International 11, 373–387.

Stephenson, D., Bryan, K., 1992. Large-scale electric and magnetic fields generated by the oceans. Journal of Geophysical Research 97 (C10), 15467.

Sun, J., Egbert, G. D., 2012. A thin-sheet model for global electromagnetic induction. Geophysical Journal International 189 (1), 343–356.

Tyler, R., 2005. A simple formula for estimating the magnetic fields generated by tsunami flow. Geophysical Research Letters 32 (9), L09608.

Tyler, R., 2008. Strong ocean tidal flow and heating on moons of the outer planets. Nature 456 (7223), 770–772.

Tyler, R., 2014. Comparative estimates of the heat generated by ocean tides on icy satellites in the outer Solar System. Icarus 243, 358–385.

Tyler, R., Mysak, L., 1995a. Electrodynamics in a rotating frame of reference with application to global ocean circulation. Canadian Journal of Physics 73 (5-6), 393–402.

Tyler, R., Mysak, L., 1995b. Motionally-induced electromagnetic fields generated by idealized ocean currents. Geophysical and Astrophysical Fluid Dynamics 80, 167–204.

Tyler, R. H., 2006. Weak influences of the Earth's magnetic field on ocean circulation. Geophysical Research Letters 33 (14), 4.

Tyler, R. H., Boyer, T. P., Minami, T., Zweng, M. M., Reagan, J. R., 2016. Electrical conductivity of the global ocean, (submitted).

Tyler, R. H., Maus, S., Lühr, H., 2003. Satellite Observations of Magnetic Fields Due to Ocean Tidal Flow. Science 299 (5604), 239–241.

Tyler, R. H., Sanford, T. B., Oberhuber, J. M., 1997. Geophysical challenges in using large-scale ocean-generated EM fields to determine the ocean flow. Journal of Geomagnetism and Geoelectricity 49 (11-12), 1351–1372.

Tyler, R. H., Sanford, T. B., Unsworth, M. J., 1998. Propagation of electromagnetic fields in the coastal ocean with applications to underwater navigation and communication. Radio Science.

Tyler, R. H., Vivier, F., Li, S., 2004. Three-dimensional modelling of ocean electrodynamics using gauged potentials. Geophysical Journal International 158 (3), 874–887.

Vance, S., Harnmeijer, J., Kimura, J., Hussmann, H., 2007. Hydrothermal systems in small ocean planets. The Astrophysical Journal 7 (6), 987–1005.

A Electrodynamics in a rotating frame

This section reviews some of the basic steps in Tyler and Mysak (1995a) to obtain the equations governing electrodynamics in a rotating frame. The Equivalence Principle from General Relativity states that non-inertial reference frames are equivalent to inertial frames with gravitational fields present. The Covariance Principles for tranformations of the four-dimensional electromagnetic tensors can then be used to transform the tensors to a rotating frame, given the appropriate metric. Additionally one needs to transform the constitutive relationships and this was done assuming the Co-Moving Hypothesis. The most general results of the transformed equations are described in Tyler and Mysak (1995a). These were greatly simplified when it is was assumed that the velocities involved were non-relativistic, and the following set of equations comparable to a Maxwell-Minkowski formulation were shown:

$$\nabla \times \mathbf{e} = -\partial_t \mathbf{b} \tag{A.1}$$

$$\nabla \cdot \mathbf{b} = 0 \tag{A.2}$$

$$\nabla \cdot \left(\varepsilon \mathbf{e} - \varepsilon N^{-2} \tilde{\mathbf{u}} \times \mathbf{b}\right) = \rho_e \tag{A.3}$$

$$\nabla \times \left(\mu^{-1} \mathbf{b} - \varepsilon N^{-2} \tilde{\mathbf{u}} \times \mathbf{e}\right) = \partial_t \left(\varepsilon \mathbf{e} - \varepsilon N^{-2} \tilde{\mathbf{u}} \times \mathbf{b}\right) + \mathbf{j} \tag{A.4}$$

together with

$$\mathbf{j} = \rho_e \mathbf{u}_c + \sigma \left(\mathbf{e} + \mathbf{u}_c \times \mathbf{b}\right) \tag{A.5}$$

which is similar to the usual form of Ohm's Law for a moving conductor (governing conduction electric currents) but with advection currents (i.e. electric currents due to flow advection of spatial charge density) added. Here, $\varepsilon = \varepsilon_r \varepsilon_0$ is the absolute electrical permittivity (ε_r is the relative permittivity, ε_0 is the permittivity of free space), $\mu = \mu_r \mu_0$ is the magnetic permeability (μ_r is the relative permeability, μ_0 is the permeability of free space), $N = (\mu_r \varepsilon_r)^{1/2}$ is the index of refraction, and

$$\tilde{\mathbf{u}} = \mathbf{u}_s + (1 - N^2)\mathbf{u}_c \tag{A.6}$$

is a velocity involving the solid-body rotation $\mathbf{u}_s$ of the coordinate system and the relative velocity $\mathbf{u}_c$ of material (e.g. the fluid ocean) in that coordinate system. Here the notation in Tyler and Mysak (1995a) is preserved, where lower case $\mathbf{e}$ and $\mathbf{b}$ are used to refer to the fields observed in the rotating frame (this should not be confused with the use of $\mathbf{b}$ in the main text to refer to the ocean-generated component of the magnetic field.)

Because these equations include a dependence on the inhomogeneous velocity of the reference frame, it is immediately clear that the equations governing the electrodynamics are not invariant to a transformation to a rotating/accelerating frame. To state that "Maxwell's equations" are similarly not invariant, even when non-relativistic approximations have been

applied, is similarly true, although with some caveats because the specific form of the Maxwell equations presented can vary as they usually incorporate constitutive relationships (which have quite different transformation properties than the electromagnetic fields). Basically, outside of the special case of homogeneous (i.e. no material charge or electric currents) Maxwell-Minkowski equations—which are indeed invariant in the transformation—the electromagnic field components represent macro-scale averages over micro-scale processes in the media and the transformation of these fields gains properties of the tranformation of the constitutive relationships.

Importantly, additional approximations (beyond simply an assumption of non-relativistic speeds, i.e. $\tilde{\mathbf{u}} \cdot \tilde{\mathbf{u}}/c^2 << 1$) were used in Tyler and Mysak (1995a) to show that (A.1, A.2, A.4, A.5) can be reduced to their non-rotating forms. These approximations involve assumptions about the electrical properties of the material as well as an assumption that the relative amplitude of the magnetic field in the process considered (with respect to the amplitude of background fields) must be larger than the squared relative speeds $\tilde{\mathbf{u}} \cdot \tilde{\mathbf{u}}/c^2$.

As (A.1, A.2, A.4, A.5) are the equations needed in forming the induction equation, the induction equation is approximately invariant to rotation. The remaining equation retains what was termed a "generalized Schiff's charge density" Tyler and Mysak (1995a). In adopting the usual induction equation for applications in the rotating frame, one assumes that displacement (first term on right side of A.4) and advection electric currents (first term on right of A.5), even in their modified form, can be ignored relative to conduction currents.

B Gauge potentials

The gauge potentials, usually written as $\mathbf{A}$, ϕ comprise the magnetic vector potential $\mathbf{A}$ and the electric scalar potential ϕ. These are sometimes treated together as the electromagnetic four-vector. These variables are arguably more fundamental than the usual variables $\mathbf{E}$, $\mathbf{B}$. General solutions can be obtained from formulations involving either, although one may note that outside of relativistic calculations (where the Lorentz gauge must be adopted for dynamic consistency) the choice of $\mathbf{A}$, ϕ is not unique as there is freedom in choosing the gauge. The relationships between $\mathbf{A}$, ϕ, and $\mathbf{E}$, $\mathbf{B}$ can be found in Tyler et al. (2004), which uses a gauge formulation exploiting the gauge freedom for calculations of ocean electrodynamics. The formulation in Tyler et al. (2004) is more general than provided in the induction equation (e.g. displacement currents are allowed) but the relationships described can also be used to calculate $\mathbf{A}$, ϕ from $\mathbf{E}$, $\mathbf{B}$ (and vice versa) for the restricted applications consistent with the induction equation.

C Galvanic vs. inductive current sources

It is helpful to provide some description on the nature of electric currents and sources ultimately driving the electrodynamics. Specifically, we shall provide a description of the distinctions between galvanic, induced, and motionally-induced electric currents.

First note an important distinction between field variables such as the electric and magnetic fields ($\mathbf{E}$, $\mathbf{B}$) that can exist in a vacuum region, and material properties and variables that can only be defined within material media. Indeed, the homogeneous Maxwell equations obtained by setting the material charge density ρ_e, and electric current density $\mathbf{J}$ to zero still support electromagnetic waves. While this is true even in regions where no material is present, it is expected that these vacuum electromagnetic fields must ultimately be driven by material sources either outside of the domain (such that the fields are driven by prescribed boundary conditions) or previously present within the domain. The Maxwell's equations can then be described as involving the field variables $\mathbf{E}$, $\mathbf{B}$ and the intensive material properties/variables ρ_e, $\mathbf{J}$, σ, $\mathbf{u}$. The electric charge density ρ_e evidently describes an excess over neutrality of material electric charge (as averaged over the very small scales where the assumptions of continuum electrodynamics breaks down). As we are only considering conduction electric currents, $\mathbf{J}$ is due to material electric charges moving through the medium and we do not include in $\mathbf{J}$ displacement electric currents or the advection electric currents due to the transport of ρ_e with the material flow. An implicit assumption is then that $|\rho_e \mathbf{u}| << |\mathbf{J}|$, and more generally that conduction electric currents either dominate all other electric currents or are at least isolated for study. The material velocity $\mathbf{u}$ shall also be regarded here as an intensive material variable as it is the ratio of the momentum density and mass density (both intensive material properties). The electrical conductivity is an intensive material property describing the ratio of electric current density to the in situ electric field. These "intensive" properties are distinguished from "extensive" properties that depend on the "extent" or amount of material present. As examples, electric charge or electric current are extensive variables while their associated material densities ρ_e $\mathbf{J}$ are intensive variables as described.

A second important distinction is in the nature of sources generating the electric field. In a wide range of applications, the electric field is often a field effect of two quite distinct physical processes in the material media. This can be made most clear with the gauge-potential variables $\mathbf{A}$, ϕ as they are more fundamental than $\mathbf{E}$, $\mathbf{B}$ (see Appendix B). Specifically, the two sets of field variables are related as

$$\mathbf{E} = -\partial_t \mathbf{A} - \nabla\phi, \tag{C.1}$$

$$\mathbf{B} = \nabla \times \mathbf{A} \tag{C.2}$$

from which we see now that $\mathbf{E}$ has two components:

The second component ($-\nabla\phi$) involves the gradient of the scalar electric potential. This simply describes an electromotive force on a charge down the gradient of ϕ. A resulting electric current can be referred to as a "direct" or "galvanic" current. "Galvanic current" is probably the better choice for distinguishing the physical process as "direct current" or "DC" is often used to distinguish temporally stationary currents from alternating currents ("AC"). While "direct currents" may typically be driven by the gradient of electric potential, this physical distinction does not appear to be a requirement in the use of the term and so in this paper "galvanic currents" is exclusively used to refer to electric currents driven in this way. Similarly, in many related studies the use of the term "toroidal currents" is used to refer to the galvanic currents but this is also avoided here as the toroidal/poloidal decomposition does not exclusively distinguish the galvanic processes.

The first component ($-\partial_t\mathbf{A}$) describes the "inductive" component of the electric field and is perhaps less intuitive. Toward helping to describe it, note that from Maxwell's equations together with (C.1, C.2) and the Coulomb gauge $\nabla\cdot\mathbf{A}=0$, we may write write

$$\nabla^2\phi = -\rho_e/\epsilon_0 \tag{C.3}$$

$$\nabla^2\mathbf{A} = -\mu_o\mathbf{J} \tag{C.4}$$

from which we may regard ϕ as the field quantity associated with ρ_e, and $\mathbf{A}$ as the field quantity associated with $\mathbf{J}$. (In a more general treatment that allows freely propagating electromagnetic waves and consistency with relativity, the Laplacian operators above are replaced with D'Alembertian wave operators.) While ϕ is the Coulomb potential associated with ρ_e, $\mathbf{A}$ is evidently dependent on the motion or time rate of change of this Coulomb "cloud" ϕ. In some simplistic cases, $\mathbf{A}$ can be regarded as the advection of ϕ at the drift velocity of the conduction charge carriers.

While ρ_e is confined to the material (conductive) media, ϕ (and therefore $\mathbf{A}$) is not and may be felt in a second conductor separated from the first by an electrical insulator. In many applications, one may think of the inductive component ($-\partial_t\mathbf{A}$) of $\mathbf{E}$ as creating the tendency of accelerating charge to entrain the motion of other charges that may even be galvanically isolated in a second conductor. This mysterious "reach" between conductors is of course just a restatement of the mysterious difference between field and material variables. While ϕ and therefore the galvanic component ($-\nabla\phi$) of the electric field can also reach through insulators and into a second conductor, the tendency to create electric current in the second conductor is quickly cancelled by a spatial charge density redistribution. The electric currents responsible for this redistribution of spatial charge have a nature overlapping with other forms of displacement current that are ignored in this treatment where only conduction currents are assumed to be significant.

D Depth integration

The utility of the thin-shell formulation is primarily restricted to cases where the shell is electromagnetically thin (i.e. the frequency-dependent skin depth within the conducting shell must be much larger than the geometric thickness of the shell). In the application to the oceans this criterion usually excludes high-frequency applications that are anyway inconsistent with other assumptions. Where the thin shell extends onto land and conductivity drops, the criterion can be formally more limiting, although one may note that a violation in this case is not likely to change the solution for the electric currents (and therefore associated magnetic fields) as these remain primarily in the oceans. Because of the galvanic isolation and electromagnetic thinness of the shell, the radial component of the magnetic field, and the horizontal components of the electric field are to good approximation uniform with depth in the shell.

Now note that in the thin shell induction equation, repeated here generically as

$$\mathbf{g}\cdot\partial_t\mathbf{B} = \nabla\cdot(\{\mathbf{u}\times\mathbf{B}\}\times\mathbf{g} - K\{\nabla\times\mathbf{B}\}\times\mathbf{g}), \tag{D.1}$$

and where we take $\mathbf{g}$ to be perpendicular to the shell and at least approximately uniform within the sheet (as would be the case where $\mathbf{g}$ represents the radial unit vector), the vector inside the divergence operator represents $\mathbf{E}_H\times\mathbf{g}$ and is therefore also depth-uniform within the shell.

Although $\mathbf{E}_H\times\mathbf{g}$ is depth uniform, the two terms comprising it are individually not, necessarily. The first term involves $\mathbf{B}$ but this shall usually be replaced with a prescribed background field and so this whole term is prescribed. The second term, however, involves the product of the parameter K and a function (curl) of the solution variable. Outside of idealized cases, there will be an error if we assume that the depth average of this product will is equivalent to the product of the depth averages. Basically, we do not in advance of the solution know how the two covary with depth. This can be avoided by exploiting the depth-uniformity of $\mathbf{E}_H$. We note that because $\overline{(K^{-1}\mathbf{E}_H)} = \overline{(K^{-1})}\overline{\mathbf{E}_H}$, where the overbar represents the depth average, we may write

$$\bar{\mathbf{E}}_H = \frac{\overline{(K^{-1}\mathbf{E}_H)}}{\overline{(K^{-1})}} = \frac{\overline{(\sigma\mathbf{E}_H)}}{\overline{(\sigma)}} = \bar{\mathbf{B}}^*_H, \tag{D.2}$$

where (2.25) has been used for the last equality, and use this instead in forming the depth average of $\mathbf{E}_H\times\mathbf{g}$ where needed in the main text.

E Toroidal component

The toroidal/poloidal decomposition is a mathematical decomposition in vector calculus that can be viewed as a restricted form of the more general Helmholtz decomposition. For vectors with zero divergence (as for magnetic fields), the toroidal/poloidal decomposition is often a convenient representation in spherical coordinates. A specific discussion of this decomposition for ocean-domain applications is found in Chave (1983) and Sun and Egbert (2012).

In the thin-shell study described in the main text, the toroidal component is not resolved as fields are averaged over the shell thickness. (The part that is resolved is the poloidal component). Within the assumptions that the ocean is both electrically and geometrically thin, one can, however, estimate toroidal magnetic field components quite simply (e.g. Tyler and Mysak 1995b; Tyler et al. 1997). Essentially, the assumption that the shell is both electrically and geometrically thin allows one to assume quasi-stasis (i.e the electromagnetic adjustment radially through the shell is instantaneous), and ignore horizontal derivatives relative to radial derivatives. The toroidal magnetic field $\mathbf{b}_H^{(T)}(h_0 < r < a)$ is easily found by integrating the equation

$$\partial_r \mathbf{b}_H^{(T)} = -\sigma\mu_0 B_r \left(\mathbf{u}_H - \bar{\mathbf{u}}_H^*\right) \tag{E.1}$$

from either one of the thin-shell interfaces where $\mathbf{b}_H^{(T)} = 0$.

F Simplified formulations for idealized cases

F.1 Cases with spherical symmetry throughout all domains

When the magnetic diffusivity parameter is a function only of radius (i.e. $K = K(r)$) (2.12) can be written as

$$\partial_t B_r + \nabla_H \cdot (B_r \mathbf{u}_H) - K\nabla^2 B_r = \nabla_H \cdot (u_r \mathbf{B}_H)\,. \tag{F.1}$$

This equation can be interpreted as a dynamical equation for B_r whereby B_r changes with time due to advection and convergences in the flow, diffusion, and tilting in which non-uniformities in radial flow u_r redirect $\mathbf{B}_H$ to gain a radial component.

While (3.14) is a projection of the induction equation onto a spherical surface, radial derivatives are involved in the Laplacian operator and there remains the coupling term on the right. There are, however, applications with configurations or approximations such that (3.14) becomes an uncoupled scalar partial-differential equation that is separable. In this case, the partial-differential equation can be replaced by algebraic equations and the solution of an ordinary-differential equation for the radial dependence.

Recall that applications where one may assume radial symmetry in electrical conductivity throughout all domains are not the target for the specialized methods described in this study. Indeed, one expects that a primary challenge that must be addressed in these specialized methods is to allow for at least one electrically inhomogeneous layer. The thin-shell formulation allows for this inhomogeneity while also imposing dynamical constraints and approximations. The radial symmetry is, however, assumed in this and the next few sections simply for the purpose of seeking analytical solutions.

The following sections consider applications addressed using the thin-shell formulation. In this section we start, however, by considering an application using (3.14) in which thin-shell assumptions have not yet been applied.

An important and common family of applications is one where a time-dependent external magnetic field is incident on a stationary (or uniformly rotating) conductor and the electrical response must be calculated. Let us consider here the conductor to be a sphere with $K = K(r)$. Let us further assume that $K(r)$ is described by $j = 1...J$ concentric shells, each with a value K_j that is uniform within the layer. Finally, let us assume a harmonic time dependency such that the symbol ∂_t can be here regarded simply as a complex coefficient. In this case, (3.14) reduces to a Helmholtz equation

$$\left(\frac{\partial_t}{K_j}\right) B_r^{(j)} - \nabla^2 B_r^{(j)} = 0 \tag{F.2}$$

applied within each layer j. These $1....J$ equations must be solved together with appropriate boundary conditions, as well as matching conditions to ensure B_r and $\partial_r B_r$ are continuous across the interfaces between the layers.

The standard method for solving (F.2) is to first apply the method of separation of variables; a spherical-harmonic expansion describes the horizontal dependence and the radial dependence is satisfied in general by the spherical Bessel functions with argument kr, where $k = \left(\frac{i\partial_t}{K_j}\right)^{1/2}$. In the case where a layer is an insulator (i.e. $K \to \infty$) the spherical Bessel functions reduce to simpler potential-field base functions. Because the number of layers J is arbitrary, one can include as many layers as needed to model an arbitrary $K(r)$. The method described then replaces the solution of the partial differential equations with an algebraic system of equations for the $2J$ coefficients (two coefficients are needed for the two base functions in each of the J shell domains.) These $2J$ equations are derived from 2 boundary equations and $2(J-1)$ matching conditions across the $J-1$ interfaces.

F.2 Quasi-static formulations

The word *electrodynamics* is used in the title of this paper to emphasize target applications that extend beyond those that can be treated under quasi-static assumptions. Courses in physics typically describe formulae and calculations for cases of *electrostatics* (involving stationary electric charge) and *magnetostatics* (involving stationary electric current) before delving into formulations for electrodynamics where these simplifying quasi-static assumptions no longer apply. Indeed, the upward step in computational complexity is typically significant and so a first step in addressing an application should be to determine whether the problem can reasonably be treated as quasi-static such that the simpler formulations may be used. Even if the application to be considered is not expected to be quasi-static, the quasi-static solutions can be helpful in validating and interpreting results from more complete and complex dynamical calculations.

The criterion for deciding whether the case is quasi-static is not as simple or immediate as some may think. Even the formulation for the criterion is very much application dependent and what is clear from the outset is that in applications of large-scale near-surface electrodynamics magnetic diffusion time scales sometimes quoted to gain this criteria are grossly misleading. The source of confusion seems to be a lack of appreciation for the fact that electromagnetic adjustment in the thin shell is quite different than what is usually described for conducting media. The reason for the difference is that the adjustment fundamentally involves propagation through the surrounding insulators rather than directly through the conducting media. Considering propagation away from a point source in the ocean at mid-depth, say, the direct path through the conductor is only important for a horizontal range of about two ocean depths. Beyond that, the paths are primarily up-over-down or down-over-up paths where the fields propagate through the ocean only up to the surface (or down to the seafloor) where the fields then propagate horizontally through the surrounding poor conductors and then refract back into the ocean. Strange "beach-mode" paths can even exist where fields propagate landward, curl around the beach and then propagate seaward, combining the up-over-down and down-over up paths (Tyler et al., 1998). What is clearly important here is that there are no applications involving primary direct paths through the conductor that do not violate the thin-shell assumptions. The direct paths are important only for horizontal scales less than about two ocean depths, as mentioned. Further, the assumption that the thin shell is electromagnetically thin means that the only time scales considered are much larger than the time needed for the direct path to the interfaces of the thin shell. Therefore, it is expected that there are no thin-shell applications for which the simple descriptions of magnetic diffusion time scales (usually calculated with plane-wave assumptions) are appropriate.

The topic of estimating appropriate time scales for the electromagnetic adjustment (such as would be needed to decide whether the application can be treated as quasi-static) is discussed in Sections 3.1 and 5.1. Here we describe useful formulations that can be used if quasi-stasis applies.

A quick way of understanding the computational advantage of the quasi-static assumption comes from looking at the gauge formulation (see Section cite). In the gauge formulation, one must generally solve four partial differential equations (one for each of the components of the four-vector $\{\mathbf{A}, \phi\}$ simultaneously. For sufficiently low-frequencies or long time scales, however, the equation for ϕ uncouples from the others, allowing the equations to be solved sequentially rather than simultaneously. The simplification in the quasi-static assumption can be traced to an electro-static assumption for the behavior of the electric field. While the electric field $\mathbf{E} = -\partial_t \mathbf{A} - \nabla\phi$ generally has two physically distinct components (see Section C for description), in the quasi-static assumption $\mathbf{E} \approx -\nabla\phi$ and one can immediately take the divergence of Ohm's Law (2.5) together with (2.3) to obtain

$$\nabla \cdot (\sigma \nabla\phi - \sigma \mathbf{u} \times \mathbf{B}) = 0, \tag{F.3}$$

which is a simple elliptic equation for ϕ in three dimensions, assuming σ, $\mathbf{u}$ and $\mathbf{B}$ are prescribed. In many applications, $\nabla \cdot (\sigma \mathbf{u} \times \mathbf{B}) \approx \nabla \cdot (\sigma \mathbf{u} \times \mathbf{F})$, where $\mathbf{F}$ is the background main geomagnetic field. A solution strategy is then to first solve

$$\nabla \cdot (\sigma \nabla\phi) = -\nabla \cdot \mathbf{J}^{(p)}, \tag{F.4}$$

for ϕ, where $\mathbf{J}^{(p)}$ (in this case, $\mathbf{J}^{(p)} = -\sigma \mathbf{u} \times \mathbf{F}$) is an arbitrary prescribed component of the electric current density. The total electric current density may be described as $\mathbf{J} = \mathbf{j} + \mathbf{J}^{(p)}$, where $\mathbf{j}$ is the component of the electric current density that must be resolved through solution. Once ϕ is found, the electric current and electric field can be calculated using (2.5), and the magnetic field can be calculated using (2.3).

F.2.1 Quasi-static thin-shell formulations

Integration of (F.4) over the thin shell depth h_0, gives

$$\nabla_H \cdot (\Sigma \nabla_H \phi) - j_r(r = a) + j_r(r = a - h_0) = -\nabla \cdot \left(\int_{a-h_0}^{a} \mathbf{J}_H^{(p)} dr \right) - J_r^{(p)}(r = a) + J_r^{(p)}(r = a - h_0). \tag{F.5}$$

If we assume that the thin layer is surrounded by insulators, then both j_r terms on the left side of (F.5) vanish as a consequence of the fact that $\mathbf{j}$ must be continuous across the boundaries. One has then to solve a simple elliptic equation in two dimensions given prescribed sources.

Alternatively, one need not assume the regions adjacent to the thin shell are insulators. One may couple (F.5) with an equation (F.4) describing the exterior regions by requiring again continuity of the normal vector component of the electric current. In this case, the thin shell does not remove the galvanic mode but may provide simplification when assumptions about parameters or other choices are different in the two domains. For example, the intrinsically three-dimensional problem of the oceans plus mantle can be reduced to solving a one-dimensional and a two-dimensional set of equations under the simplifying assumption of a radially symmetric conductivity distribution (such as in Section 2.4.3). Let (F.5) represent the inhomogeneous ocean/surface conductance shell. Following (F.4) with $\sigma = \sigma(r)$, and $\mathbf{J}^{(p)} = 0$,

$$\nabla \cdot (\sigma_m \nabla \phi_m) = \sigma_m \nabla_H^2 \phi_m + \frac{1}{r^2} \partial_r \left(r^2 \sigma_m \partial_r \phi_m \right) = 0, \tag{F.6}$$

governs the electric potential in the mantle (ϕ_m).

F.2.2 Electric stream function, electric potential

The electric stream function is useful for assumed two-dimensional electric currents $\mathbf{J}$ (where $\mathbf{J}$ may represent either a two-dimensional electric current in a three-dimensional medium, or a depth average over a thin layer). One must also assume that the motional induction term is a vector also lying in the local plane of electric currents, or that adjacent insulators confine the electric currents to remain in this plane. By application of Helmholtz' theorem for an assumed two-dimensional vector, we may expand $\mathbf{J}$ as $\mathbf{J} = \nabla \Theta_J + \nabla \times (A_J \hat{\mathbf{n}})$, where Θ_J is a scalar potential and $A_J \hat{\mathbf{n}}$ is the one component of the vector potential (perpendicular to the plane of electric current) remaining after the two-dimensional assumption. We have by (2.3), however, that $\nabla \cdot \mathbf{J} = \nabla^2 \Theta_J = 0$ such that we may (outside of unusual boundary conditions) assume simply $\Theta_J = 0$. The scalar A_J can then be regarded as a stream function for the electric current as $\mathbf{J} = \nabla \times (A_J \hat{\mathbf{n}}) = \nabla A_J \times \hat{\mathbf{n}}$. Using these relationships (together with $\mathbf{E} = -\nabla \phi$) in (2.5) we derive the following elliptic equation for the electric stream function, where $\mathbf{u}_H$ refers to the projection of the flow velocity tangent to the plane of electric current.

$$\nabla \cdot \left(\sigma^{-1} \nabla A_J + (\hat{\mathbf{n}} \cdot \mathbf{B}) \, \mathbf{u}_H \right) = 0. \tag{F.7}$$

Interestingly, the electric stream function approach can be generalized to non-static cases. Indeed, in the thin-shell formulation treated next, the magnetic potential at the surface of the thin shell is proportional to a stream function (call it ψ_e) for the depth integrated electric currents within the shell as

$$\psi_e = \frac{2}{\mu_0} M. \tag{F.8}$$